Causality Is All You Need: A Stochastic Perspective On 2D Quantum Gravity

Ryan Barouki

Merton College

University of Oxford

A thesis submitted for the degree of

Doctor of Philosophy

Michaelmas 2025

Acknowledgements

Firstly, I thank my supervisor, John Wheater, for his constant guidance and collaboration. You have taught me how to be an independent researcher and patiently listened to and answered my ill-posed questions for just over four years. I am eternally grateful for that.

To my biggest collaborator and friend, Davide Laurenzano, with whom I have shared many head-scratching moments and triumphant epiphanies. Of course, my other collaborators: Henry Stubbs, Giacomo Marocco and second supervisor Subir Sarkar, who guided my initial time at Oxford.

I am grateful to Merton College for spending their endowment on me, from travel costs to language courses, and to the STFC for funding my studentship.

My time at Oxford was shaped by the lifelong friends I made here. Aleksy Kwiatkowski, with whom I have lived since day one, you have been a constant source of support and fun; without your countless dinners, I may well have perished.

To my long-time friend, Aidan Murray, thank you for staying in touch all these years despite the distance and for being my number one fan on Strava. Our regular climbing trips in Fontainebleau were a highlight.

Liam Gladden, for our long office conversations at lunch and mutual encouragement during moments of self-doubt.

Eugene Lin, for being my regular climbing partner at the Gallery, a place we both went to find a guaranteed sense of accomplishment.

Thomas Kite, you have always sung my praises and enabled so many experiences. Our time in Boston will always be a fond memory.

Isaac Layton, we started our physics journey together on our first day at Manchester University. Your ability to think deeply about physics was an inspiration and fuelled my own curiosity. I honestly would not be here without our long, meandering chats.

I thank my parents for their endless support. I have never felt pressured to pursue any particular path and have always been encouraged to follow my interests. I am very grateful for that.

Finally, to my partner Arunima, the brightest highlight of all. You have opened me up to a new world of ideas from our late-night conversations and ever-growing reading lists. You challenge me and inspire me to think differently. Most importantly, your love and care were more crucial than I can express, especially during the final push to the finish line. I am so grateful to have you in my life.

Abstract

This thesis develops a causality–first perspective on two-dimensional quantum gravity. Working within Causal Dynamical Triangulations (CDT) and closely related solvable models, we combine stochastic methods, matrix models and renormalisation group techniques to investigate how matter couples to causal random geometry.

A central toy model of matter in this thesis is the Ising model and its coupling to CDT. In Chapter 4 we consider the conformal dimensions of the Ising conformal field theory operators on a CDT graph. We construct topological defects and Dehn-twist operators directly on causal triangulations and follow them to the continuum, showing that (for the Ising model and more generally in the settings considered) the critical exponents are those of the flat lattice—i.e. there is no Knizhnik-Polyakov-Zamolodchikov (KPZ) dressing on CDT. The argument relies on the continuity of the causal stochastic process and the fusion category structure of defects.

In Chapter 5, we formulate and analyse a matrix model for Ising spins on CDT using the Functional Renormalisation Group. Within a single-trace truncation we derive beta functions, identify Gaussian and pure-CDT fixed points, and find non-trivial fixed points with three relevant directions—matching the three primary operators of the Ising CFT.

In the final chapter, the stochastic approach once again comes into its own where we use it to show how hyperbolic geometry emerges from CDT in two different ways. The first builds on the previous work in [1], making it rigorous and finding a new stochastic process which incorporates the average hyperbolic profile as well as the fluctuations around it. The second is a consequence of a stochastic time-reparameterisation known as a Lamperti time-change. This change of time transforms the process that describes the spatial length of CDT from a Bessel type process to an exponential Brownian process. The emergent constant negative curvature is then direct.

It is clear that the stochastic approach to analysing continuum CDT is very powerful and has the potential to solve many of the remaining questions in CDT by leveraging the vast machinery of stochastic calculus. However, underlying the ability to describe CDT as a stochastic process in the first place is the central tenet of causality. It appears to tame the two-dimensional gravitational path integral; you might say that, *"causality is all you need"*.

Statement Of Originality

This thesis is the work of the author, except where otherwise stated. It has not been submitted in whole or in part for any other qualification. Chapters 4 and 5 contain material that has appeared in the following publications; the text has been adapted and expanded for the purposes of this thesis.

Chapter 4 is based on:

- Ryan Barouki, Henry Stubbs, and John Wheater, "Conformal dimensions on causal random geometry," *Journal of High Energy Physics* **07** (2025) 173, arXiv:2501.17930 [hep-th].

Chapter 5 is based on:

- Ryan Barouki and Davide Laurenzano, "A Renormalization Group Analysis of the Ising Model Coupled to Causal Dynamical Triangulations," *Journal of High Energy Physics* **10** (2025) 198, arXiv:2504.01134 [hep-th].

Except where specifically cited, the remaining chapters and all linking material represent original work completed by the author—all em dashes are my own.

Contents

An author is a fool who, not content with boring those he lives with, insists on boring future generations.

— Charles de Montesquieu

1 Introduction

1.1 Motivation

The search for a consistent quantum theory of gravity remains one of the central open problems in theoretical physics. It is one of the necessary pieces for the holy grail: a "theory of everything". Despite the successes of string theory which promises to be such a theory, there are many features which leave a lot to be desired. In the absence of any evidence of compact higher dimensions or supersymmetry, it is natural to explore other avenues to quantizing gravity. Our perspective, along with that of many others, is to tackle the gravitational path integral head on.

Directly quantizing four-dimensional general relativity confronts severe conceptual and technical obstacles: perturbative non–renormalizability [2–4], the absence of a fixed background geometry, and the challenge of defining genuinely diffeomorphism-invariant observables [5]. Lower-dimensional models provide an indispensable laboratory in which these issues can be isolated, sharpened, and in many cases, solved explicitly. In particular, two-dimensional quantum gravity admits multiple complementary formulations: continuum field-theoretic (Liouville) approaches [6–13], discretised (dynamical triangulation and matrix model) approaches [14–22], and probabilistic / stochastic descriptions related to random planar maps and the Brownian map [23–30]. Their mutual agreement in

appropriate scaling limits provides rare, concrete evidence that the gravitational path integral can be given a mathematically controlled meaning.

Quantum gravity in two dimensions is equivalent to studying random surfaces. Random surfaces have been studied thoroughly in the physics literature and are already relevant to string theory (the string world-sheet) as well as to conformal field theory. These models are also of interest from a statistical physics point of view. For example, results of various scaling exponents of random walks on a regular $\mathbb{Z}^2$ lattice were first calculated exactly on a random surface and then mapped to the fixed lattice [31].

Within the discretised programme, imposing or relaxing causal structure leads to qualitatively different universality classes. Euclidean random triangulations reproduce Liouville gravity but exhibit highly fractal geometries with Hausdorff dimension $d_H = 4$ [24]. Causal Dynamical Triangulations (CDT) [32–37] introduce a distinguished foliation and a microscopic notion of time, enabling a well-defined Wick rotation, suppressing certain pathological baby-universe proliferations, and yielding continuum limits with geometric properties closer to semiclassical expectations [38]. CDT has been remarkably successful in the non-perturbative study of two-dimensional quantum gravity, with many analytic and numerical results [34–37, 39–44]. Understanding precisely how causality constraints modify scaling behaviour, critical exponents, and matter coupling is therefore of both conceptual and practical importance. Moreover, considerable progress has been made in four-dimensional CDT using numerical methods [45–47].

Coupling matter to fluctuating geometry is essential: only then can we probe how geometry back-reacts on quantum fields and vice versa. Even in two dimensions, non-trivial interplay arises. Matrix-model techniques efficiently enumerate discretised surfaces decorated with matter degrees of freedom [22], while functional renormalisation group (FRG) methods can uncover continuum fixed points directly in (multi-)matrix theories [48–55]. This thesis leverages and interrelates these perspectives. A unifying theme of this thesis is to explore how causality constraints shape critical phenomena, conformal data, and effective continuum descriptions.

Broadly, the goals are:

- To review and connect continuum, discrete, and stochastic formulations of two-dimensional quantum gravity.
- To analyse causal ensembles and their geometric and scaling properties relative to Euclidean counterparts.
- To compute conformal dimensions and scaling relations in causal random geometry using probabilistic tools.
- To investigate matter–geometry interaction in CDT via matrix-model plus FRG techniques, identifying fixed points and relevant directions consistent with conformal field theory expectations.
- To investigate the emergence of hyperbolic space from CDT that lies latent in CDT using stochastic methods.

In combination these strands aim to sharpen our understanding of universality in two-dimensional quantum gravity and to highlight the power of the stochastic approach to tackling problems in CDT and two-dimensional causal geometry as a whole.

1.2 Outline

The remainder of the thesis is organised as follows.

Chapter 2 Introduces two-dimensional quantum gravity in continuum and discrete guises, contrasting Liouville theory with (causal) dynamical triangulations and setting notational and conceptual conventions. We also review 2D Hořava–Lifshitz gravity and give a brief introduction to matrix models.

Chapter 3 Collects stochastic calculus tools (e.g. martingales, measure changes, Doob h-transforms) as a primer for the rest of the thesis.

Chapter 4 Considers conformal dimensions on causal random geometry, contrasting with Liouville predictions and examining how causality modifies scaling relations.

Chapter 5 Applies the Functional Renormalisation Group to the matrix model describing CDT coupled to Ising matter, identifying fixed points, and classifying relevant directions.

Chapter 6 Formulates a rigorous description of the emergence of hyperbolic space from CDT as well as from a stochastic time-reparameterisation of the original CDT time.

Each chapter is written to be as self-contained as possible while building cumulatively: early chapters lay the theoretical foundations; later chapters combine discrete, continuum, and stochastic insights to address the interplay of matter, causality, and geometry.

2

2D Quantum Gravity

Contents

We begin the theoretical background with a discussion of *two-dimensional quantum gravity* which sets the background for the work in this thesis. This is a broad topic with many avenues to explore and so we provide a streamlined cut through the relevant literature in order to prepare the reader for the latter chapters.

In Lorentzian space-time, we define *quantum gravity* on the two dimensional manifold M as the path integral

$$Z(\Lambda) = \int \mathcal{D}[g]\, \mathcal{D}[\Phi]\, e^{iS_{EH}(g)+iS_m(\Phi,g)}\,. \tag{2.1}$$

Here $[g]$ denotes the equivalence class of Lorentzian metrics g on M up to diffeomorphisms, and $[\Phi]$ the configuration of, for the moment unspecified, matter degrees of freedom

living on M. $S_{EH}(g)$ is the Einstein-Hilbert action

$$S_{EH}(g) = \frac{1}{16\pi G_N} \int_M d^2x\sqrt{g}(2\Lambda - R)\,, \tag{2.2}$$

where G_N is Newton's constant, Λ is the cosmological constant, and R is the Ricci scalar curvature. $S_m(\Phi, g)$ is the diffeomorphism invariant action for the matter degrees of freedom. For simplicity we have omitted the Gibbons-Hawking-York term for manifolds with boundary. We often work with the Euclidean gravity model which is similarly defined by

$$Z(\Lambda) = \int \mathcal{D}[g]\,\mathcal{D}[\Phi]\, e^{-S_{EH}(g)-S_m(\Phi,g)}\,, \tag{2.3}$$

where now the functional integration is over Euclidean, rather than Lorentzian, metrics. Note, however, that the relationship between Lorentzian and Euclidean models cannot be simply seen as the Wick rotation $t \to -it$, as for field theory in flat space-time, because this transformation does not commute with diffeomorphisms [56–59].

In two dimensions, Euclidean manifolds are completely characterised by their genus g and the number of boundaries b. Moreover, the curvature part of the Einstein-Hilbert action is a topological invariant due to the Gauss-Bonnet theorem

$$\int_M d^2x\sqrt{g}R = 4\pi\chi(M), \tag{2.4}$$

where $\chi(M) = 2 - 2g - b$ is the Euler characteristic of the manifold. Hence for a fixed topology, every geometry receives the same factor (2.4) in the path integral and can be factored out leaving only the cosmological constant term, so we henceforth set $8\pi G_N = 1$. The physics of the model then lies largely in the proper definition of the functional integral over the metric. The approach taken in this thesis is to discretise the manifold into simplices (triangles) and turn the continuum path integral into a combinatorial problem. Before we elaborate on the discrete approach, it behoves us to briefly mention a continuum approach introduced by Polyakov [6] known as Liouville gravity.

2.1 Liouville Gravity

We outline the basic features here; see [8, 9] for a detailed review of the topic. It is known that any 2D metric can be written as $g = e^{\phi}\hat{g}$, where ϕ is a dynamical degree

of freedom and $\hat{g}$ is a fixed background metric which can always be taken to be flat Euclidean space, assuming a suitable topology. The Euclidean Einstein-Hilbert action reduces to the Liouville action for the scalar field ϕ given by

$$S_L = \int d^2z\sqrt{\hat{g}}(\hat{g}^{ab}\partial_a\phi\partial_b\phi + Q\hat{R}\phi + \Lambda e^{\gamma\phi}) + S_{CFT}\,. \tag{2.5}$$

Here $\hat{R}$ is the Ricci curvature associated with $\hat{g}$, Λ is the cosmological constant and S_{CFT} is the action of some conformal matter with central charge c. The requirement that there is no conformal anomaly then determines $Q = \frac{2}{\gamma} + \frac{\gamma}{2}$, where γ is given by

$$\gamma = \frac{1}{\sqrt{6}}(\sqrt{25-c} - \sqrt{1-c}). \tag{2.6}$$

For example, pure gravity ($c = 0$) corresponds to $\gamma = \sqrt{8/3}$ whereas the scaling limit of the Ising model ($c = \frac{1}{2}$) corresponds to $\gamma = \sqrt{3}$.

The Liouville path integral for pure gravity, taking the background metric $\hat{g}_{ab} = \delta_{ab}$, is written formally as

$$Z[\Lambda] = \int \mathcal{D}\phi\, e^{-\int d^2z\,\partial_a\phi\partial^a\phi + \Lambda e^{\gamma\phi}}\,. \tag{2.7}$$

We will return to the topic of Liouville gravity in Chapter 4 where we give it a stochastic flavour, and connect with rigorous probabilistic constructions [12, 13, 27, 28].

2.2 Hořava–Lifshitz Gravity

Another approach to continuum quantum gravity is given by Hořava–Lifshitz (HL) gravity [60, 61]. Its unique feature is the restriction of spacetime to have a global time foliation, hence the theory is only invariant under foliation preserving diffeomorphisms. Because of the preferred time direction, it is convenient to use the ADM decomposition of the metric, given by

$$ds^2 = -N(t,x)^2\,dt^2 + g_{ij}\left(dx^i + N^i dt\right)\left(dx^j + N^j dt\right), \tag{2.8}$$

where $N(t,x)$ is the *lapse function* and $N^i(t,x)$ is called the *shift vector*. In d spatial dimensions the HL action in ADM variables (N, N_i, g_{ij}) is

$$\begin{aligned} I &= \frac{1}{\kappa}\int dt\, d^dx\,\sqrt{g}\,N\Big(K_{ij}K^{ij} - \lambda K^2 + R - 2\Lambda\Big), \\ K_{ij} &= \frac{1}{2N}\Big(\partial_0 g_{ij} - \nabla_i N_j - \nabla_j N_i\Big), \end{aligned} \tag{2.9}$$

where K_{ij} is the extrinsic curvature built from the covariant derivative ∇_i of g_{ij}, with trace $K = g^{ij}K_{ij}$, and R is the intrinsic Ricci scalar of g_{ij}. The parameter λ sets the relative weight of K^2 and reproduces the GR kinetic term when $\lambda = 1$; Λ plays the role of a cosmological constant, and κ is a gravitational coupling constant [43].

We further restrict this action to the *projectable* case, meaning that we force the lapse function $N(t)$ to depend only on time. Furthermore, since this thesis concerns 2D quantum gravity, let us consider the action in $1+1$ dimensions. Let the spatial metric $g_{11} = g$ and $\varphi := \sqrt{g}$, then the extrinsic curvature reduces to

$$K \;=\; \frac{1}{N}\left(\frac{1}{\varphi}\partial_0\varphi - \frac{1}{\varphi^2}\partial_1 N_1 + \frac{N_1}{\varphi^3}\partial_1\varphi\right), \tag{2.10}$$

and the 1+1 action is

$$S_{HL} \;=\; \int dt\, dx\, N\,\varphi\Big[(1-\lambda)\,K^2 - 2\Lambda\Big] \;=:\; \int dt\, dx\, N\varphi\,\mathcal{L}. \tag{2.11}$$

Note that we set $\kappa = 1$, since it is dimensionless in $1+1$, and $R = 0$ in $d = 1$. The momentum conjugate to φ is

$$\pi_\varphi \;=\; \frac{\partial\mathcal{L}}{\partial(\partial_0\varphi)} \;=\; 2(1-\lambda)\,K, \qquad \{\varphi(x,t), \pi_\varphi(y,t)\} = \delta(x-y), \tag{2.12}$$

where $\{\cdot,\cdot\}$ is the Poisson bracket. The Hamiltonian can be written as $H = \int dx\,(N\,\mathcal{H} + N_1\mathcal{H}^1)$ with

$$\mathcal{H} \;=\; \varphi\left(\frac{\pi_\varphi^2}{4(1-\lambda)} + 2\Lambda\right), \qquad \mathcal{H}^1 \;=\; -\frac{\partial_1\pi_\varphi}{\varphi}. \tag{2.13}$$

The momentum constraint $\mathcal{H}^1 = 0$ implies $\pi_\varphi(t,x) = \pi_\varphi(t)$ (spatially constant), which further reduces the Hamiltonian to

$$H \;=\; N(t)\left[\frac{L(t)\,\pi_\varphi(t)^2}{4(1-\lambda)} + 2\Lambda\,L(t)\right], \tag{2.14}$$

where we have defined the spatial length

$$L(t) \;:=\; \int dx\,\varphi(x,t)\,. \tag{2.15}$$

The Hamiltonian constraint fixes π_φ to a constant on-shell; when $(\lambda-1)\Lambda > 0$,

$$\pi_\varphi^2 \;=\; 8(\lambda-1)\Lambda. \tag{2.16}$$

Eliminating π_φ in favour of L and passing to the Lagrangian form gives

$$S \;=\; \int dt \left[\frac{\dot{L}^{\,2}}{4N(t)\,L(t)} - \tilde{\Lambda}\,N(t)\,L(t)\right], \qquad \tilde{\Lambda} := \frac{\Lambda}{2(1-\lambda)}. \tag{2.17}$$

The momentum conjugate to L is

$$\Pi \;=\; \frac{\partial \mathcal{L}}{\partial \dot{L}} \;=\; \frac{\dot{L}}{2NL}, \tag{2.18}$$

so the Hamiltonian (with $\{L, \Pi\} = 1$) is

$$H \;=\; N(t)\Big(L\,\Pi^2 + \tilde{\Lambda}\,L\Big). \tag{2.19}$$

If we gauge fix (2.19) to the proper time

$$T(t) \;=\; \int_0^t ds\, N(s), \tag{2.20}$$

the lapse function drops out and the classical Hamiltonian becomes $H = L\Pi^2 + \tilde{\Lambda}L$. Performing path integral quantization in this gauge, we can define the transition amplitude from length L_1 to L_2 in proper time $T := T(1)$ by the Euclidean path integral

$$G(L_1, L_2; T) = \langle L_2|\, e^{-T\hat{H}}\, |L_1\rangle = \int \mathcal{D}L(t)\; \exp\!\left\{-\int dt \left[\frac{\dot{L}^{\,2}}{4L} + \tilde{\Lambda}\,L\right]\right\}. \tag{2.21}$$

We can also perform canonical quantisation by promoting Π to an operator $\hat{\Pi} = -i\frac{d}{dL}$, leading to the canonical commutation relation $[\hat{L}, \hat{\Pi}] = i$. Quantizing $L\Pi^2$ admits three natural orderings:

$$(L\Pi^2)_0 \;=\; -\frac{d}{dL}\,L\,\frac{d}{dL}\,; \qquad (L\Pi^2)_{-1} \;=\; -\,L\,\frac{d^2}{dL^2}\,; \qquad (L\Pi^2)_{+1} \;=\; -\,\frac{d^2}{dL^2}\,L\,, \tag{2.22}$$

which are Hermitian with respect to the measures dL, dL/L, and $L\,dL$, respectively. We will come back to the origin of these three quantum Hamiltonians in Section 2.3.3 $\hat{H}_i$, $i \in \{-1, 0, +1\}$ when we look at a discrete description of the 2D gravitational path integral: Causal Dynamical Triangulations (CDT). This model turns out to be a lattice regularisation of 2D projectable HL gravity [43, 62–64]. We can recover all three of these Hamiltonians from CDT by setting up the discrete problem in different ways. However, before we can discuss this further, we must introduce discrete geometry and the discrete gravitational path integral.

2.3 Discrete Geometry

It is natural, when tackling hard problems, to break them down into smaller, more manageable pieces. This is exactly the philosophy behind the discrete approach to quantum gravity. Spacetime is broken into discrete simplices (triangles in two dimensions) and the functional integral is replaced by a sum over discrete geometries. This approach not only provides a UV cut-off in the form of the lattice spacing but is naturally non-perturbative. The use of generalised triangulations to approximate the geometry of manifolds in general relativity goes back to the work of Regge [14] on coordinate-independent computational methods. Here we focus on the approximation of a two-dimensional manifold M and its geometry g by triangulations composed of piece-wise flat equilateral triangles each of the same area α. Heuristically, a given continuum configuration of fixed area A can be approximated progressively more accurately by increasing the number of triangles, N_α and decreasing the area α such that $N_\alpha \alpha = A$ is held fixed. Additionally, for fixed N_α, a given triangulation defines a set of graph distances $\{d(v_i, v_j)\}$ between vertices that approximate the set of geodesic distances on M; hence each distinct triangulation approximates a distinct metric g. A triangulation is naturally a graph, so we gather some relevant graph theory definitions here.

Definition 2.3.1 (Graphs and Maps)**.**

(i) A graph $G = (V, E)$ consists of a set of vertices V and a set of edges E that are unordered pairs of distinct vertices $\langle u, v\rangle$, such that no two vertices share more than one edge.

(ii) A map $M = (V, E, F)$ is an embedded graph on a two-dimensional topological manifold Σ_g of genus g, with no intersecting edges. The embedding produces a set of faces F such that the Euler characteristic $\chi(\Sigma_g) = |V| - |E| + |F| = 2 - 2g$.

(iii) A planar map is a graph embedded on a sphere (or plane).

(iv) We denote by $d(u, v)$ the graph distance between vertices u and v.

(v) A rooted map M is a map with one marked vertex called the root v_0.

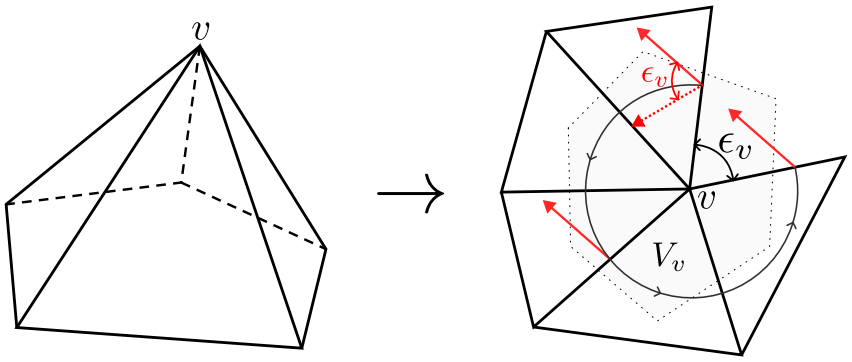

Figure 2.1: Positive curvature around v results in a positive deficit angle. The shaded region around the vertex is the dual volume V_v.

(vi) The dual map M^* is constructed from M by placing a vertex in every face, and joining the new vertices with edges such that each new edge intersects only one edge of M. Essentially, vertices are mapped to faces, edges to edges and faces to vertices.

(vii) A triangulation T is a rooted map where every face is a triangle.

(viii) A tree is planar map with no cycles.

Although we have distinguished between graphs and maps in this definition, we often refer to maps as graphs in the remaining text. It should however be clear where the graph is embedded and so should not cause confusion.

2.3.1 Geometry from triangulations

The way that curvature is captured in this discrete picture is quite intuitive in two dimensions. Let's first consider the Euclidean case – the curvature of a simplicial manifold is concentrated at the co–dimension 2 simplices, which in two dimensions are the vertices of the triangulation. To see this, consider the parallel transport of a vector around the point v in figure 2.1 which has the metric structure of a cone. As the vector moves around the piecewise flat triangles it maintains its original angle but when the spacetime is stitched back together, the final vector makes an angle to the original equal to the deficit angle $\epsilon_v = 2\pi - \sum_i \theta_i$, where θ_i are the angles of the triangles incident to v.

In both the Euclidean and Lorentzian case, the Gaussian curvature is given by

$$K_v = \frac{\epsilon_v}{V_v}, \tag{2.23}$$

where V_v is the dual volume around the vertex v. In two dimensions the Ricci curvature is simply $R = 2K$, hence we can write the discrete Ricci term as

$$\int_{\mathcal{M}} d^2x\sqrt{g}R \to \sum_{v\in T} K_v V_v = \sum_{v\in T} \epsilon_v. \tag{2.24}$$

Again, this is equal to $4\pi\chi(M)$, where the Euler characteristic is given by $\chi(M) = V - E + F$ in terms of the total number of vertices V, edges E and faces F of the graph representing the discrete manifold.

2.3.2 Discrete partition functions

Now we have discretised the two-dimensional surface, we must construct the discrete equivalent of the path integral. We first consider the pure gravitational system with no matter degrees of freedom on a disk M. Let $\mathcal{E}(M)$ be the set of unrestricted triangulations of M and define the partition function

$$W(\tilde{g}, z) = \sum_{T\in\mathcal{E}(M)} \frac{1}{C(T)} \tilde{g}^{\Delta(T)} z^{|\partial T|}\,. \tag{2.25}$$

Here we denote by $\Delta(T)$ the number of triangles in T, $|\partial T|$ the number of edges in the boundary of T and $C(T)$ the size of the automorphism group of the triangulation which ensures that we are only summing over the equivalence classes of metrics.

It is worth spending some time to get a better understanding of this object. The variables $\tilde{g}$ and z are formal variables that mark, respectively, the bulk number of triangles (discrete area) and the boundary length in the generating function. Writing

$$W(\tilde{g}, z) = \sum_{n\geq 0}\sum_{l\geq 0} N_{n,l}\, \tilde{g}^{\,n} z^{\,l}, \tag{2.26}$$

the coefficients $N_{n,l}$ count triangulations with $\Delta(T) = n$ and $|\partial T| = l$. From a purely combinatorial perspective therefore, $\tilde{g}$ and z serve as bookkeeping variables and enable the computation of moments by taking logarithmic derivatives, e.g.

$$\langle\Delta\rangle_{\tilde{g},z} = \tilde{g}\,\partial_{\tilde{g}} \log W, \qquad \langle|\partial T|\rangle_{\tilde{g},z} = z\,\partial_z \log W, \tag{2.27}$$

with higher-order moments defined analogously. Extracting coefficients

$$[\tilde{g}^{\,n} z^{\,l}]\, W = N_{n,l} \tag{2.28}$$

implements a canonical (fixed-area/perimeter) ensemble, while $(\tilde{g}, z)$ furnish the conjugate grand-canonical variables.

From an analytical point of view, these variables exhibit critical values and take on the physical meaning of bulk and boundary cosmological constants as we shall see. For a fixed z, the sum has a finite radius of convergence $\tilde{g}_c(z)$ determined by the exponential growth of $N_{n,l}$ in n. Similarly, for a fixed $\tilde{g}$, there exists a boundary critical value $z_c(\tilde{g})$. As a critical point is approached (e.g., $\tilde{g} \uparrow \tilde{g}_c$), the averages $\langle\Delta\rangle$ and higher moments diverge, and the series becomes dominated by large triangulations. The singular part of W near criticality displays universal, non-analytic behavior governed by model-dependent susceptibility exponents. This specific regime is precisely what gives rise to a continuum limit.

The combinatorics of $\mathcal{E}(M)$ was first elucidated by Tutte in [65–68]. Crucially, the number of triangulations $T \in \mathcal{E}(M)$ such that $\Delta(T) = n$ grows more slowly than $\tilde{g}_c^{-n}$ with $0 < \tilde{g}_c < 1$. It follows that the sum in (2.25) converges and W exists for $\tilde{g} < \tilde{g}_c$.

It was proposed in [16, 17] that the sum over triangulations in (2.25), taken in the limit $\tilde{g} \uparrow \tilde{g}_c$ where arbitrarily large triangulations dominate, can be identified with the Euclidean functional integral over the metric. Setting $\tilde{g} \to \tilde{g}_c e^{-\Lambda\alpha}$, identifying the area

$$\alpha\Delta(T) \to \int_{\mathcal{M}} d^2x\sqrt{g}\,, \tag{2.29}$$

and the triangulation sum

$$\sum_{T\in\mathcal{E}(M)} \frac{1}{C(T)} \tilde{g}_c^{\Delta(T)}(.) \to \int \mathcal{D}[g](.)\,, \tag{2.30}$$

we see that $W[\tilde{g}, 1]$ formally reproduces $Z[\Lambda]$ (2.3) (the curvature term can be ignored as it is topological). There is now a great deal of evidence that this identification is correct and that the Euclidean functional integral over the metric can indeed be defined as a sum over triangulations. Much of this evidence comes through the connection between $\mathcal{E}(M)$ and matrix models which was established in [69–72]; for a modern review see [21].

The ensemble $\mathcal{E}(M)$ of random planar maps has been studied in great detail; one particularly interesting result is that the Hausdorff dimension of very large planar maps is $d_H = 4$ almost surely [23]. Such a map must have very non-trivial fractal structure since it is assembled piecewise from two-dimensional triangles (or, more generally, polygons).

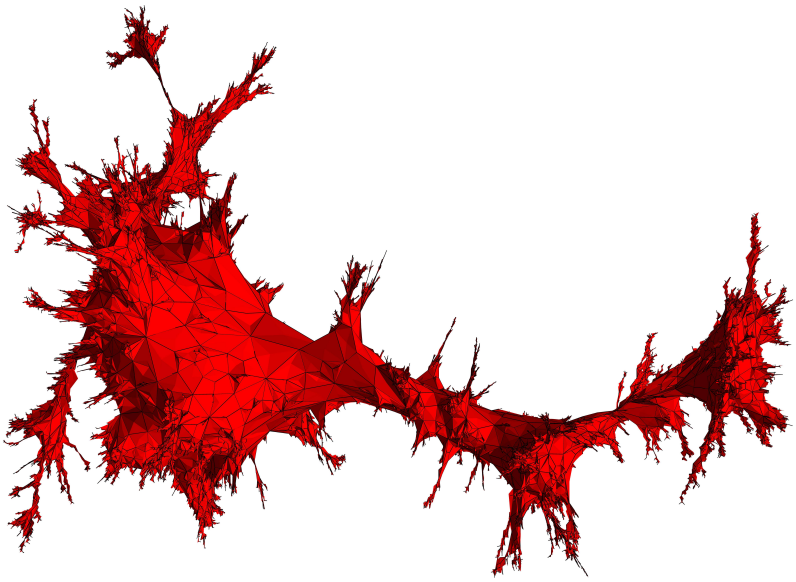

Figure 2.2: An instance of a large planar map with 30,000 vertices generated by Jérémie Bettinelli [73].

Figure 2.2 shows a striking example of a planar map with a large number of vertices; it is a discrete approximation of the Brownian map [24]. We will return to the characterisation of such maps in Section 4.3.

2.3.3 Discrete Lorentzian Geometry

Euclidean triangulations provide a definition of the Euclidean path integral but it is not immediately clear how results in this theory are related to physical quantities in the Lorentzian theory (2.1). This led Ambjørn and Loll [32] to introduce the causal triangulation (CT).

Definition 2.3.2. *A causal triangulation (CT) C of the disk M is a triangulation where all vertices at a fixed graph distance t from the root form a cycle $S_t(C)$. Furthermore, there is no face for which all three of its vertices are at the same distance from the root. Its height $h(C)$ is the maximum graph distance of the vertices from the root*

$$h(C) = \max_{v \in C} \{d(v, v_0)\}.$$

Let's understand this definition a bit better. A CT only triangulates manifolds that are globally hyperbolic, i.e. they have a time slicing. Time is discretised into integer steps $t = 0, 1, 2, \ldots$, and a slice at fixed t is a one-dimensional spatial loop made of

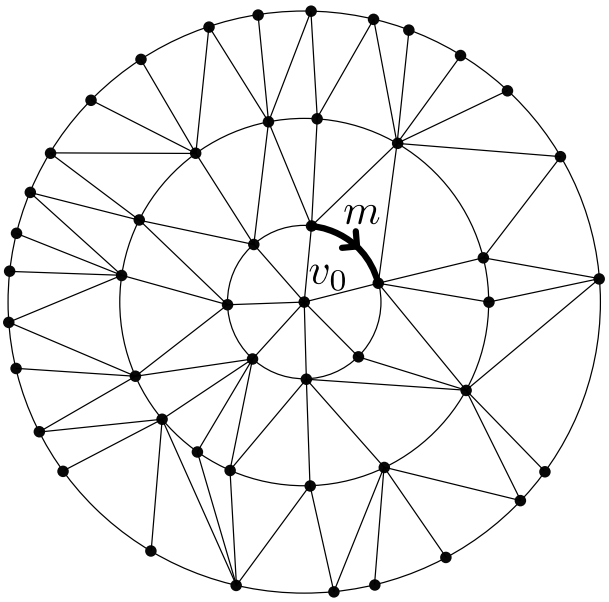

Figure 2.3: Example of a causal triangulation (CT) of the disk M. The marked edge m is shown on the first layer by the solid arrow.

l space-like edges (see Figure 2.3). Global hyperbolicity is enforced by requiring that each space-like slice has a well-defined proper-time ordering, and by forbidding spatial topology changes. Consequently the edges in a CT are either time-like or space-like which allows for a well-defined Wick rotation between Euclidean and Lorentzian signatures. The sum over geometries becomes a sum over all inequivalent gluings of triangles consistent with these causal constraints [32, 41, 74].

The model is most often solved in Euclidean signature but a consistent way to define Lorentzian triangles and angles that satisfy the usual Euclidean additivity conditions exists and was described in [75]. Every triangle has 2 time-like edges and 1 space-like edge (see Figure 2.3). Without loss of generality, we take the time-like edges with squared length $l_t^2 = -a^2$ and space-like edges $l_s^2 = a^2$. Then the angle between a space-like and time-like edge is $\theta_{st} = \frac{\pi}{2} + i \log\left(\frac{1+\sqrt{5}}{2}\right)$ and between a pair of time-like edges is $\theta_{tt} = -2i \log\left(\frac{1+\sqrt{5}}{2}\right)$. Flat Minkowski space can be triangulated with 6 Lorentzian triangles at every point. We can show this by calculating the deficit angle formed by these triangles. Every 6-valent vertex has 2 space-like edges and 4 time-like edges, or equally, four space-time angles and two time-time angles. Hence the deficit angle is $\epsilon_v = 2\pi - (4\theta_{st} + 2\theta_{tt}) = 0$ as expected.

It is clear from the definition that each vertex of C at height $t > 0$ has 2 spatial

neighbours, several future neighbours σ_v^f and a number of past neighbours σ_v^p such that the total number of neighbours is $\sigma_v = 2 + \sigma_v^f + \sigma_v^p$. The definition is easily extended to annular topology by marking a vertex at height $t = 1$ then deleting the root and the edges attached to it.

Letting $\mathcal{C}(M)$ be the set of causal triangulations of the annulus M with a marked edge on the entrance loop, we define the Causal Dynamical Triangulation (CDT) model through the partition function

$$G(x, y, \tilde{g}; t) = \sum_{C \in \mathcal{C}(M):\, h(C)=t} |S_1(C)|\, \tilde{g}^{\Delta(C)} x^{|S_1(C)|}\, y^{|S_t(C)|}\,. \tag{2.31}$$

Note that, in contrast to the Euclidean triangulation case, we now have a natural 'time' t. From the gravitational point of view, G is essentially the discretised path integral for the Euclidean amplitude that a universe evolves from an initial boundary of length $l_1 := |S_1(C)|$ to a final boundary of length $l_2 := |S_t(C)|$ in time t. Another way to look at G is as a combinatorial generating function for the number of ways to triangulate a surface of t slices from an initial boundary length of l_1 vertices to a final boundary length of l_2 vertices. In this way, we can consider the generating function $G(x, y, \tilde{g}; t)$ as a discrete Laplace transform of $G(l_1, l_2, \tilde{g}; t)$ which allows us to move between two representations:

$$G(x, y, \tilde{g}; t) = \sum_{l_1, l_2} x^{l_1} y^{l_2} G(l_1, l_2, \tilde{g}; t). \tag{2.32}$$

The t-step propagator satisfies the convolution (transfer-matrix) relation:

$$G(l_1, l_2, \tilde{g}; t) = \sum_{l=1}^{\infty} G(l_1, l, \tilde{g}; 1)\; G(l, l_2, \tilde{g}; t-1), \tag{2.33}$$

or in terms of the boundary variables x, y

$$G(x, y, \tilde{g}; t) = \oint \frac{dz}{2\pi i\, z}\; G(x, z^{-1}, \tilde{g}; 1)\, G(z, y, \tilde{g}; t-1), \tag{2.34}$$

ensuring that $G(\cdot, \cdot, \tilde{g}; 1)$ defines a positive, symmetric transfer matrix and thus a self-adjoint Hamiltonian in the continuum limit. Note that G denotes the 'marked' propagator which has special marked edge on the loop of length l_1 to make the combinatorial problem easier. To recover the unmarked propagator we simply divide by the entrance loop

l_1 (c.f. [32]). It is clear that if we know the one-step propagator then we can iterate (2.33) t times to find the t-step propagator.

In what follows we work with the disk for simplicity and consider a marked edge on $S_k(C)$, so that we can treat the combinatorics problem as if it were a linear chain of triangles. Furthermore, this forces the first triangle from the marked edge to be pointing 'up' (see Figure 2.3). Hence, the number of ways to triangulate a layer between $S_k(C)$ with l_k vertices and $S_{k+1}(C)$ with l_{k+1} vertices amounts to choosing which of the remaining $l_k - 1$ triangles from a total of $l_k + l_{k+1} - 1$ point up. The one-step propagator is therefore

$$G(l_k, l_{k+1}, \tilde{g}; 1) = \binom{l_k + l_{k+1} - 1}{l_k - 1} \tilde{g}^{l_k + l_{k+1}}. \tag{2.35}$$

or in conjugate variables

$$G(x, y, \tilde{g}; 1) = \sum_{l_k, l_{k+1}=1}^{\infty} \binom{l_k + l_{k+1} - 1}{l_k - 1} \tilde{g}^{l_k + l_{k+1}} x^{l_k} y^{l_{k+1}} = \frac{\tilde{g}^2 xy}{(1 - \tilde{g}x)(1 - \tilde{g}x - \tilde{g}y)}. \tag{2.36}$$

Now consider the grand canonical partition function for a disk of height t, denoted $Z(\tilde{g}; t)$. This is defined in terms of the t-step propagator as

$$Z(\tilde{g}; t) = \sum_{l_t=1}^{\infty} G(1, l_t, \tilde{g}; t)\, \tilde{g}^{l_t} \tag{2.37}$$

and using (2.33) to expand in terms of the one-step propagator we find

$$Z(\tilde{g}; t) = \tilde{g} \sum_{l_1=1}^{\infty} \sum_{l_2=1}^{\infty} \cdots \sum_{l_t=1}^{\infty} \left(\prod_{k=1}^{t-1} \binom{l_k + l_{k+1} - 1}{l_k - 1} \right) \tilde{g}^{2(l_1 + l_2 + \cdots + l_t)}. \tag{2.38}$$

Remarkably, one can make progress by using the binomial expansion of $(1 - x)^{-n}$:

$$(1 - x)^{-n} = \sum_{k=0}^{\infty} \binom{n + k - 1}{k} x^k. \tag{2.39}$$

Starting with the sum over l_1 we get

$$Z(\tilde{g}; t) = \tilde{g} \left(\frac{\tilde{g}^2}{1 - \tilde{g}^2} \right) \sum_{l_2=1}^{\infty} \cdots \sum_{l_t=1}^{\infty} \prod_{k=2}^{t-1} \frac{\tilde{g}^{2l_2}}{(1 - \tilde{g}^2)^{l_2}} \binom{l_k + l_{k+1} - 1}{l_k - 1} \tilde{g}^{2(l_3 + l_4 + \cdots + l_t)}. \tag{2.40}$$

Let us define

$$X_{k+1} := \frac{\tilde{g}^2}{1 - X_k}, \quad X_1 := \tilde{g}^2, \tag{2.41}$$

and continue summing over $l_2, l_3, \ldots, l_t$ to find

$$Z(\tilde{g};t) = \tilde{g}\left(\frac{X_1}{1-X_1}\right)\left(\frac{X_2}{1-X_2}\right)\sum_{l_3=1}^{\infty}\cdots\sum_{l_t=1}^{\infty}\prod_{k=3}^{t-1}\binom{l_k+l_{k+1}-1}{l_k-1}X_3^{l_3}\tilde{g}^{2(l_4+l_5+\cdots+l_t)}$$
$$= \tilde{g}\prod_{k=1}^{t}\frac{X_k}{1-X_k}. \tag{2.42}$$

It remains to solve the recursion (2.41) for X_k.

Lemma 2.3.1. *Let $(X_k)_{k\geq 1}$ be defined by*

$$X_{k+1} = \frac{\tilde{g}^2}{1-X_k}, \qquad X_1 = \tilde{g}^2, \tag{2.43}$$

for a fixed parameter $\tilde{g} \in \mathbb{C}$. Then, with

$$\lambda_\pm = \frac{1 \pm \sqrt{1-4\tilde{g}^2}}{2},$$

one has, for all $k \geq 1$,

$$X_k = 1 - \frac{\lambda_+^{k+2} - \lambda_-^{k+2}}{\lambda_+^{k+1} - \lambda_-^{k+1}} = \tilde{g}^2\,\frac{\lambda_+^k - \lambda_-^k}{\lambda_+^{k+1} - \lambda_-^{k+1}}. \tag{2.44}$$

In the degenerate case $1-4\tilde{g}^2 = 0$ (i.e. $\lambda_+ = \lambda_- = \frac{1}{2}$),

$$X_k = \frac{1}{2}\frac{k}{k+1} \qquad (k \geq 1). \tag{2.45}$$

Moreover, if $|\tilde{g}| < \frac{1}{2}$, then $X_k \to \lambda_- = \dfrac{1-\sqrt{1-4\tilde{g}^2}}{2}$ as $k \to \infty$.

Proof. Set

$$X_k = 1 - \frac{Y_{k+1}}{Y_k}. \tag{2.46}$$

Then (2.43) gives

$$1 - \frac{Y_{k+2}}{Y_{k+1}} = \frac{\tilde{g}^2}{1-X_k} = \frac{\tilde{g}^2}{\frac{Y_{k+1}}{Y_k}} = \tilde{g}^2\,\frac{Y_k}{Y_{k+1}},$$

which is equivalent to the linear recurrence

$$Y_{k+2} - Y_{k+1} + \tilde{g}^2\,Y_k = 0. \tag{2.47}$$

From $X_1 = \tilde{g}^2$ and (2.46) we may take $Y_1 = 1$, $Y_2 = 1-\tilde{g}^2$ (the normalisation $Y_1 = 1$ is harmless since (2.46) is scale-invariant). The characteristic equation of (2.47) is $r^2 - r + \tilde{g}^2 = 0$, with roots $\lambda_\pm$ above. Solving,

$$Y_k = \frac{\lambda_+^{k+1} - \lambda_-^{k+1}}{\lambda_+ - \lambda_-} \qquad (k \geq 1).$$

Substituting into (2.46) yields the first expression in (2.44); using $\lambda_+ + \lambda_- = 1$ and $\lambda_+\lambda_- = \tilde{g}^2$ gives the equivalent form. When $\lambda_+ = \lambda_- = \frac{1}{2}$, (2.47) has solution $Y_k = \dfrac{k+1}{2^k}$, which inserted into (2.46) gives (2.45). Finally, if $|\tilde{g}| < \frac{1}{2}$, then $|\lambda_+| < 1$ and $|\lambda_-| < 1$ with $|\lambda_-| < |\tilde{g}| < |\lambda_+|$; the ratio in (2.44) converges to λ_-, the attracting fixed point of $x \mapsto \dfrac{\tilde{g}^2}{1-x}$. □

Lemma 2.3.1 shows that there is a critical value $\tilde{g}_c = \frac{1}{2}$ such that the sum in (2.31) converges for $\tilde{g} < \tilde{g}_c$ for all t; in the limit $\tilde{g} \uparrow \tilde{g}_c$ arbitrarily large triangulations dominate as the partition function becomes non-analytic and we recover the path integral for the point-to-boundary amplitude in two-dimensional projectable Hořava-Lifshitz gravity [43] with $\lambda \neq 0$.

Although the sum to determine $Z(\tilde{g}; t)$ can be evaluated by elementary means for finite t [32], this gives us little information about the nature of the CTs that contribute at criticality. It was observed in [76] that $\mathcal{C}(M)$ can also be studied by exploiting the existence of a bijection $\beta : \mathcal{C} \to \mathcal{T}$ with the set of planar rooted trees, see [37] for a recent review.

The tree bijection

Definition 2.3.3. *The bijective map $\beta(C)$ is defined by:*

1. *Mark an edge coming out of v_0 and add a root vertex r to C connected by a single edge to v_0 placed in the face to the right of the marked edge as seen from v_0.*

2. *Remove all edges in the cycles $S_t(C), \forall t > 0$. i.e. the space-like edges.*

3. *For every $v \in S_t(C)$ where $1 \leq t < h(C)$ remove the rightmost edge of the σ_v^f edges as seen from v.*

The resulting graph T is a tree with a new root vertex r and every vertex from C as shown in Figure 2.4. It is straightforward to show that the inverse map β^{-1} exists.

The partition functions for annulus and disk functions can be calculated using the tree bijection. Let's first define the auxiliary object $w_{t+1}(g, z)$ to be the partition function

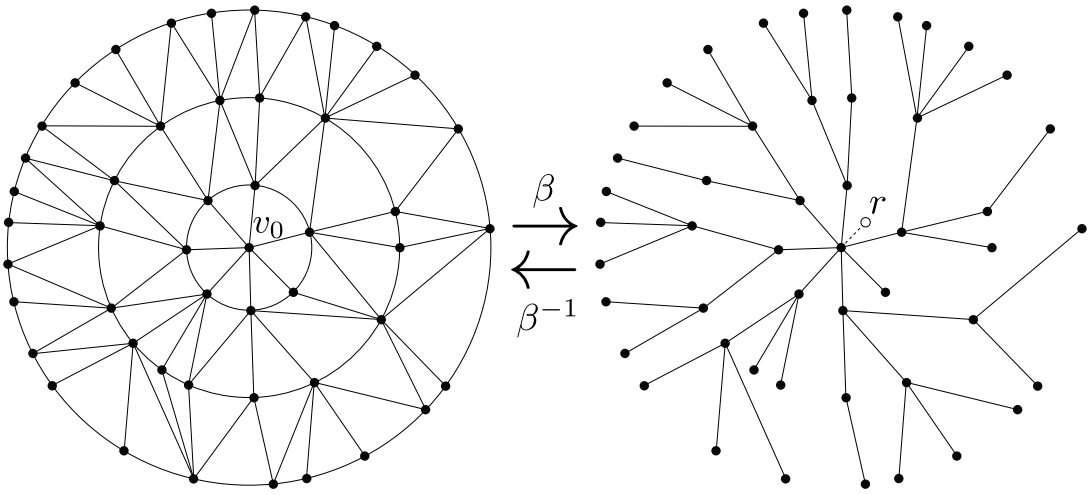

Figure 2.4: A causal triangulation of height 3, and the action of the map β to its associated tree.

for trees of height $\leq t+1$. We assign each vertex $v \in T \setminus r$ a weight $\tilde{g}^{2(\sigma_v-1)}$ and every boundary vertex at height $t+1$ a weight $z/\tilde{g}$

$$w_{t+1}(g,z) = \sum_{t' \leq t+1} \sum_{T \in \mathcal{T}^{(t')}} (z/\tilde{g})^{|S_{t+1}(T)|} \prod_{v \in V(T) \setminus r} \tilde{g}^{2(\sigma_v-1)}. \tag{2.48}$$

Note that the only z contributions come from those trees of height $t+1$. Using the tree bijection, we return to a CT of disk topology, $C = \beta^{-1}(T)$. One can see that the number of triangles in a CT is given by

$$\Delta(C) = 2 \sum_{k=1}^{h(C)} |S_k(C)|. \tag{2.49}$$

Given that each vertex v in the tree at height k contributes $\sigma_v - 1$ vertices to the layer at height $k+1$, we can rewrite $w_{t+1}(g,z)$ as

$$w_{t+1}(g,z) = \sum_{t' \leq t} \sum_{C \in \mathcal{C}^{(t')}} (z/\tilde{g})^{|S_t(C)|} \tilde{g}^{\Delta(C)}. \tag{2.50}$$

Since z contributions only come from those trees of height $t+1$, or equally CTs of height t, we can differentiate with respect to z to suppress CTs of height $< t$. Hence the CT disk function is given by

$$G(z,\tilde{g};t) = z\frac{\partial}{\partial z} w_{t+1}(g,z). \tag{2.51}$$

The reason for introducing the auxiliary object is that it's much easier to calculate from a combinatorial perspective. The rooted trees of height $t+1$ can be decomposed into a sum of trees of height t attached to the vertex adjacent to the root vertex r. Every tree of height t is connected by an edge to the vertex at height 1, contributing a factor of g^2. Therefore, $w_{t+1}(g,z)$ satisfies the recursion

$$w_{t+1}(g,z) = \sum_{k=0}^{\infty} (g^2 w_t(g,z))^k = \frac{1}{1-g^2 w_t(g,z)}, \quad w_1(g,z) = z g^{-1}, \tag{2.52}$$

It is convenient to set $X_h := g^2 w_h$; then

$$X_{h+1} = \frac{g^2}{1-X_h}, \qquad X_1 = g\,z, \tag{2.53}$$

which is the same Möbius recursion as (2.41), only with a different initial condition (reflecting the boundary fugacity z).

By choosing the parameterisation $g^{-1} = 2\cosh\theta$, the solution can be given in the following closed form expression [37]

$$w_{t+1}(g,z) = 2\cosh\theta\, \frac{\sinh(t\theta) - z\,\sinh((t-1)\theta)}{\sinh((t+1)\theta) - z\,\sinh(t\theta)}, \tag{2.54}$$

and hence the disk function by

$$G(z,g;t) = 2\cosh\theta\, \frac{z\,\sinh^2\theta}{\Big(\sinh((t+1)\theta) - z\,\sinh(t\theta)\Big)^2}. \tag{2.55}$$

To couple two boundaries with fugacities (x,y) we repeat the decomposition leading to (2.52), but with a change at the *last* step of the iteration: every offspring of the vertex adjacent to the root carries weight $g^2(x/g) = xg$ instead of g^2, while the far boundary is encoded by y through $w_t(g,y)$. Therefore

$$\begin{aligned} G(x,y,g;t) &= y\,\partial_y \left[\frac{1}{1-xg\,w_t(g,y)}\right] \\ &= \frac{x\,y\,\sinh^2\theta}{\Big(\sinh(t\theta) - (x+y)\sinh((t-1)\theta) + xy\,\sinh((t-2)\theta)\Big)^2}. \end{aligned} \tag{2.56}$$

Clearly, the radius of convergence in $\tilde{g}$ is unchanged from the disk case shown in Lemma 2.3.1. The full region of convergence is given by $\tilde{g} < 1/2, x < 1, y < 1$ and is explicitly verified in [39].

Galton-Watson Trees

It has been shown that the ensemble (2.50) at criticality, i.e. $\tilde{g} = \frac{1}{2}$, is equivalent to another process, known as a critical Galton-Watson (GW) process [37]. A GW process is a branching process specified by a set of probabilities $p_n, n = 0, 1, ...$, called the *offspring probabilities*, having unit mean i.e., $\sum_{n=0}^{\infty} np_n = 1$ [77, 78]. The process can be viewed as a tree in which p_n is the probability of a single vertex having n offspring. Recalling that by definition, the root vertex has a single offspring with probability one, the probability distribution on finite trees $T \in \mathcal{T}$ is then given by

$$\pi(T) = \prod_{i \in T \setminus r} p_{\sigma_i - 1}. \tag{2.57}$$

Choosing $p_n = 2^{-n-1}$ we see that $\pi(T)$ reproduces the weights in $G_{\text{disk}}(\frac{1}{2}, 1; t)$; they define the generic random tree ensemble [39]. It is convenient to introduce the generating function for offspring probabilities

$$f(s) = \sum_{n=0}^{\infty} p_n s^n. \tag{2.58}$$

Then $f(1) = 1$, $f'(1) = 1$, and for the generic random tree $f(s) = (2 - s)^{-1}$.

The definition 2.3.2 of CTs is easily extended to triangulations that have infinite height $h(C) = \infty$ and no boundary; these form the set $\mathcal{C}_\infty$ and cover the plane. Applying the bijection β (2.3.3) to $C \in \mathcal{C}_\infty$ then yields an infinite tree $T \in \mathcal{T}_\infty$. It was shown in [37] that one can extend the probability distribution $\pi(T)$ on finite trees to a measure $\nu(T)$ on $T \in \mathcal{T}_\infty$. Provided only that $f''(1) < \infty$, $\nu(T)$ is concentrated on single spine trees [37, 79]. The spine is a sequence of vertices $r, s_1, s_2, ...$ starting at the root and going off to infinity with no backtracking. Attached to each spine vertex, with probability p'_n generated by $sf'(s)$, is a set of n finite trees with vertices distributed according to $f(s)$. The ensemble defined by the set of triangulations $\mathcal{C}_\infty$ and the probability measure on them $\mu(C) = \nu(\beta^{-1}(C))$ is called the Uniform Infinite Causal Triangulation (UICT).

The Continuum Limit

As discussed, at the critical point $\tilde{g} = \tilde{g}_c = \frac{1}{2}$ the partition function $Z(\tilde{g}; t)$ diverges and the ensemble of triangulations is dominated by large triangulations. This is where the

continuum limit is defined. In Chapter 4 we find the continuum limit of the partition functions via an alternative approach. We make use of the tree bijection to construct a limiting stochastic differential equation for the length of the spatial slices at height t and the Feynman–Kac formula to write down an expression for the partition functions. This involves heavy use of stochastic calculus which we will prepare the reader for in Chapter 3. Therefore, we present a more traditional approach to the continuum limit here along the lines of that in [37] and done originally in [32].

Expanding (2.55) about $\theta = 0$ at fixed t and $y < 1$ gives

$$G(z, g; t) = \frac{2z}{\Big(t(1-z)+1\Big)^2} + O(\theta^2). \tag{2.59}$$

As $t \to \infty$ the disk function approaches zero which reflects the fact that even at the critical point very tall causal triangulations are unlikely. However, if we also scale the discrete time variable such that $t(1-z) = \text{const.}$ then we can get large macroscopic universes.

The physically non-trivial limit is obtained by setting

$$\tilde{g} = \tfrac{1}{2}\,\operatorname{sech}\theta, \qquad z = 1 - Z\theta\,\Lambda^{-1/2}, \qquad t = T\theta^{-1}\Lambda^{1/2},$$

and taking $\theta \to 0$. The scaling amplitudes are then defined to be

$$\begin{aligned} G_\Lambda(Z;T) &:= \lim_{\theta\to 0} G\left(\tfrac{1}{2}\,\operatorname{sech}\theta,\ 1 - Z\theta\Lambda^{-1/2},\ T\theta^{-1}\Lambda^{1/2}\right) \\ &= \frac{2\Lambda}{\Big(\sqrt{\Lambda}\cosh\Big(\sqrt{\Lambda}T\Big) + Z\,\sinh\Big(\sqrt{\Lambda}T\Big)\Big)^2}. \end{aligned} \tag{2.60}$$

and

$$\begin{aligned} G_\Lambda(X,Y;T) &:= \lim_{\theta\to 0}\ \theta^2\, G\left(\tfrac{1}{2}\,\operatorname{sech}\theta,\ 1 - X\theta\Lambda^{-1/2},\ 1 - Y\theta\Lambda^{-1/2},\ T\theta^{-1}\Lambda^{1/2}\right) \\ &= \frac{\Lambda^2}{\Big((\Lambda + XY)\sinh\Big(\sqrt{\Lambda}T\Big) + \sqrt{\Lambda}(X+Y)\cosh\Big(\sqrt{\Lambda}T\Big)\Big)^2}. \end{aligned} \tag{2.61}$$

The pre-factor θ^2 is needed here because the marked boundary relative to the disk causes the partition function to diverge. This is nothing but a wavefunction renormalisation which in general is expected when taking the continuum limit.

These functions represent the amplitude for a continuous two–dimensional universe to evolve from an initial boundary to a final boundary with cosmological constants

X, Y respectively in a time T. T is chosen to have length dimension $[T] = 1$, so that $[\Lambda] = -2$, and $[X] = [Y] = -1$, giving continuum definitions with sensible units. A formula that we will refer back to often is the two–boundary amplitude in the conjugate length variables L_1, L_2 which is obtained from (2.61) by inverse laplace transforming $X \to L_1, Y \to L_2$ and reads

$$G_\Lambda(L_1, L_2; T) = \frac{L_1 L_2}{\sqrt{L_1 L_2}} \frac{\sqrt{\Lambda}}{\sinh\left(\sqrt{\Lambda} T\right)} e^{-\sqrt{\Lambda}(L_1+L_2)\coth\left(\sqrt{\Lambda}T\right)} I_1\left(\frac{2\sqrt{\Lambda L_1 L_2}}{\sinh\left(\sqrt{\Lambda}T\right)}\right), \quad (2.62)$$

where I_1 is the modified Bessel function of the first kind. Note that this is the doubly–marked amplitude, to unmark the initial boundary / final boundary we divide by L_1 / L_2 respectively.

The CDT Hamiltonians

The transfer-matrix relation (2.33) (or (2.34) in Laplace variables) implies that the t-step propagator is generated by repeated composition of the one-step kernel. Taking the one-step propagator (2.36) and inserting it into (2.34) gives the iterative relation

$$G(x, y, \tilde{g}; t) = \frac{\tilde{g}^2 x}{1 - \tilde{g}x} G\left(\frac{\tilde{g}}{1 - \tilde{g}x}, y, \tilde{g}; t - 1\right) \quad (2.63)$$

Taking the continuum scaling of the previous section directly at the level of (2.63) yields a first-order evolution equation in Laplace space:

$$\partial_T G_\Lambda(X, Y; T) \;=\; -\partial_X\Big[(X^2 - \Lambda)\, G_\Lambda(X, Y; T)\Big], \qquad G_\Lambda(X, Y; 0) = \frac{\Lambda}{(X + Y)^2}. \quad (2.64)$$

One can verify that (2.61) is indeed a solution of (2.64) with the given initial condition. Equivalently,

$$\partial_T G_\Lambda(X, Y; T) \;=\; -\hat{H}_X\, G_\Lambda(X, Y; T), \qquad \hat{H}_X := (X^2 - \Lambda)\, \partial_X + 2X. \quad (2.65)$$

Inverse Laplace transforming $X \mapsto L_1$ turns (2.64) into a heat-type equation with a local, second-order generator acting on the initial boundary length:

$$\partial_T G_\Lambda(L_1, L_2; T) \;=\; -\,\hat{H}_{L_1}\, G_\Lambda(L_1, L_2; T), \qquad \hat{H}_{L_1} = -L_1 \partial_{L_1}^2 + \Lambda L_1, \quad (2.66)$$

with $L_1 > 0$ and initial condition for the doubly marked kernel

$$G_\Lambda(L_1, L_2; 0) \;=\; \Lambda L_1\, \delta(L_1 - L_2). \quad (2.67)$$

The operator $\hat{H}_L$ is self-adjoint on $L^2(\mathbb{R}_+, \frac{dL}{L})$, in accordance with the symmetry of the discrete transfer matrix. The Hamiltonian for the unmarked propagators is given by

$$\hat{H}_L^{(u)} = -\partial_L^2(L\,\cdot) + \Lambda L = -L\partial_L^2 - 2\partial_L + \Lambda L, \tag{2.68}$$

and is self-adjoint on $L^2(\mathbb{R}_+, L\,dL)$. As we saw in Section 2.2, if one starts by quantizing 2D projectable Hořava–Lifshitz gravity, one obtains three Hamiltonians depending on the choice of operator ordering. These are summarised in the following table

Hamiltonian	Self-adjoint on	SDE
$\hat{H}_L^{(m)} = -L\,\partial_L^2 + \Lambda L$	$L^2(\mathbb{R}_+, dL/L)$	$dL_t = \sqrt{2L_t}\,dW_t$
$\hat{H}_L^{(u)} = -\partial_L^2(L\,\cdot) + \Lambda L$	$L^2(\mathbb{R}_+, L\,dL)$	$dL_t = 2dt + \sqrt{2L_t}\,dW_t$
$\hat{H}_L^{(\text{open})} = -\partial_L(L\,\partial_L) + \Lambda L$	$L^2(\mathbb{R}_+, dL)$	$dL_t = dt + \sqrt{2L_t}\,dW_t$

Table 2.1: Three Hamiltonians from quantizing 2D projectable Hořava–Lifshitz gravity and their corresponding stochastic differential equations (SDEs).

The first two are the Hamiltonians we have already encountered, while the third one corresponds to the generator for a universe with open boundaries [43, 80] (in contrast to our cylinder universes encountered thus far) and is self-adjoint in the flat measure dL. Considering these Hamiltonians as generators of diffusion processes leads to the stochastic differential equations (SDEs) in Table 2.1. The process W_t is the Wiener process (or standard Brownian motion; see Chapter 3) which will appear again in Chapters 4 and 6 and we defer further discussion until then.

Physical observables

In 2D gravity with a single (possibly marked) geodesic boundary the relevant observables are amplitudes for creating a spatial loop of length L "from nothing", for evolving a loop of length L_1 into one of length L_2 during a proper time T, and correlation functions of loop length functionals. We briefly collect the standard results, emphasising the role of the two operator orderings already encountered.

Hartle–Hawking (disk) wavefunctions. The Hartle–Hawking ("no–boundary") wavefunction is obtained by integrating the propagator over all positive proper time with one of the boundary lengths shrunk to zero. Operationally one fixes the operator ordering (hence the functional measure), then defines

$$W_\Lambda^{(\cdot)}(L) := \int_0^\infty dT\; G_\Lambda^{(\cdot)}(L_0, L; T)\Big|_{L_0\to 0}, \tag{2.69}$$

whenever the integral converges. In Laplace variables this is equivalent to extracting the stationary (T–independent) solution of the evolution equation. For the marked sector one finds the particularly simple result

$$W_\Lambda^{(m)}(X) = \frac{1}{X+\sqrt{\Lambda}}, \qquad \Longleftrightarrow \qquad W_\Lambda^{(m)}(L) = e^{-\sqrt{\Lambda}L}. \tag{2.70}$$

Unmarking the boundary amounts to dividing by L in length space; correspondingly

$$W_\Lambda^{(u)}(L) = \frac{e^{-\sqrt{\Lambda}L}}{L}\,. \tag{2.71}$$

Wheeler–DeWitt equations. The above wavefunctions are annihilated by the Hamiltonian constraint (Wheeler–DeWitt equation) of the theory.

$$\hat{H}^{(m)} W_\Lambda^{(m)}(L) = 0, \qquad \hat{H}^{(u)} W_\Lambda^{(u)}(L) = 0. \tag{2.72}$$

which can be verified by direct substitution. Note that these wavefunctions are non-normalisable but there is no requirement that the wavefunction of the universe should be normalisable.

Expectation values and stochastic interpretation. Using the diffusion picture (Table 2.1) the evolution of loop length observables follows directly from Itô calculus (see Chapter 3). For the unmarked process $dL_T = 2\,dT + \sqrt{2L_T}\,dW_T$ one has

$$\frac{d}{dT}\langle L_T\rangle = 2, \qquad \Rightarrow \qquad \langle L_T\rangle = L_0 + 2T. \tag{2.73}$$

These relations give a direct probabilistic derivation of the Hausdorff dimension $d_H = 2$ by reading off the exponent of T in the average spatial volume $\langle V(T)\rangle = \int_0^T \langle L(T)\rangle\; dT \sim T^2$. In contrast, the Euclidean $d_H = 4$ and this difference will be revisited when we consider the Ising model coupled to CDT in Chapter 4.

2.4 Matrix Models

So far we have seen how discrete surfaces can be used to define a non-perturbative theory of 2D quantum gravity. The challenge of computing the gravitational path integral was reduced to a combinatorial problem of counting planar maps. Another approach to this combinatorial problem is provided by matrix models. The foundational work started with 't Hooft in 1974 [81]. They have since been used extensively to study many aspects of two-dimensional quantum gravity with some notable recent examples [82–84]. See [85] for an older review and [21] for a more recent one.

2.4.1 Why matrices?

The basic idea is that the Feynman diagram expansion of certain matrix integrals can be interpreted as a sum over discretised surfaces. Most readers will be used to the idea that the Feynman diagram expansion of a quantum field theory boils down to the enumeration of graphs. Which begs the question: why do we need matrices? Aren't the graphs we get from scalar field theory good enough to represent the graphs representing a discretised surface? The short answer is no. To understand the longer answer, we first need to talk about the connection between Gaussian integrals and graphs and about the distinction between a *graph* and a *map*.

2.4.2 Gaussian integrals and graphs

Consider the generating function for the set of graphs $\mathcal{G}^{(4)}$ with 4–valent vertices

$$Z = \sum_{G \in \mathcal{G}^{(4)}} \frac{1}{|\Gamma(G)|} g^{|G|}, \tag{2.74}$$

where $|G|$ denotes the number of vertices in G and $\Gamma(G)$ is the automorphism group of the graph G. Before proceeding, it is worth spending some time with the definition of the automorphism group.

Definition 2.4.1. *The automorphism group $\Gamma(G)$ of a graph $G = (V, E)$ is the group of permutations of the vertex set V that keep the edge set E invariant. That is, given an element $\sigma \in \Gamma(G)$ of the automorphism group,*

$$(v_1, v_2) \in E \quad \Longleftrightarrow \quad (\sigma(v_1), \sigma(v_2)) \in E, \quad \forall\, (v_1, v_2) \in E.$$

It is clear that every permutation has an inverse, there is an identity permutation and the composition of two automorphisms is again an automorphism. Hence, the set of all such permutations forms a subgroup of the full permutation group. To gain some intuition for the above definition, consider the following example.

Example 2.4.2. *Let the graph G be the square with vertices $V = \{1, 2, 3, 4\}$ and edges $E = \{(1, 2), (2, 3), (3, 4), (4, 1)\}$. Graphically, we can represent this as*

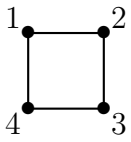

(2.75)

Now, consider the following permutation of the vertex set $\sigma = (1234)$. Applying this to every element of E we get $\sigma(E) = \{(2, 3), (3, 4), (4, 1), (1, 2)\} = E$, leaving the edge set invariant, hence $\sigma \in \Gamma(G)$. Now consider the permutation $\sigma' = (12) \notin \Gamma(G)$ because $(\sigma'(2), \sigma'(3)) = (1, 3)$ is not an edge in E.

The automorphism group of a graph naturally captures its symmetry. In the above example, the permutation $\sigma = (1234)$ represents a rotation of the square by 90° anti-clockwise. Whereas σ' would involve cutting some edges and re-gluing them, this does not represent a symmetry of the graph and hence is not in the automorphism group.

We are actually interested in a more general graph structure that allows for multiple edges and loops, which are edges that start and end at the same vertex. Consider the following, more involved, graphs

$G_1 =$ 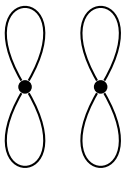 $G_2 =$  $G_3 =$ 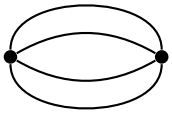

(2.76)

In order to deal with such graphs, we need to extend our definition to *multigraphs*.

Definition 2.4.3. *A **multigraph** is a tuple $G = (V, E)$ where V is a set of vertices and E is a multiset of unordered pairs of vertices. That is, the edge set E can contain multiple copies of the same edge and loops (e.g. (1,1)) are allowed.*

For example, the multigraph $G_1 = (\{1,2\}, \{(1,1)_1, (1,1)_2, (2,2)_1, (2,2)_2\})$. To complicate things further, the graphs that arise from Wick contractions of Gaussian integrals also have *half-edges*. These are edges that are only connected to one vertex. We will see why these arise in a moment. To couch the above in a more formal language, we introduce the notion of a Feynman graph.

Definition 2.4.4. *A **Feynman graph** is a quadruple*

$$G = (V, H, \phi, \iota),$$

where

- V *is a finite set of* vertices*;*
- H *is a finite set of* half-edges*;*
- $\phi : H \to V$ *assigns each half-edge to the vertex where it is incident;*
- $\iota : H \to H$ *is a fixed-point-free involution* ($\iota^2 = \mathrm{id}$) *pairing half-edges into* edges*. Each orbit* $\{h, \iota(h)\}$ *is an edge.*

We distinguish:

- Internal edges*: pairs* $\{h, \iota(h)\}$ *where both half-edges are incident to vertices in* V*;*
- External legs*: half-edges left unpaired (if* ι *is allowed to have fixed points).*

An automorphism *of* G *is a pair of permutations* (σ_V, σ_H) *on* V *and* H *such that* $\forall h \in H$

$$\phi(\sigma_H(h)) = \sigma_V(\phi(h)), \qquad \sigma_H(\iota(h)) = \iota(\sigma_H(h)).$$

The automorphisms are therefore the permutations of the vertices and of the half edges that keep the edge set invariant. This slightly mysterious definition becomes clearer with an example.

Example 2.4.5 (Double figure-8 graph with two vertices)**.** *Consider the Feynman graph* $G = (V, H, \phi, \iota)$ *defined as follows:*

- *The set of vertices is*

$$V = \{1, 2\}.$$

- *The set of half-edges is*

$$H = \{h_{11}, h_{12}, h_{13}, h_{14}, h_{21}, h_{22}, h_{23}, h_{24}\},$$

  where the first index indicates the vertex and the second index distinguishes half-edges.

- *The incidence map $\phi : H \to V$ is given by*

$$\phi(h_{1j}) = 1 \quad (j = 1, \ldots, 4), \qquad \phi(h_{2j}) = 2 \quad (j = 1, \ldots, 4).$$

- *The involution $\iota : H \to H$ pairs half-edges into loops:*

$$\iota(h_{11}) = h_{12}, \quad \iota(h_{12}) = h_{11}, \qquad \iota(h_{13}) = h_{14}, \quad \iota(h_{14}) = h_{13},$$
$$\iota(h_{21}) = h_{22}, \quad \iota(h_{22}) = h_{21}, \qquad \iota(h_{23}) = h_{24}, \quad \iota(h_{24}) = h_{23}.$$

Thus G has two vertices, each carrying two loops.

To find the size of the automorphism group we must consider permutations of vertices and half-edges that keep the edge set invariant. Its automorphism group is generated by

- *swapping the two vertices ($1 \leftrightarrow 2$);*
- *permuting the two loops at each vertex ($S_2 \times S_2$);*
- *flipping each of the four loops ($\mathbb{Z}_2^4$).*

Hence

$$\Gamma(G) \cong \mathbb{Z}_2 \times (S_2 \times S_2) \times (\mathbb{Z}_2)^4, \qquad |\Gamma(G)| = 2^7 = 128.$$

This definition of *Feynman graphs* and its automorphism group now mirrors the usual physics definition of the symmetry factors of Feynman diagrams which additionally count the $\mathbb{Z}^2$ factors associated with flipping loops. Note that without the additional structure of the half-edges on top of the multiset, the automorphism group would not distinguish between loop flips and the size of the automorphism group would be $2^3 = 8$ instead of $2^7 = 128$.

The remarkable insight of Feynman was exactly that the Wick contractions of Gaussian integrals can be enumerated by counting the above definition of *Feynman graphs*. To elaborate, consider the following Gaussian integral

$$\mathcal{Z} = \int_{-\infty}^{\infty} \frac{dx}{\sqrt{2\pi}} \exp\left(-\frac{1}{2}x^2 + g\,\frac{x^4}{4!}\right). \tag{2.77}$$

We claim that the generating function Z in (2.74) can be computed by the above Gaussian integral $\mathcal{Z}$, i.e. $Z = \mathcal{Z}$. To see this, we can expand the exponential in powers of g to get

$$\mathcal{Z} = \sum_{n=0}^{\infty} \frac{g^n}{n!} \left(\frac{1}{4!}\right)^n \int_{-\infty}^{\infty} \frac{dx}{\sqrt{2\pi}}\, x^{4n}\, e^{-\frac{1}{2}x^2} = \sum_{n=0}^{\infty} \frac{g^n}{n!} \left(\frac{1}{4!}\right)^n \left\langle x^{4n} \right\rangle_{g=0}. \tag{2.78}$$

The expectation value $\langle x^{4n}\rangle_{g=0}$ can be computed using standard Gaussian integrals (or Wick's theorem) and is given by

$$\left\langle x^{4n} \right\rangle_{g=0} = (4n-1)!! \tag{2.79}$$

The graphs G_1, G_2, G_3 are all the distinct Feynman graphs with two 4–valent vertices. Therefore, in order for $\mathcal{Z}$ to reproduce the generating function Z, the coefficient of g^2 in (2.77) must be equal to $\sum_{i=1}^{3} \frac{1}{|\Gamma(G_i)|}$. Indeed, we have already shown that $|\Gamma(G_1)| = 128$. We leave the remaining factors as an exercise to show that $|\Gamma(G_2)| = 2^4$ and $|\Gamma(G_3)| = 2 \cdot 4!$. It can be easily verified that $\frac{7!!}{2!(4!)^2} = \frac{105}{2!(4!)^2} = \left(\frac{1}{128} + \frac{1}{16} + \frac{1}{48}\right)$, confirming that $\mathcal{Z}$ is counting correctly at the order of g^2. In fact, this is true of any order of g and so this Gaussian integral gives us an alternative approach to the combinatorial problem of counting graphs and is an object we can get a better analytic control of. Note that the power of the non-quadratic part in the exponential in $\mathcal{Z}$ is what determines the valency of the vertices in the graphs we are counting. For example, if we had $gx^3/3!$ instead of $gx^4/4!$, we would be counting 3–valent graphs.

We can also add different vertex valencies by adding more non-gaussian terms to the exponential. For example, if we wanted to count graphs with both 3–valent and 4–valent vertices, we would consider

$$\mathcal{Z} = \int_{-\infty}^{\infty} \frac{dx}{\sqrt{2\pi}} \exp\left(-\frac{1}{2}x^2 + g_3\,\frac{x^3}{3!} + g_4\,\frac{x^4}{4!}\right). \tag{2.80}$$

Even more powerful is the ability to add different types of vertices by considering multiple variables. For example, if we wanted to count graphs with 3–valent vertices of two different types, say *red* and *blue*, we would consider

$$\mathcal{Z}_A = \int_{-\infty}^{\infty} \frac{dx\,dy}{2\pi} \exp\left(-\frac{1}{2}\vec{\mathbf{x}}^{\mathsf{T}} A\vec{\mathbf{x}} + g_{\text{red}}\frac{x^3}{3!} + g_{\text{blue}}\frac{y^3}{3!}\right), \tag{2.81}$$

where $\vec{\mathbf{x}} = (x, y)^{\mathsf{T}}$ and A is a 2×2 symmetric matrix that determines the propagators. The matrix must be symmetric because there is a contraction with symmetric indices in the exponential so any anti-symmetric part vanishes. The propagators are given by

$$\left\langle x^2 \right\rangle = A^{-1}_{11}, \quad \left\langle y^2 \right\rangle = A^{-1}_{22}, \quad \langle xy \rangle = A^{-1}_{12} = A^{-1}_{21}, \tag{2.82}$$

where the expectation value is taken with $g_{\text{red}} = g_{\text{blue}} = 0$ as usual, representing the 'free' theory. This allows us to control which types of vertices can connect to each other by choosing the matrix A^{-1} appropriately. For example if we only wanted red vertices to connect with blue vertices and vice versa, we would choose the off diagonal matrix

$$A^{-1} = \begin{pmatrix} 0 & 1 \\ 1 & 0 \end{pmatrix} \quad \Rightarrow \quad A = \begin{pmatrix} 0 & 1 \\ 1 & 0 \end{pmatrix}. \tag{2.83}$$

This is readily extended to n variables and hence many more types of vertices by integrating over a higher dimensional vector x_i, $i = 1, 2, ..., n$ and choosing a symmetric $n \times n$ matrix A. We usually say that the diagrams are constructed from 'propagators' and 'vertices' which carry the factors we found above and whose graphical representations are the building blocks of the full graphs. They are drawn as follows

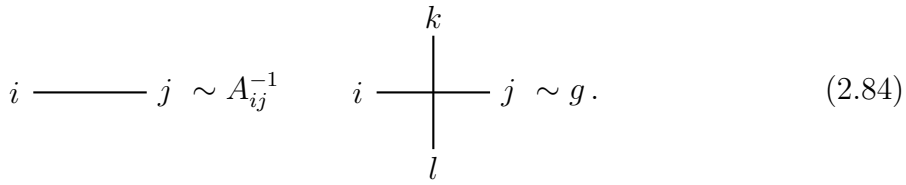

(2.84)

Aside. *Let us take a non-rigorous leap of faith and consider the limit $n \to \infty$. Formally, this would allow us to count graphs with infinitely many types of vertices. This infinite object is something akin to a functional integral and is a nice way to formally define a quantum field theory via the path integral. The infinite index i becomes a continuous variable x labelling the position in spacetime and the matrix A^{-1} becomes a kernel $A^{-1}(x, y)$, which*

is the Green's function of some differential operator. This is the path integral formulation of quantum field theory where we have our familiar Feynman diagrams.

It is clear that the above approach to counting graphs is very powerful and flexible. However, graphs do not have any notion of planarity or genus. To be able to use a similar approach to count discretised surfaces, we need to be able to distinguish between planar and non-planar graphs. For that we need a graph with faces, which is called a *map*. It turns out that the right extension to the above integrals in order to count maps is to increase the number of indices on the objects we are integrating over. Instead of a vector x_i with one index, we need an object with two indices, i.e. a matrix M_{ij}.

2.4.3 Matrix integrals and maps

To that end, consider the Hermitian $N \times N$ matrix M with Gaussian action

$$\mathcal{Z} = \int \mathcal{D}M \ \exp\left(-N\,\frac{1}{2}\ \mathrm{Tr}\, M^2\right). \tag{2.85}$$

The measure $\mathcal{D}M = \prod_i dx_{ii} \prod_{j<k} dx_{jk} dy_{jk}$, $x_{ij} = \mathrm{Re}(M_{ij})$, $y_{ij} = \mathrm{Im}(M_{ij})$ and the trace ensures that every index is contracted, thereby generating closed diagrams with no unmatched edges. Just as before, this object will generate Feynman graphs, that is to say multigraphs with half-edges, but with additional structure that allows us to generate well-defined surfaces. We may calculate the propagator

$$\langle M_{ij} M_{kl} \rangle := \int \mathcal{D}M \ M_{ij} M_{kl} \ \exp\left(-N\,\frac{1}{2}\ \mathrm{Tr}\, M^2\right) = \frac{1}{N}\,\delta_{il}\delta_{jk}, \tag{2.86}$$

using standard Gaussian integrals. This is the matrix equivalent of A^{-1} we had before but now each matrix has two indices, hence this inverse must be a four index object. The double line structure of the propagator is represented graphically as

$$\begin{array}{l} i \longleftarrow l \\ j \longrightarrow k \end{array} \ \sim \frac{1}{N}\,, \tag{2.87}$$

and we emphasise that each internal leg in the diagrams contributes a factor of N^{-1}. The vertices of the graphs are generated by higher order terms in the action as usual. For example, a quartic interaction

$$S_{\mathrm{int}}[M] = N\, g\ \mathrm{Tr}\, M^4 \tag{2.88}$$

generates four-valent vertices, diagrammatically represented as

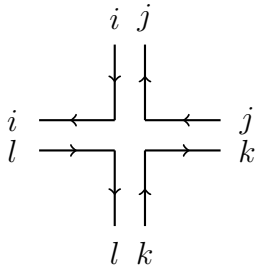

$$\sim Ng\,. \tag{2.89}$$

These 'thickened' graphs are called *ribbon graphs* and it is this thickness that enables us to talk about graphs with faces or *maps*.

To see how these Feynman rules enumerate maps, consider the following example with a quartic vertex generated by (2.88). Expanding the exponential as we did before, we must calculate expectations like $\langle(\operatorname{Tr} M^4)^n\rangle$. Let's focus on the simplest case of $n = 1$, then we have

$$\left\langle \operatorname{Tr} M^4 \right\rangle = \langle M_{ij} M_{jk} M_{kl} M_{li} \rangle\,. \tag{2.90}$$

Using Wick's theorem, we can compute this in terms of 2–point functions

$$\begin{aligned} \langle M_{ij} M_{jk} M_{kl} M_{li} \rangle &= \langle M_{ij} M_{jk} \rangle \langle M_{kl} M_{li} \rangle \\ &\quad + \langle M_{ij} M_{kl} \rangle \langle M_{jk} M_{li} \rangle \\ &\quad + \langle M_{ij} M_{li} \rangle \langle M_{jk} M_{kl} \rangle\,. \end{aligned} \tag{2.91}$$

Using (2.86) it is straightforward to show that $\langle \operatorname{Tr} M^4 \rangle = 2N + N^{-1}$. Let's investigate this diagrammatically. Starting with a single vertex (i.e. (2.89)) and considering all the ways you can join these half-edges together with propagators we get the diagrams in Figure 2.5.

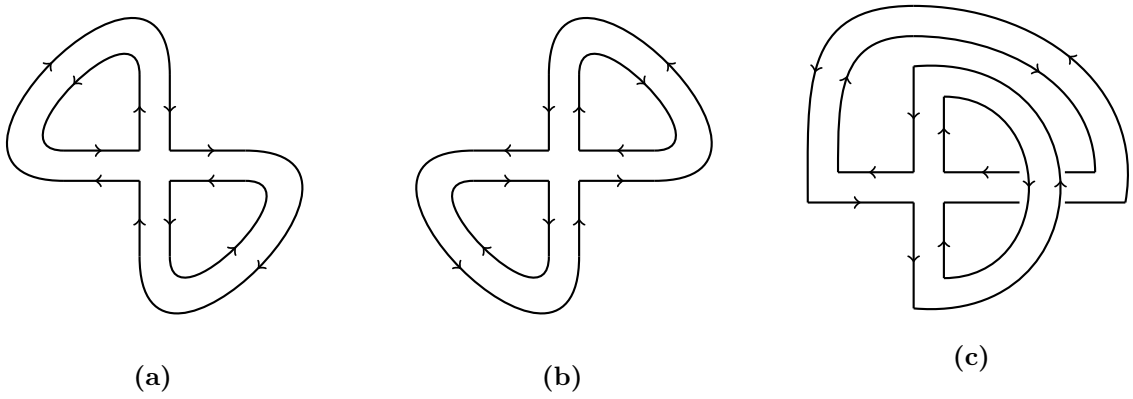

Figure 2.5: Wick contractions of $\operatorname{Tr} M^4$ as ribbon-graphs. Sub-figures (a) and (b) are planar and scale as N^2, while (c) is non-planar (genus one) and scales as N^0.

Adding back the factor of gN that comes from expanding the exponential in $\mathcal{Z}$, we see that the overall factor for a diagram is given by $g^V N^{V-E+F}$ where V, E, F is the number of vertices, propagators (edges) and faces (loops) respectively in the diagram. But $V-E+F$ is nothing more than the Euler characteristic of the surface Σ on which you can draw the graph and is equal to $\chi_h(\Sigma) = 2-2h$, where h is the genus of Σ. Therefore we say that the diagrams arrange themselves according to their topology. For the diagrams we considered, their contribution is given by $g(2N^2+1)$, where the first term represents the planar ($h=0$) contribution and the second term represents the ($h=1$) torus contribution.

The matrix integral

$$\mathcal{Z}_N(g) = \int \mathcal{D}M \ \exp\left(-N\,\frac{1}{2}\ \mathrm{Tr}\, M^2 + N\, g\ \mathrm{Tr}\, M^4\right) \tag{2.92}$$

counts all connected and non-connected Feynman graphs with quartic vertices. As a general rule of generating functions, to count only connected graphs, we consider the free energy

$$\mathcal{F}_N(g) = -\log\frac{\mathcal{Z}_N(g)}{\mathcal{Z}_N(0)} = g(2N^2+1) + \mathcal{O}(g^2), \tag{2.93}$$

which we have seen can be perturbatively arranged in powers of N as

$$\mathcal{F}_N(g) = \sum_{h=0}^{\infty} N^{2-2h}\mathcal{F}^{(h)}(g), \tag{2.94}$$

where $\mathcal{F}^{(h)}(g)$ counts connected ribbon graphs that can be drawn on surfaces of genus h i.e.

$$\mathcal{F}^{(h)}(g) = \sum_{V=0}^{\infty} C_V g^V, \tag{2.95}$$

where C_V is the number of connected ribbon graphs with V vertices that can be drawn on a genus h surface, weighted by the inverse size of their automorphism group. It is clear that in the large N limit, only the planar diagrams survive, which is why this limit is often called the 'planar limit'. This is the essence of the 't Hooft large N expansion [81].

Continuum limits

For a particular genus h, the generating function $\mathcal{F}^{(h)}(g)$ will have a finite radius of convergence $g < g_c$. As we have discussed in Section 2.3.3, approaching the region of non-analyticity, where graphs with very large numbers of vertices dominate, is where one may define a continuum limit.

It can be shown (see [21]) that the non-analytic part of $\mathcal{F}^{(h)}(g)$ close to g_c behaves as

$$\lim_{g\to g_c} \mathcal{F}^{(h)}_{\text{n.a.}}(g) \sim \begin{cases} (g-g_c)^{5/2} & h=0, \\ \log(g-g_c) & h=1, \\ (g-g_c)^{5\chi_h/4} & h\geq 2. \end{cases} \tag{2.96}$$

So we have two limits, the planar limit $N\to\infty$ and the continuum limit $g\to g_c$. If one takes these two limits sequentially, one obtains the planar continuum limit and all higher genus contributions are suppressed. Is there a way to take both limits simultaneously and retain contributions from all genera? The answer is yes, and this is called the *double scaling limit* [18–20]. The idea is to take $N\to\infty$ and $g\to g_c$ while keeping a certain combination fixed. It follows that the large N expansion near g_c is given by

$$\mathcal{F}_N(g) \approx N^2\mathcal{F}^{(0)}(g_c) + \sum_{h=0}^{\infty} f_h N^{\chi_h}(g-g_c)^{5\chi_h/4}, \tag{2.97}$$

where f_h are constants of proportionality. This motivates us to define the double scaling limit as

$$N\to\infty, \quad g\to g_c, \quad \kappa^{-1} = N(g-g_c)^{5/4} = \text{fixed}, \tag{2.98}$$

which gives rise to the following quantity of interest

$$\mathcal{F}_{\text{ds}}(\kappa) = \lim_{\substack{N\to\infty,\, g\to g_c \\ \kappa \text{ fixed}}} \left(\mathcal{F}_N(g) - N^2\mathcal{F}^{(0)}(g)\right) = \sum_{h=0}^{\infty} f_h \kappa^{-\chi_h}. \tag{2.99}$$

This quantity sums over all genera and is a candidate for a non-perturbative definition of 2D quantum gravity where one also cares about topology change.

We have laid out the basic framework and motivation behind matrix models. The aim was to show why and how Gaussian integrals over a matrix variable are a natural tool to count discretised surfaces. There is much more to say about them, especially non-perturbatively, where many analytical tools exist to solve them exactly. Since every Hermitian matrix can be diagonalised by a unitary transformation, it is natural to ask about the eigenvalue distribution of the ensemble of matrices. This reduces the problem to only N degrees of freedom—a huge simplification that goes a long way to solving these models. However, for the purposes of this thesis, we are mostly interested in the combinatorial aspects of the perturbative expansion. In Chapter 5, we will see how

we can apply functional renormalisation group techniques to study these models non-perturbatively. For more details on matrix models and their applications to 2D quantum gravity, we refer the reader to [21, 22, 85, 86].

3

Essential Stochastic Calculus

Contents

Much of the material in this thesis is expressed in the language of stochastic calculus. This chapter provides a brief overview of the key concepts and results needed to understand the subsequent chapters. For a more comprehensive treatment, refer to [87–89].

3.1 Probability Spaces

Definition 3.1.1 (Probability Space)**.** *A* ***probability space*** *is a triple* $(\Omega, \mathcal{F}, \mathbb{P})$*, where:*

- Ω *is the* ***sample space****, representing all possible outcomes of an experiment.*
- $\mathcal{F}$ *is a* σ*-****algebra****. A* σ*-algebra is a collection of subsets of* Ω *satisfying:*

  1. $\Omega \in \mathcal{F}$,

2. *if* $A \in \mathcal{F}$, *then* $A^c \in \mathcal{F}$,

3. *if* $A_1, A_2, \cdots \in \mathcal{F}$, *then* $\bigcup_{i=1}^{\infty} A_i \in \mathcal{F}$.

- $\mathbb{P} : \mathcal{F} \to [0,1]$ *is a* ***probability measure*** *satisfying:*

  1. $\mathbb{P}(\Omega) = 1$,

  2. $\mathbb{P}$ *is countably additive: for disjoint* $A_i \in \mathcal{F}$,

$$\mathbb{P}\left(\bigcup_{i=1}^{\infty} A_i\right) = \sum_{i=1}^{\infty} \mathbb{P}(A_i).$$

- *A set* $A \in \mathcal{F}$ *is called a* ***measurable set*** *or an* ***event****.*

The intuition behind this definition is that Ω is the set of all possible, mutually exclusive, 'atomic' outcomes of an experiment, e.g. the outcome of n die rolls. The σ-algebra $\mathcal{F}$ represents the collection of questions we can ask about said outcomes and assign probabilities to. Note that $\mathbb{P}$ acts on the sets in $\mathcal{F}$ and not directly on the elements of Ω so we can only ask questions about the events in $\mathcal{F}$.

Definition 3.1.2 (Random Variable)**.** *Let* $(\Omega, \mathcal{F}, \mathbb{P})$ *be a probability space and let* $\mathcal{B}(\mathbb{R})$ *denote the Borel* σ*-algebra on* $\mathbb{R}$*, which is simply the smallest* σ*-algebra containing all intervals* $[a, b] \subset \mathbb{R}$*. A function*

$$X : \Omega \longrightarrow \mathbb{R}$$

is called an $\mathcal{F}$***-measurable*** *random variable if*

$$\forall\, B \in \mathcal{B}(\mathbb{R}), \quad X^{-1}(B) \in \mathcal{F}.$$

Building on the previous intuition, an $\mathcal{F}$-measurable random variable is a function for which we can always calculate the probability of its outcomes since the pre-image of any interval (or union of intervals) is a **measurable** set in $\mathcal{F}$—the set of questions we can ask.

Definition 3.1.3 (Stochastic Process)**.** *A* ***stochastic process*** *is a collection of random variables* $\{X_t\}_{t \geq 0}$ *defined on a common probability space* $(\Omega, \mathcal{F}, \mathbb{P})$.

Definition 3.1.4 (Independence)**.** *Let $(\Omega, \mathcal{F}, \mathbb{P})$ be a probability space.*

1. ***Independence of events.*** *Two events $A, B \in \mathcal{F}$ are called independent if*

$$\mathbb{P}(A \cap B) = \mathbb{P}(A)\,\mathbb{P}(B).$$

2. ***Independence of σ-algebras.*** *Two σ-algebras $\mathcal{G}, \mathcal{H} \subseteq \mathcal{F}$ are called independent if for all $G \in \mathcal{G}$ and $H \in \mathcal{H}$,*

$$\mathbb{P}(G \cap H) = \mathbb{P}(G)\,\mathbb{P}(H).$$

3. ***Independence of random variables.*** *Random variables $X, Y : \Omega \to \mathbb{R}$ are called independent if the σ-algebras they generate are independent: i.e. for all Borel sets $B, C \in \mathcal{B}(\mathbb{R})$,*

$$\mathbb{P}\Big(X \in B,\ Y \in C\Big) = \mathbb{P}(X \in B)\,\mathbb{P}(Y \in C).$$

3.2 Conditional Expectation and Filtration

Definition 3.2.1 (Conditional Expectation)**.** *Let $(\Omega, \mathcal{F}, \mathbb{P})$ be a probability space and let $X \in L^1(\Omega, \mathcal{F}, \mathbb{P})$. Given a sub-$\sigma$-algebra $\mathcal{G} \subset \mathcal{F}$, the* ***conditional expectation*** *of X given $\mathcal{G}$ is the $\mathcal{G}$-measurable random variable $\mathbb{E}[X \mid \mathcal{G}]$ such that*

$$\int_G \mathbb{E}[X \mid \mathcal{G}]\, d\mathbb{P} = \int_G X\, d\mathbb{P} \quad \textit{for all } G \in \mathcal{G}.$$

To help gain an intuition of this definition, imagine $\mathcal{G}$ is generated by a partition of Ω into finitely many blocks $A_1, A_2, ..., A_n$ with $\mathbb{P}(A_i) \neq 0,\ i = 1, 2, ..., n$. The definition of conditional expectations then forces

$$\int_{A_i} \mathbb{E}[X \mid \mathcal{G}]\, d\mathbb{P} = \int_{A_i} X d\mathbb{P}, \quad i = 1, 2, ..., n.$$

but since $\mathbb{E}[X \mid \mathcal{G}]$ is $\mathcal{G}$-measurable, the expectation is a constant c_i on the subset A_i. Therefore we have that

$$c_i\,\mathbb{P}(A_i) = \int_{A_i} X d\mathbb{P}, \quad i = 1, 2, ..., n.$$

or equally

$$c_i = \frac{1}{\mathbb{P}(A_i)} \int_{A_i} X d\mathbb{P}, \quad i = 1, 2, ..., n.$$

which matches the more familiar notion of a conditional expectation which is taken with respect to the conditional probability of Bayes' theorem

$$\mathbb{P}(A \mid B) = \frac{\mathbb{P}(A \cap B)}{\mathbb{P}(B)}.$$

Proposition 3.2.1 (Basic Properties of Conditional Expectation)**.** *Let $(\Omega, \mathcal{F}, \mathbb{P})$ be a probability space, $X, Y \in L^1(\Omega, \mathcal{F}, \mathbb{P})$, and let $\mathcal{H} \subseteq \mathcal{G} \subseteq \mathcal{F}$ be sub-σ-algebras. Then:*

1. ***Linearity:***

$$\mathbb{E}[aX + bY \mid \mathcal{G}] = a\,\mathbb{E}[X \mid \mathcal{G}] + b\,\mathbb{E}[Y \mid \mathcal{G}], \quad a, b \in \mathbb{R}.$$

2. ***Monotonicity:***

$$X \leq Y \quad \Longrightarrow \quad \mathbb{E}[X \mid \mathcal{G}] \leq \mathbb{E}[Y \mid \mathcal{G}] \quad a.s.$$

   where 'a.s.' stands for 'almost surely' (i.e. with probability one).

3. ***Tower Property (Iterated Conditioning):***

$$\mathbb{E}\Big[\mathbb{E}[X \mid \mathcal{G}] \,\Big|\, \mathcal{H}\Big] = \mathbb{E}[X \mid \mathcal{H}] \quad \textit{and} \quad \mathbb{E}[\,\mathbb{E}[X \mid \mathcal{H}] \mid \mathcal{G}\,] = \mathbb{E}[X \mid \mathcal{H}].$$

4. ***Taking Out What Is Known:*** *If Y is $\mathcal{G}$-measurable and $Y\,X \in L^1$, then*

$$\mathbb{E}[Y\,X \mid \mathcal{G}] = Y\,\mathbb{E}[X \mid \mathcal{G}].$$

5. ***Contractivity (Jensen's Inequality):*** *For any convex function $\varphi : \mathbb{R} \to \mathbb{R}$ with $\varphi(X) \in L^1$,*

$$\varphi\Big(\mathbb{E}[X \mid \mathcal{G}]\Big) \leq \mathbb{E}\Big[\varphi(X) \mid \mathcal{G}\Big] \quad a.s.$$

6. ***Law of Total Expectation:***

$$\mathbb{E}\Big[\mathbb{E}[X \mid \mathcal{G}]\Big] = \mathbb{E}[X].$$

7. ***Independence:*** *If X is independent of $\mathcal{G}$, then*

$$\mathbb{E}[X \mid \mathcal{G}] = \mathbb{E}[X].$$

The tower property is particularly useful in calculations and we will make heavy use of it. Note that it is the smallest sigma algebra $\mathcal{H}$ that prevails in the end because this is the most coarse-grained average.

Additionally, consider $\mathcal{G} = \{\emptyset, \Omega\}$ then $\mathbb{E}[X \mid \mathcal{G}] = \mathbb{E}[X]$ since $\mathcal{G}$ contains minimal information. In the other extreme, where $\mathcal{G} = \mathcal{F}$, $\mathbb{E}[X \mid \mathcal{G}] = X$ since X is a random variable and by definition is $\mathcal{F}$-measurable. We can view this as moving along a spectrum of information ranging from knowing nothing to knowing everything with $\mathbb{E}[X \mid \mathcal{G}]$ giving the "best guess" of X based on the information contained in $\mathcal{G}$. When looking at stochastic processes we observe the trajectory up to some time t; the following definition formalises how we deal with this increasing information content.

Definition 3.2.2 (Adapted Process and Filtration)**.** *A **filtration** is a family $\{\mathcal{F}_t\}_{t\geq 0}$ of sub-σ-algebras of $\mathcal{F}$ such that $\mathcal{F}_s \subseteq \mathcal{F}_t$ for all $0 \leq s \leq t$. A stochastic process $\{X_t\}_{t\geq 0}$ is said to be **adapted** to the filtration if X_t is $\mathcal{F}_t$-measurable for all t.*

Being $\mathcal{F}_t$-measurable for all t means that the information contained in $\mathcal{F}_t$ at time t is sufficient to determine the value of X_t. So the value of X_t does not depend on any events after t.

Definition 3.2.3 (Martingale)**.** *Let $(\Omega, \mathcal{F}, \{\mathcal{F}_t\}, \mathbb{P})$ be a filtered probability space. A stochastic process $\{M_t\}_{t\geq 0}$ is a **martingale** with respect to the filtration $\{\mathcal{F}_t\}$ if:*

1. *M_t is $\mathcal{F}_t$-measurable for all $t \geq 0$,*
2. *$\mathbb{E}[|M_t|] < \infty$ for all $t \geq 0$,*
3. *For all $0 \leq s \leq t$, $\mathbb{E}[M_t \mid \mathcal{F}_s] = M_s$ almost surely.*

A property of martingales is that they have constant expectation which is a consequence of the last property in the definition. In particular $\mathbb{E}[M_t] = \mathbb{E}[M_t \mid \mathcal{F}_0] = M_0$, since $\mathcal{F}_0 = \{\emptyset, \Omega\}$.

3.3 The Wiener Process

Definition 3.3.1 (Wiener Process)**.** *A* ***Wiener process*** *(or Brownian motion) is a stochastic process* $\{W_t\}_{t\geq 0}$ *on a filtered probability space* $(\Omega, \mathcal{F}, \{\mathcal{F}_t\}_{t\geq 0}, \mathbb{P})$ *satisfying:*

1. $W_0 = 0$ *almost surely.*
2. W_t *has independent increments: for* $0 \leq s < t$*, the increment* $W_t - W_s$ *is independent of* $\mathcal{F}_s$*.*
3. W_t *has stationary increments: the distribution of* $W_t - W_s$ *depends only on* $t - s$*.*
4. $W_t - W_s \sim \mathcal{N}(0, t-s)$*, where* $\mathcal{N}(0, t-s)$ *is a normal distribution with mean 0 and variance* $t - s$*.*
5. W_t *has continuous paths almost surely.*

Remark 3.3.2. *The Wiener process is a Gaussian process with covariance function* $\mathbb{E}[W_s W_t] = \min(s, t)$*.*

Definition 3.3.3 (Quadratic Variation)**.** *Let* $\{X_t\}_{t\geq 0}$ *be a stochastic process with continuous paths on a filtered probability space* $(\Omega, \mathcal{F}, \{\mathcal{F}_t\}, \mathbb{P})$*. For any partition* $\Pi = \{0 = t_0 < t_1 < \cdots < t_n = T\}$ *of* $[0, T]$*, define the quadratic variation sum*

$$Q(\Pi; X)_T \;=\; \sum_{i=0}^{n-1} \Big(X_{t_{i+1}} - X_{t_i}\Big)^2.$$

If, as $\|\Pi\| = \max_i (t_{i+1} - t_i) \to 0$*, the random variables* $Q(\Pi; X)_T$ *converge in probability (or almost surely) to a limit, we call that limit the* ***quadratic variation*** *of* X *over* $[0, T]$ *and denote*

$$[X, X]_T \;=\; \lim_{\|\Pi\| \to 0} \sum_{i=0}^{n-1} \Big(X_{t_{i+1}} - X_{t_i}\Big)^2.$$

In particular, for a standard Wiener process $\{W_t\}$, one has almost surely

$$[W, W]_T \;=\; T.$$

The quadratic variation of the Wiener process can be expressed in the informal differential notation as

$$(dW_t)^2 \;=\; dt,$$

with the additional rules

$$dW_t\,dt = 0, \qquad (dt)^2 = 0.$$

In other words, when expanding stochastic differentials via Itô's calculus, one treats

$$dW_t\,dW_t \;=\; dt, \quad dW_t\,dt \;=\; 0, \quad dt\,dt \;=\; 0,$$

reflecting the fact that the only non-negligible second-order term is the quadratic variation of W, which accumulates at rate 1. An important result is Lévy's characterization theorem which states that any continuous martingale with quadratic variation $[M, M]_t = t$ is a Wiener process [89].

3.4 Itô Integrals

The informal differential notation introduced above is formalised via Itô integrals. They allow us to talk about integrals and differentials of functions of stochastic processes. In particular, Itô's lemma is the stochastic calculus analogue of the chain rule and a central result that we will use extensively throughout this thesis.

Definition 3.4.1 (Itô Integral)**.** *Let $\{W_t\}_{t\geq 0}$ be a Wiener process and let $\{X_t\}_{t\geq 0}$ be an adapted process. Then the* ***Itô integral***

$$\int_0^T X_t\,dW_t$$

is defined as the L^2-limit of Riemann sums:

$$\sum_{i=0}^{n-1} X_{t_i}(W_{t_{i+1}} - W_{t_i}),$$

where $\{t_i\}$ is a partition of $[0, T]$ and X_{t_i} is evaluated at the left endpoint.

Proposition 3.4.1 (Itô Isometry and Martingale Property)**.** *Let $\{W_t\}_{t\geq 0}$ be a Wiener process on a filtered probability space $(\Omega, \mathcal{F}, \{\mathcal{F}_t\}, \mathbb{P})$, and let $\{X_t\}_{t\geq 0}$ be an adapted process such that*

$$\mathbb{E}\left[\int_0^T X_t^2\,dt\right] < \infty.$$

Then the Itô integral

$$M_t := \int_0^t X_s\,dW_s$$

defines a stochastic process $\{M_t\}_{t\geq 0}$ satisfying:

1. *(**Itô Isometry**) For each $T \geq 0$,*

$$\mathbb{E}\left[M_T^2\right] = \mathbb{E}\left[\int_0^T X_t^2 \, dt\right].$$

2. *(**Martingale Property**) The process $\{M_t\}_{t\geq 0}$ is a martingale with respect to $\{\mathcal{F}_t\}$.*

The following lemma is concerned with a particular type of stochastic process known as an *Itô process*. Simply put, given the functions $\mu_t(x)$ and $\sigma_t(x)$, an *Itô process* is an adapted process that satisfies a stochastic differential equation of the form $dX_t = \mu_t(X_t)\,dt + \sigma_t(X_t)\,dW_t$. Further integrability conditions and precise definitions can be found in the aforementioned references [87–89].

Theorem 3.4.1 (Itô's Lemma)**.** *Let $f(t,x)$ be a $C^{1,2}$ function and let X_t be an Itô process satisfying*

$$dX_t = \mu_t\,dt + \sigma_t\,dW_t.$$

Then $Y_t = f(t, X_t)$ satisfies

$$df(t,X_t) = \left(\frac{\partial f}{\partial t} + \mu_t \frac{\partial f}{\partial x} + \frac{1}{2}\sigma_t^2 \frac{\partial^2 f}{\partial x^2}\right) dt + \sigma_t \frac{\partial f}{\partial x}\, dW_t.$$

Proof. Let

$$dX_t = \mu_t\,dt + \sigma_t\,dW_t, \qquad Y_t = f\big(t, X_t\big),$$

with $f \in C^{1,2}$. Expand f to second order in dt and dX:

$$df = f_t\,dt + f_x\,dX + \tfrac{1}{2}\,f_{xx}\,(dX)^2 + \text{higher orders}.$$

Since

$$dX = \mu\,dt + \sigma\,dW, \qquad (dW)^2 = dt, \quad dW\,dt = 0, \quad (dt)^2 = 0,$$

we have

$$(dX)^2 = \sigma^2\,(dW)^2 = \sigma^2\,dt.$$

Substituting back gives

$$\begin{aligned} df &= f_t\,dt + f_x\big(\mu\,dt + \sigma\,dW\big) + \tfrac{1}{2}\,f_{xx}\,\sigma^2\,dt \\ &= \left(f_t + \mu\,f_x + \tfrac{1}{2}\,\sigma^2\,f_{xx}\right) dt + \sigma\,f_x\,dW, \end{aligned}$$

which is exactly Itô's Lemma. □

3.5 Cameron–Martin/Girsanov's Theorem

The Cameron–Martin/Girsanov theorem describes how the dynamics of a stochastic process change under a change of measure. It allows us to transform a Brownian motion with drift into a standard Brownian motion by adjusting the underlying probability measure.

Theorem 3.5.1 (Girsanov's Theorem)**.** *Let $(\Omega, \mathcal{F}, \{\mathcal{F}_t\}, \mathbb{P})$ be a filtered probability space supporting a Wiener process W_t. Suppose $(\theta_t)_{t\geq 0}$ is an $\{\mathcal{F}_t\}$–adapted process satisfying*

$$\int_0^T \theta_t^2 \, dt < \infty \quad \text{almost surely.}$$

Define the exponential martingale

$$Z_t \;=\; \exp\Big(-\int_0^t \theta_s \, dW_s \;-\; \frac{1}{2}\int_0^t \theta_s^2 \, ds\Big), \quad t \in [0,T].$$

Due to the martingale property, $\mathbb{E}[Z_T] = 1$ and the measure $\mathbb{Q}$ defined by

$$\left.\frac{d\mathbb{Q}}{d\mathbb{P}}\right|_{\mathcal{F}_T} \;=\; Z_T$$

is a probability measure on $(\Omega, \mathcal{F}_T)$, and under $\mathbb{Q}$ the process

$$\widetilde{W}_t \;:=\; W_t \;+\; \int_0^t \theta_s \, ds$$

is a standard Wiener process with respect to $\{\mathcal{F}_t\}$.

Remark 3.5.1. *Girsanov's theorem describes how the drift of a Brownian motion can be "removed" (or introduced) by an equivalent change of measure, using the Radon–Nikodym derivative Z_T. In particular, if under $\mathbb{P}$ one has*

$$dX_t = \mu_t \, dt + \sigma_t \, dW_t,$$

then under the new measure $\mathbb{Q}$ with $\theta_t = \mu_t/\sigma_t$, X_t becomes a local martingale, i.e. driftless.

3.6 The Feynman–Kac Formula

The Feynman–Kac formula provides a link between stochastic processes and the partial differential equations that describe the generators of those processes.

Theorem 3.6.1 (Feynman–Kac Formula)**.** *Let X_t satisfy the Itô SDE*

$$dX_t \;=\; \mu(X_t)\,dt + \sigma(X_t)\,dW_t, \quad X_0 = x,$$

and let $r(x) \geq 0$ and $g(x)$, $f(t,x)$ be sufficiently smooth functions. Define

$$u(t,x) \;=\; \mathbb{E}^x\Big[\exp\Big(-\int_0^t r(X_s)\,ds\Big)\,g\Big(X_t\Big)\Big] \;+\; \int_0^t \mathbb{E}^x\Big[\exp\Big(-\int_0^s r(X_u)\,du\Big)\,f\Big(s,X_s\Big)\Big]ds,$$

where $\mathbb{E}^x$ denotes expectation over the stochastic process with $X_0 = x$. Then $\forall t \geq 0$, $u(t,x)$ is the unique classical solution of the PDE

$$\frac{\partial u}{\partial t} \;=\; \mathcal{L}u - r(x)u + f(t,x), \quad u(0,x) = g(x),$$

where

$$\mathcal{L}u \;=\; \mu(x)\,\frac{\partial u}{\partial x} \;+\; \frac{1}{2}\,\sigma^2(x)\,\frac{\partial^2 u}{\partial x^2}.$$

Proof. Let

$$A_s = \exp\Big(-\int_0^s r(X_u)\,du\Big), \qquad Y_s = u(t-s,\,X_s),$$

and define

$$Z_s = A_s\,Y_s + \int_0^s A_v\,f(t-v,X_v)\,dv.$$

Since A_s has finite variation,

$$dA_s = -r(X_s)\,A_s\,ds.$$

By Itô's lemma applied to $Y_s = u(t-s,X_s)$, writing $\dot{u}(t,x) = \partial_t u(t,x)$, $u'(t,x) = \partial_x u(t,x)$, and $u''(t,x) = \partial_x^2 u(t,x)$ we get

$$dY_s = \Big(-\dot{u}(t-s,X_s) + \mathcal{L}u(t-s,X_s)\Big)\,ds + \sigma(X_s)\,u'(t-s,X_s)\,dW_s.$$

Therefore

$$d(A_sY_s) = A_s\,dY_s + Y_s\,dA_s = A_s\Big(-\dot{u}(t-s,X_s) + \mathcal{L}u(t-s,X_s)\Big)\,ds + A_s\,\sigma(X_s)\,u'(t-s,X_s)\,dW_s.$$

Using the PDE $\dot{u}(t-s, X_s) = \mathcal{L}u(t-s, X_s) - r(X_s)\, u(t-s, X_s) + f(t-s, X_s)$ we get

$$d(A_s Y_s) = -A_s\, f(t-s, X_s)\, ds + A_s\, \sigma(X_s)\, u'(t-s, X_s)\, dW_s.$$

Adding the differential of the integral term in Z_s yields

$$dZ_s = A_s\, \sigma(X_s)\, u'(t-s, X_s)\, dW_s,$$

demonstrating by Proposition 3.4.1 that Z_s is a martingale and hence that $\mathbb{E}^x[Z_t] = Z_0$. At $s = 0$, $Z_0 = u(t, x)$, while at $s = t$,

$$Z_t = e^{-\int_0^t r(X_v)\, dv}\, g(X_t) + \int_0^t e^{-\int_0^v r(X_u)\, du}\, f(t-v, X_v)\, dv.$$

Taking expectations under $\mathbb{P}^x$ gives

$$u(t, x) = \mathbb{E}^x[Z_t],$$

which is exactly the Feynman–Kac representation. □

The term $r(x)$ appearing in the PDE is called the "killing term" in the following sense.

3.7 Killing Terms

Definition 3.7.1 (Killed Process)**.** *Given a stochastic process X_t and a nonnegative killing (or rate) function $r(x) \geq 0$, the **killed process** is defined by*

$$X_t^* \;=\; \begin{cases} X_t, & t < \tau, \\ \dagger, & t \geq \tau, \end{cases}$$

*where τ is the **exit (or killing) time***

$$\tau \;=\; \inf\Big\{ t \geq 0 : \int_0^t r\big(X_s\big)\, ds \geq \mathbf{e} \Big\},$$

and $\mathbf{e} \sim \mathrm{Exp}(1)$ is an independent exponential random variable. The state $\dagger$ is called the cemetery state and indicates absorption.

Proposition 3.7.1. *Let $u(t, x) = \mathbb{E}^x\big[h(X_t)\, \mathbb{1}_{\{t<\tau\}}\big]$. Then u satisfies the PDE with a killing term*

$$\frac{\partial u}{\partial t} = \mathcal{L}u - r(x)\, u, \quad u(0, x) = h(x).$$

Proof. Observe that the event $\{t < \tau\}$ is the same as the event $\{\mathbf{e} > \int_0^t r(X_s)\,ds\}$, hence by conditioning on the entire path $\{X_s\}_{s\le t}$ we have

$$\begin{aligned} u(t,x) &= \mathbb{E}^x\Big[h(X_t)\,\mathbb{1}_{\{t<\tau\}}\Big] \\ &= \mathbb{E}^x\left[h(X_t)\,\mathbb{E}\left[\mathbb{1}_{\{\mathbf{e}>\int_0^t r(X_s)\,ds\}} \mid \{X_s\}_{s\le t}\right]\right] \\ &= \mathbb{E}^x\Big[e^{-\int_0^t r(X_s)\,ds}\,h(X_t)\Big] \end{aligned}$$

Then by the Feynman–Kac formula, the function $u(t,x) = \mathbb{E}^x\Big[e^{-\int_0^t r(X_s)\,ds}h(X_t)\Big]$ is the unique solution of

$$\frac{\partial u}{\partial t} = \mathcal{L}u - r(x)\,u, \qquad u(0,x) = h(x).$$

□

3.8 Doob h–Transforms

The Doob h–transform is a way of conditioning a stochastic process (and more generally a Markov process) on a rare event (e.g. never hitting a boundary, or reaching a particular point). It defines a new process whose dynamics are altered to make the event "typical" which preserves the Markov property.

Definition 3.8.1 (Generator of a Markov process)**.** *Let $\{X_t\}_{t\ge0}$ be a Markov process on a state space E. Its **infinitesimal generator** is defined by*

$$\mathcal{L}f(x) = \lim_{h\downarrow 0}\frac{\mathbb{E}^x[f(X_h)] - f(x)}{h}, \quad f \in \mathcal{D}(\mathcal{L}),$$

whenever the limit exists.

This is a generalisation of the generator $\mathcal{L}$ we have already met in the previous sections to any Markov process.

Definition 3.8.2 (Doob h–Transform)**.** *Let $X = (X_t)_{t\ge0}$ be a time-homogeneous Markov process with infinitesimal generator $\mathcal{L}$, and let $h : \mathbb{R} \to (0,\infty)$ be a strictly positive C^2 function satisfying*

$$\mathcal{L}h = \lambda h$$

for some constant $\lambda \in \mathbb{R}$. Define a new probability measure $\mathbb{Q}^h$ on path space by

$$\frac{d\mathbb{Q}^h}{d\mathbb{P}^x}\Big|_{\mathcal{F}_t} = \frac{h(X_t)}{h(x)} e^{-\lambda t},$$

*where $\mathbb{P}^x$ is the law of X starting from $X_0 = x$. Then under $\mathbb{Q}^h$, the process X is called the **Doob** h–**transform** of the original process.*

Proposition 3.8.1. *Let $u(t,x)$ solve the PDE*

$$\frac{\partial u}{\partial t} = \mathcal{L}u, \quad u(0,x) = f(x).$$

Then the Doob h–transform X_t satisfies the PDE

$$\frac{\partial u^h}{\partial t} = \mathcal{L}^h u^h, \quad u^h(0,x) = f(x),$$

where the transformed generator $\mathcal{L}^h$ is given by

$$\mathcal{L}^h f = \frac{1}{h}\mathcal{L}(hf) - \lambda f.$$

Proof. Let $u(t,x) = \mathbb{E}^x[f(X_t)]$, then under the Doob h–transform, the expectation becomes

$$u^h(t,x) = \mathbb{E}_{\mathbb{Q}^h}\Big[f(X_t)\Big] = \mathbb{E}_{\mathbb{P}^x}\left[f(X_t)\frac{h(X_t)}{h(x)}e^{-\lambda t}\right].$$

Define $v(t,x) = \mathbb{E}^x[f(X_t)h(X_t)]$, then

$$u^h(t,x) = \frac{1}{h(x)}e^{-\lambda t}v(t,x).$$

We know $v(t,x)$ solves

$$\frac{\partial v}{\partial t} = \mathcal{L}v, \quad v(0,x) = f(x)h(x).$$

Therefore,

$$\frac{\partial u^h}{\partial t} = \frac{1}{h(x)}e^{-\lambda t}\left[\frac{\partial v}{\partial t} - \lambda v\right] = \frac{1}{h(x)}e^{-\lambda t}\left[\mathcal{L}(v) - \lambda v\right].$$

Substituting back $v = hu^h e^{\lambda t}$ gives

$$\frac{\partial u^h}{\partial t} = \frac{1}{h(x)}\Big[\mathcal{L}(hu^h) - \lambda h u^h\Big] = \frac{1}{h}\mathcal{L}(hu^h) - \lambda u^h,$$

which is the PDE governed by the transformed generator $\mathcal{L}^h$. □

Example 3.8.3 (Conditioning Brownian Motion to Stay Positive (3D Bessel Process))**.** *Let W_t be standard Brownian motion whose generator is $\mathcal{L} = \frac{1}{2}\frac{d^2}{dx^2}$ and define the function $h(x) = x$ on $(0, \infty)$. Then h satisfies*

$$\frac{1}{2}h''(x) = 0$$

so $\mathcal{L}\,h = 0$ with $\lambda = 0$. The Doob h–transform of Brownian motion via $h(x) = x$ is a diffusion process with generator

$$\mathcal{L}^h f(x) = \frac{1}{x} \cdot \frac{1}{2}\frac{d^2}{dx^2}(xf(x)) = \frac{1}{2}\frac{d^2 f}{dx^2} + \frac{1}{x}\frac{df}{dx},$$

which is the infinitesimal generator of the 3D Bessel process. Hence, the Doob h–transform of Brownian motion conditioned to stay positive is a 3D Bessel process.

In this way, the Doob h–transform enables us to rigorously define processes such as Brownian motion conditioned to avoid a set (e.g. hitting zero), to reach a point at a given time, or to behave in other nonstandard ways.

We can also consider time-dependent h–transforms, known as space–time harmonic transforms. These are useful for conditioning on events that depend on both space and time, such as survival up to a finite time horizon. In the rest of this chapter we will state the relevant results that extend our previous discussion to the time dependent case.

Definition 3.8.4 (Space-time harmonic function)**.** *A strictly positive function*

$$h\colon [0,T] \times D \longrightarrow \mathbb{R}_{>0}$$

is called ***space–time harmonic*** *for the family of generators $\{\partial_t + \mathcal{L}\}$ if*

$$\Big(\partial_t + \mathcal{L}\Big)\, h(t,x) = 0, \qquad (t,x) \in [0,T] \times D.$$

A space–time harmonic function can be used to define a time-dependent Doob h–transform by defining the Radon-Nikodym derivative as follows.

Proposition 3.8.2 (Martingale property of the h–transform)**.** *Let h be space–time harmonic for $\{\mathcal{L}_t\}$, and assume $h(0, X_0) > 0$. Define*

$$M_t \;=\; \frac{h(t, X_t)}{h(0, X_0)}, \qquad t \in [0,T].$$

Then $\{M_t\}$ is a $\mathbb{P}$–martingale. Consequently, one may define a new probability measure $\mathbb{Q}$ on $\mathcal{F}_t$ by

$$\left.\frac{d\mathbb{Q}}{d\mathbb{P}}\right|_{\mathcal{F}_t} = M_t.$$

Proposition 3.8.3 (Transformed dynamics under $\mathbb{Q}$)**.** *Under the measure $\mathbb{Q}$ defined above, the process X remains Markovian with generator $\mathcal{L}_t^h$ given by*

$$\mathcal{L}_t^h f(x) \;=\; \frac{1}{h(t,x)}\Big(\partial_t + \mathcal{L}_t\Big)\Big[h(t,\cdot)\, f(\cdot)\Big](x).$$

This is the time-dependent analogue of Proposition 3.8.1.

We can use time-dependent Doob h-transforms to condition a stochastic process to hit a particular point at a specified time, such as in the case of the Brownian bridge.

Example 3.8.5 (Brownian bridge)**.** *Let B_t be a Brownian motion in $\mathbb{R}$ with generator $\mathcal{L} = \frac{1}{2}\partial_x^2$. For fixed $T > 0$ and target $y \in \mathbb{R}$, define*

$$h(t,x) = p(T-t,x,y) = \frac{1}{\sqrt{2\pi(T-t)}} \exp\!\Big(-\tfrac{(x-y)^2}{2(T-t)}\Big).$$

Then the new generator is given by

$$\mathcal{L}^h = \frac{1}{h(t,x)}\Big(\partial_t + \mathcal{L}\Big)h(t,x) = \frac{1}{2}\,\partial_x^2 + \frac{\partial_x h(t,x)}{h(t,x)}\,\partial_x,$$

where

$$\frac{\partial_x h(t,x)}{h(t,x)} = -\frac{x-y}{T-t}\,.$$

The equivalent SDE for the process under $\mathbb{Q}$ is

$$dB_t = -\frac{B_t - y}{T-t}\,dt + dW_t^Q,$$

which is the classical Brownian bridge from X_0 to y over $[0,T]$.

In the above example, the space–time harmonic function $h(t,x)$ is the transition kernel of Brownian motion from x to y in time $T-t$. The Doob h–transform conditions the Brownian motion to be at y at time T. To see why this is the case, consider an $\mathcal{F}_t$-measurable random variable $G(X_t)$. Then the expectation under $\mathbb{Q}$ is given by

$$\mathbb{E}_{\mathbb{Q}}[G(X_t)] = \mathbb{E}_{\mathbb{P}^x}\Big[G(X_t)\,\frac{p(T-t,X_t,y)}{p(T,x,y)}\Big] = \int G(z)\,\frac{p(T-t,z,y)}{p(T,x,y)}\,p(t,x,z)\,dz,$$

but this is exactly the conditional expectation $\mathbb{E}^x[G(X_t) \mid X_T = y\,]$ under $\mathbb{P}^x$.

We can go further and consider a *killed* process and use a space–time harmonic function to condition it to survive (i.e. never reach the cemetery state) up to a finite time horizon T. Let $(X_t)_{t\geq 0}$ be a stochastic process with infinitesimal generator $\mathcal{L}$ and a state-dependent killing rate $r \geq 0$. We define the survival function

$$u(t,x) = \mathbb{E}^x\Big[\mathbb{1}_{\{t<\tau\}}\Big] = \mathbb{P}^x\{t < \tau\},$$

where τ is the killing time given by

$$\tau = \inf\Big\{t \geq 0 : \int_0^t r(X_s)\,ds \geq \mathbf{e}\Big\}, \quad \mathbf{e} \sim \mathrm{Exp}(1).$$

Then by Theorem 3.6.1, $u(t,x)$ solves the Feynman–Kac PDE

$$\partial_t\, u(t,x) = \mathcal{L}\, u(t,x) - r(x)\, u(t,x), \quad u(0,x) = 1.$$

Proposition 3.8.4 (Conditioning on survival to time T)**.** *Define*

$$h(s,x) = u(T-s,x), \quad 0 \leq s \leq T\,.$$

Then h is strictly positive on $[0,T)\times\mathbb{R}$ and satisfies

$$\Big(\partial_s + \mathcal{L} - r\Big)\, h(s,x) = 0,$$

i.e. h is space–time harmonic for the family $\{\partial_t + \mathcal{L} - r\}$. Assume $h(0,X_0) = u(T,X_0) > 0$. For $s \leq T$, define

$$M_s = \frac{h(s,X_s)}{h(0,X_0)}\,\mathbb{1}_{\{s<\tau\}} = \frac{u(T-s,X_s)}{u(T,X_0)}\,\mathbb{1}_{\{s<\tau\}}.$$

Then $\{M_s\}_{0\leq s\leq T}$ is a $\mathbb{P}^x$–martingale. For each $s \leq T$, define a probability measure $\mathbb{Q}^T$ on $\mathcal{F}_s$ by

$$\frac{d\mathbb{Q}^T}{d\mathbb{P}^x}\,\Big|_{\mathcal{F}_s} = M_s = \frac{u(T-s,X_s)}{u(T,x)}\,\mathbb{1}_{\{s<\tau\}}.$$

Under $\mathbb{Q}^T$, X_t is the Doob transformed process conditioned to survive up to time T.

Proof. The positivity of h follows from the fact that $u(t,x) = \mathbb{P}^x\{t < \tau\}$ is a survival probability and hence strictly positive for all finite t. The PDE satisfied by h follows directly from the PDE satisfied by u.

To show the martingale property of M_s, define the process

$$\widetilde{M}_s := h(s, X_s)e^{-\int_0^s r(X_u)\,du},$$

which can be shown to be a $\mathbb{P}^x$–martingale by the same argument as in the proof of Theorem 3.6.1. Then it follows that for $v < s < T$,

$$\begin{aligned}
\mathbb{E}_{\mathbb{P}^x}\left[\frac{h(s,X_s)}{h(0,X_0)}\,\mathbb{1}_{\{s<\tau\}} \mid \mathcal{F}_v\right] &= \frac{1}{h(0,X_0)}\mathbb{E}_{\mathbb{P}^x}[h(s,X_s)\mathbb{1}_{\{v<\tau\}}e^{-\int_v^s r(X_u)\,du} \mid \mathcal{F}_v] \\
&= \frac{\mathbb{1}_{\{v<\tau\}}}{h(0,X_0)}\mathbb{E}_{\mathbb{P}^x}\left[h(s,X_s)\frac{e^{-\int_0^s r(X_u)\,du}}{e^{-\int_0^v r(X_u)\,du}} \;\middle|\; \mathcal{F}_v\right] \\
&= \frac{h(v,X_v)}{h(0,X_0)}\mathbb{1}_{\{v<\tau\}},
\end{aligned}$$

where in the last step we used the martingale property of $\widetilde{M}_s$. □

To see that this really does condition the process to survive up to time T, consider the probability of survival under $\mathbb{Q}^T$:

$$\mathbb{Q}^T\{s < \tau\} = \mathbb{E}_{\mathbb{Q}^T}[\mathbb{1}_{\{s<\tau\}}] = \mathbb{E}_{\mathbb{P}^x}\left[\frac{h(s,X_s)}{h(0,X_0)}\,\mathbb{1}_{\{s<\tau\}}\right] = \frac{h(0,X_0)}{h(0,X_0)} = 1,$$

by the martingale property of M_s. Furthermore, for any $\mathcal{F}_s$-measurable random variable $G(X_s)$,

$$\mathbb{E}_{\mathbb{Q}^T}[G(X_s)] = \mathbb{E}_{\mathbb{P}^x}\left[G(X_s)\,\frac{u(T-s,X_s)}{u(T,x)}\,\mathbb{1}_{\{s<\tau\}}\right] = \mathbb{E}_{\mathbb{P}^x}\left[G(X_s)\,\frac{\mathbb{P}^{X_s}\{T-s<\tau\}}{\mathbb{P}^x\{T<\tau\}}\,\mathbb{1}_{\{s<\tau\}}\right],$$

which is exactly the conditional expectation $\mathbb{E}^x[G(X_s) \mid T < \tau\,]$ under $\mathbb{P}^x$. Under $\mathbb{Q}^T$, X_t remains Markovian with time-dependent generator

$$\mathcal{L}_s^T f(x) = \frac{1}{h(s,x)}\Big(\partial_s + \mathcal{L} - r\Big)\Big[h(s,x)\,f(x)\Big]$$

where $h(s,x) = u(T-s,x)$.

If instead we want to condition the process to survive up to a finite time horizon T *and* arrive at a particular point $y \in \mathbb{R}$, we can use the transition kernel of the killed process as we did for the Brownian bridge.

Before concluding this section, we can also consider the limit as $T \to \infty$ to condition the process to survive forever. Suppose the limit

$$h(x) \;=\; \lim_{T\to\infty} u(T,x)$$

exists and satisfies $h(x) > 0$ for all $x \in \mathbb{R}$. Then h solves the eigenfunction equation

$$(\mathcal{L} - r(x))\, h(x) = 0$$

Define a new measure $\mathbb{Q}^h$ on each $\mathcal{F}_s$ by

$$\frac{d\mathbb{Q}^h}{d\mathbb{P}^x}\,\Big|_{\mathcal{F}_s} = \frac{h\Big(X_s\Big)}{h(x)}\;\mathbb{1}_{\{s<\tau\}}.$$

Under $\mathbb{Q}^h$, the process X is conditioned to survive forever. The time-homogeneous transformed generator $\mathcal{L}^h$ is

$$\mathcal{L}^h f(x) = \frac{1}{h(x)}\,(\mathcal{L} - r)\Big(h\,f\Big)(x),$$

and the process never reaches the cemetery state.

The topics covered in this chapter are used throughout the rest of this thesis. The theory of stochastic calculus is incredibly rich and there is a lot more to say about it that may become useful in future analysis of causal random geometry. To that end, the reader is encouraged to consult the references for further reading [87–89].

4

Conformal dimensions on causal random geometry

Contents

4.1 Introduction

As we explained in Chapter 2, when defining quantum gravity, one is free to choose the class of random surfaces over which we sum in a path integral. We call the unrestricted

class *Liouville random surfaces* for its connection to Liouville gravity which will be explained in the following sections. Matter coupled to Liouville random surfaces has been studied thoroughly in the context of Liouville gravity. One important result is the *Knizhnik-Polyakov-Zamolodchikov* (KPZ) formula [90–92] which relates the scaling dimension x of a conformal field on a flat background to the value Δ on a Liouville random surface. The intuition for why scaling dimensions of fields get shifted is that the highly fractal and singular nature of the underlying geometry (as depicted in Figure 2.2) "dresses" the matter degrees of freedom. For example, the Ising model coupled to Liouville random surfaces has been calculated exactly with matrix model techniques [11, 85, 93, 94] and the scaling dimensions agree with those found with the KPZ formula.

In this chapter, we are interested in how matter couples to CDT—we use the Ising model as an example but the main results can be extended to so-called RSOS, or height, models. Not much is known analytically, but numerical studies suggest that the scaling dimensions of the Ising fields are not shifted from their classical values. It was shown using Monte Carlo methods and a high-temperature expansion that the critical exponents of a single Ising model ($c = 1/2$) coupled to CDT appear to retain their classical values [40]. Furthermore, a numerical study of the three-state Potts model ($c = 4/5$) found the same behaviour [42]. Perhaps more surprisingly, in a numerical study of 8 Ising models ($c = 4$) coupled to CDT, the scaling dimensions of the matter fields still remained unchanged despite a change in the gravity sector [41]. It appears that CDT coupled to unitary matter has the universal property that the critical exponents take their classical values and that this result is robust even beyond $c = 1$. Interestingly, it has been found that the scaling exponents *do* shift when coupling hard dimers to CDT in a certain phase of the model [36]. At the present time, the authors are not aware of a topological defect construction for hard dimers, but if one were found then the first part of our argument, made in Section 4.4, would be applicable to this model. However, the hard dimer model at its critical point has a central charge $c = -22/5$ and so is non-unitary. The complex weights ruin the description in terms of a positive definite stochastic process that the second part of our argument relies upon. Hence the results of this chapter do not apply to such models.

We provide a series of analytical arguments for why the scaling dimensions of fields on CDT are no different to those on a fixed lattice for the quenched model. Crucial to our arguments are the topological defect formulation of the Ising model [95] and evasion of the KPZ relation. The most useful formulation of the latter for our purposes is that of Duplantier-Sheffield (DS) [26] whose framework we adapt to CDT to show that no analogue of KPZ applies. This follows from the fact that CDT is essentially one-dimensional and can be described in terms of a stochastic differential equation (SDE) which has continuous sample paths *almost surely*. As a consequence, KPZ is evaded.

This chapter is structured as follows. We firstly explain how to couple matter to the ensemble of graphs in Section 4.2. In Section 4.3 we describe how Liouville theory can be understood in terms of a Gaussian free field along the lines of Duplantier-Sheffield [26]. In Section 4.4 we explain the plaquette formalism of the Ising model as described in [95] and use the algebra of topological defects to find algebraic relations for operators that will be crucial for finding the conformal dimensions: the Dehn twist operators. In Section 4.5 we show that one can indeed construct a Dehn twist in the continuum, from which we calculate the conformal dimensions of the Ising fields. Furthermore, we provide an alternative proof that there will be no KPZ-like relation in continuum CDT by constructing a random measure and following the arguments of DS in [26]. In Section 4.6 we extend the existing connection to Hořava–Lifshitz gravity originally found in [43]. Finally, in Section 4.7 we provide an argument for why our results may apply more generally to the model where the geometry and matter are sampled according to a joint measure (the *annealed model*), which relies solely on the continuity of the process describing the evolution of CDT.

4.2 Coupling the Ising Model to CDT

To implement the matter action S_m (2.3) in the discretised picture we introduce new degrees of freedom that live on the vertices of the graphs G in the ensemble. In this chapter we work specifically with Ising spins but the construction is easily generalised, in particular to the random height models. On each vertex $v \in V(G)$ lives a spin that takes values in $\{+1, -1\}$,

and spins on vertices that share an edge $e \in E(G)$ interact with a coupling strength J_e. The spin partition function on G is given by the sum over all spin configurations

$$Z_G[\{J\}_G] = \sum_{\{\sigma \in \{+1,-1\}^{V(G)}\}} \exp\left(\sum_{e=\langle x,y\rangle \in E(G)} J_e \sigma_x \sigma_y \right). \tag{4.1}$$

From now on we will assume that for the ensemble of Euclidean triangulations $\mathcal{E}$, $J_e = J, \forall e$, and that for the ensemble of causal triangulations $\mathcal{C}$, $J_e = J_1$ for all space-like edges and $J_e = J_2$, for all time-like edges. The discretised Euclidean and CT path integrals for the disk corresponding to (2.3) then take the form

$$W_{\mathcal{G}} = \sum_{G \in \mathcal{G}} \tilde{g}^{\Delta(G)} z^{|\partial G|} Z_G[J_{\mathcal{G}}]\,, \tag{4.2}$$

where $\mathcal{G}$ is chosen to be respectively $\mathcal{E}$ or $\mathcal{C}$. We refer to the systems described by $W_{\mathcal{G}}$ as *annealed* models.

In statistical mechanics language $W_{\mathcal{G}}$ is the grand canonical partition function. For a given $J_{\mathcal{G}}$ the sum is convergent for $\tilde{g} < \tilde{g}_c(J_{\mathcal{G}})$. Let $\mathcal{A}$ be the region of coupling strength for which $\tilde{g}_c(J_{\mathcal{G}})$ is analytic, then for $J_{\mathcal{G}} \in \mathcal{A}$, the limit $\tilde{g} \uparrow \tilde{g}_c(J_{\mathcal{G}})$ describes the same purely gravitational physics as the partition function without matter degrees of freedom. On the other hand, in the region $J_{\mathcal{G}} = J^*_{\mathcal{G}} \in \partial\mathcal{A}$ where $\tilde{g}_c(J_{\mathcal{G}})$ is not analytic the spins become critical on the very large graphs in the sum—they magnetise in the case of the Ising model. The limit $\tilde{g} \uparrow \tilde{g}_c(J^*)$ then describes a continuum theory of gravity interacting with matter. The matrix model solution [93, 94] for $W_{\mathcal{E}}$ shows that the Ising scaling exponents are shifted away from their regular $\mathbb{Z}^2$ lattice values; they are related to each other by the KPZ formula which can be understood in a number of ways as is discussed below in Section 4.3. Numerical simulations and series expansions for $\mathcal{C}$ [40] strongly suggest that the scaling exponents for Ising spins are not shifted from their regular lattice values, but no exact solution for $W_{\mathcal{C}}$ is known.

An alternative formulation of the CT interacting with matter is provided by working in the canonical ensemble with the graphs $C \in \mathcal{C}_\infty$. In principle we have a new measure $\mu_J(C)$ that reflects the relative weight of the Ising partition function $Z_C(J)$ on different graphs. As critical behaviour of the spins only occurs on very large graphs we might expect $\mu_J(C)$ to capture the same physics as the grand canonical partition function $W_{\mathcal{C}}$; unfortunately

$\mu_J(C)$ is yet to be constructed. An intermediate step is to analyse the critical properties of an Ising spin system living on a triangulation sampled from the UICT ensemble according to the measure μ, which we call the *quenched* model. In [76] it was shown that at small J this system has a unique Gibbs measure (corresponding to unmagnetised spins), while at large J (at least) two Gibbs measures co-exist (corresponding to two possible magnetised states); furthermore it was shown that almost surely (i.e. with probability one in the measure μ) the critical temperature is the same for any C. The main purpose of this chapter is to show that *if* this critical point leads to a scaling limit, *then* the corresponding field theory must contain operators with the same scaling exponents as those appearing in the scaling limit of the flat lattice Ising model.

4.3 Liouville gravity à la Duplantier-Sheffield

The Liouville gravity approach to computing the gravitational path integral was introduced by Polyakov [6]. We outline the basic features here (see [8, 9, 27] for a detailed review of the topic). Recall the Liouville path integral for pure gravity, taking background metric $\hat{g}_{ab} = \delta_{ab}$, is written formally as

$$Z[\Lambda] = \int \mathcal{D}\phi\, e^{-\int d^2z\, \partial_a\phi\partial^a\phi + \Lambda e^{\gamma\phi}}. \tag{4.3}$$

To make rigorous sense of (4.3) we must define the measure on ϕ. In the probabilistic approach to QFT, the idea is that the term $e^{-\int d^2z\, \partial_a\phi\partial^a\phi}$ is proportional to a Gaussian measure on the space of functions $\phi : D \to \mathbb{R}$ with Dirichlet boundary conditions where $D \subset \mathbb{R}^2$ [96]. This ensemble is called the *Gaussian free field* (GFF); it is a generalisation of Brownian motion to higher dimensions and is defined as follows.

Definition 4.3.1. *Let $D \subset \mathbb{R}^d$ be some domain and define the inner product on functions $f : D \to \mathbb{R}$ as*

$$\langle f, g\rangle_\nabla := \frac{1}{2\pi}\int_D \nabla f \cdot \nabla g\, d^dz\,, \tag{4.4}$$

and associated norm

$$||h||^2_\nabla := \frac{1}{2\pi}\int_D \nabla h \cdot \nabla h\, d^dz. \tag{4.5}$$

The GFF is defined to be the measure whose probability density is given by

$$\rho(h) = const.\ \exp\left\{\left(-\frac{1}{2}||h||^2_{\nabla}\right)\right\}. \tag{4.6}$$

The density $\rho(h)$ is nothing but the path integral measure for the massless free boson with Dirichlet boundary conditions. Hence the formal path integral (4.3) is defined rigorously as

$$\int \mathcal{D}\phi\, e^{-\int d^2z \partial_a\phi\partial^a\phi + \Lambda e^{\gamma\phi}} = \mathbb{E}[e^{-\int d^2z \Lambda e^{\gamma\phi}}], \tag{4.7}$$

where the expectation is over the GFF measure. Note that this measure does not exist as a well-defined function but can be considered in terms of generalised distributions. We refer the reader to [26, 97–101] for further details.

In this formulation of Liouville gravity, the cosmological constant couples to the random area

$$A = \int e^{\gamma\phi} d^2z\,, \tag{4.8}$$

generated by the GFF ϕ. On the common base space $[0,1]^2$ there are then two measures:

- The Lebesgue measure on $[0,1]^2$, d^2z;
- The random measure $d\mu_\gamma = e^{\gamma\phi}d^2z$, where ϕ is a GFF.

To visualise the random measure μ_γ, choose $\delta \in (0,1)$ and, starting with the base space $[0,1]^2$, iteratively divide squares into four quadrants to obtain the set of largest square regions $S_i \subset [0,1]^2$ such that $\mu_\gamma(S_i) \leq \delta$. This defines the *dyadic square decomposition* where each square has roughly the same quantum area δ. The decomposition is shown in figure 4.1 for a particular instance of the GFF. The strength of the fluctuations is determined by γ, which is in turn determined by the type of matter on the background through (2.6).

Duplantier and Sheffield [26] observed that a subset $K \subset [0,1]^2$ can be measured by using either the Lebesgue measure or the random measure. The random measure with fixed $\phi = 0$, *i.e.* no fluctuations in the 2D metric, is simply the Lebesgue measure, so the relationship between the two results characterises the effect of gravity on K. To make this relationship precise first define two kinds of balls:

Definition 4.3.2 (Euclidean and quantum balls)**.** *For all* $z \in [0,1]^2$:

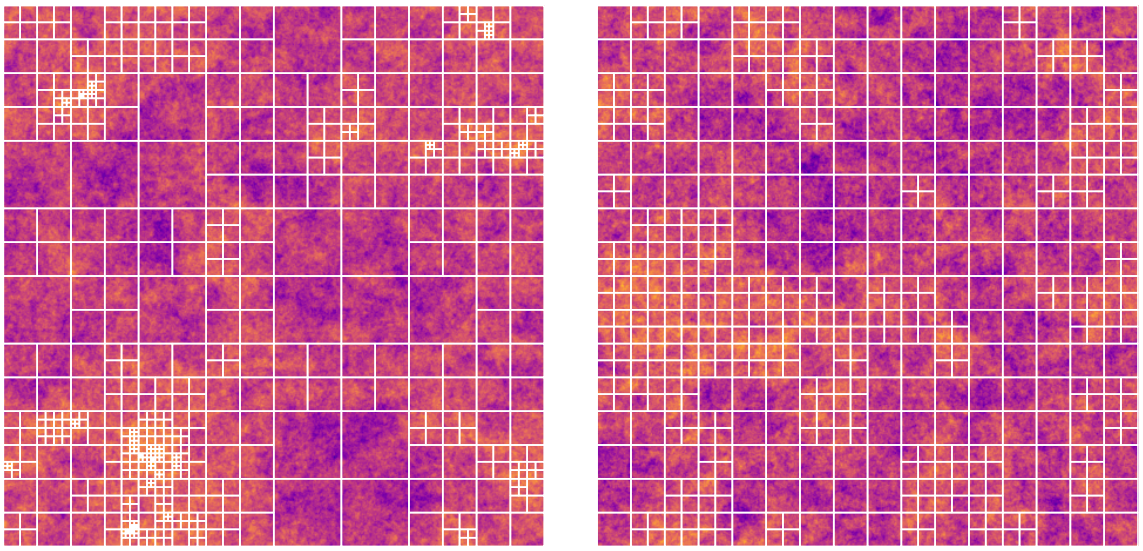

Figure 4.1: A dyadic decomposition of $e^{\gamma\phi}$ with $\gamma = 2$ (left) and $\gamma = 0.5$ (right). The colour represents the height of $e^{\gamma\phi}$.

- *$B_\epsilon(z)$ is the Euclidean ball of radius ϵ centred on z;*
- *$B^\delta(z)$ is the quantum ball centred on z and of quantum area δ i.e. It is the Euclidean ball $B_\tau(z)$ with $\tau := \sup\{r \geq 0,\ \mu_\gamma(B_r(z)) \leq \delta\}$.*

We can then define two different scaling exponents for some given (deterministic or random) subset $K \subset [0,1]^2$ [26]:

Definition 4.3.3 (Euclidean and quantum scaling)**.**

- *The **Euclidean scaling exponent** $x = x(K)$ is defined as*

$$x(K) := \lim_{\epsilon \to 0} \frac{\log \mathbb{P}[B_\epsilon(z) \cap K \neq \emptyset]}{\log \epsilon^2}, \tag{4.9}$$

  where z is sampled according to, and the probability $\mathbb{P}$ computed in, the Lebesgue measure;

- *The **quantum scaling exponent** $\Delta = \Delta(K)$ is defined as*

$$\Delta(K) := \lim_{\delta \to 0} \frac{\log \mathbb{E}[\mu_\gamma[B^\delta(z) \cap K \neq \emptyset]]}{\log \delta}, \tag{4.10}$$

  where z is sampled according to, and the expectation $\mathbb{E}$ computed in, the random measure μ_γ.

The main result of Duplantier-Sheffield [26] is the derivation of the *Knizhnik-Polyakov-Zamolodchikov* (KPZ) formula [90] that relates these two scaling dimensions by

$$x = \frac{\gamma^2}{4}\Delta^2 + (1 - \frac{\gamma^2}{4})\Delta. \tag{4.11}$$

Taking the Ising model as an example, we have $\gamma = \sqrt{3}$ and 2 primary fields ε, σ with scaling dimensions $x_\varepsilon = 1/2, x_\sigma = 1/16$. Using (4.11) we find that the quantum scaling dimensions take the shifted values

$$\Delta_\varepsilon = 2/3, \quad \Delta_\sigma = 1/6.$$

These are in agreement with the matrix model calculations of Kazakov et al [93, 94].

4.4 The Ising model and topological defects

The exact microscopic connection between topological defects in the two-dimensional Ising model and the corresponding fusion category was elucidated in [95], and then extended to general height models in [102]. In this section we review the formalism for the Ising model given in [95], and describe in detail how it can be applied to CT graphs of disk or annulus topology.

4.4.1 The Ising model in the plaquette formalism

Consider the Ising model with partition function $Z_G[\{J\}_G]$ (4.1) defined on a planar graph G. Now construct a new graph $\widetilde{G}$ formed by combining G with its dual G^* as follows: start with G and G^* overlaying each other, then join each G vertex to the nearest G^* vertices without crossing any original or dual edges, and finally remove the original and dual edges. See Figure 4.2 for the case when G is a square lattice. The graph $\widetilde{G}$ is formed of quadrilateral faces with opposite vertices belonging to the original or dual map. We call these quadrilateral faces *plaquettes*. It is important to note that the spins exist either on G or on G^*, but not both. Therefore, each plaquette only has 2 spins. Each plaquette represents an edge between spins on the original lattice.

If G is a CT, we have two types of plaquettes in $\widetilde{G}$, *horizontal* and *vertical* as shown in figure 4.3. By assigning weights to each plaquette we can rewrite the partition function as a product of these weights. First, we define u_H and u_V via

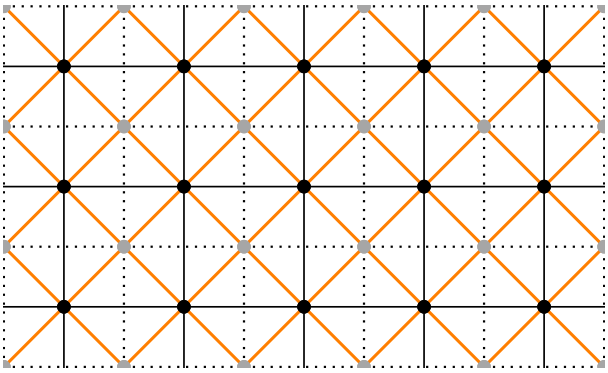

Figure 4.2: The graph $\widetilde{G}$ (orange) formed from the original square lattice (black), and its dual (gray, dashed).

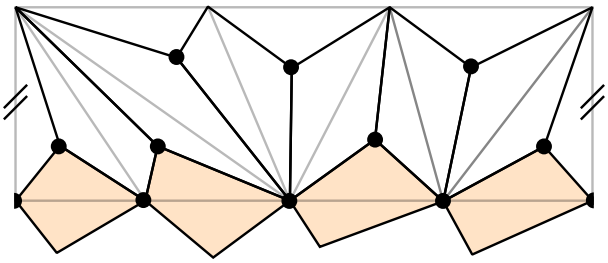

Figure 4.3: Horizontal (orange) and vertical plaquettes for a single CDT strip where the dots show the location of the weights d_v.

$$e^{2J_V} = \cot u_V, \quad e^{2J_H} = \cot\left(\frac{\pi}{4} - u_H\right), \tag{4.12}$$

where J_H and J_V are the couplings for horizontal and vertical edges respectively. It is useful in the context of defects to re-define the partition function to include a vertex factor d_v [95]

$$d_v = \begin{cases} 1 & \text{if } v \text{ has a spin;} \\ \sqrt{2} & \text{if } v \text{ is empty.} \end{cases} \tag{4.13}$$

We assign these weights to the plaquettes by splitting them between the left and right vertices. Since the vertical plaquettes only have spins on the top and bottom positions this gives an additional $\sqrt{2}$ factor. Horizontal plaquettes have spins on the left and right positions so the additional factor from the weights is 1. We then define the

weights for each plaquette

$$W_j^V(u_V) \equiv \quad = \sqrt{2}\,(\cos u_V \delta_{ab} + \sin u_V \sigma^x_{ab}) = \sqrt{2}\begin{cases}\cos u_V & a = b\\ \sin u_V & a \neq b\end{cases} \tag{4.14}$$

$$W_j^H(u_H) \equiv \quad = \frac{1}{\sqrt{2}}\,(\cos u_H + (-1)^{a+b}\sin u_H) = \begin{cases}\cos\left(\frac{\pi}{4} - u_H\right) & a = b\\ \sin\left(\frac{\pi}{4} - u_H\right) & a \neq b\end{cases}$$

where the labels are related to the spins by $\sigma = (-1)^a$. The partition function is now a product of plaquettes

$$Z_G[J_V, J_H] = \sum_{\{\sigma\}} \prod_{p \in \mathcal{P}_{\widetilde{G}}} a_p \quad c_p \ , \tag{4.15}$$

up to an analytic pre-factor, where $\mathcal{P}_{\widetilde{G}}$ denotes the set of plaquettes in $\widetilde{G}$.

4.4.2 The spin-flip defect

One can define an Ising model in the presence of a spin defect. A spin defect is a one-dimensional object that bisects a sequence of edges in the original lattice and swaps the couplings $J \to -J$, turning the interaction from ferromagnetic to anti-ferromagnetic and vice versa. We can implement this defect in the plaquette formalism by cutting a path along $\widetilde{G}$ and splitting the lattice in two – making a copy of every spin along the cut. We then insert a sequence of parallelograms which have a factor proportional to the Pauli matrix σ^x, enforcing that the spins on each side of the parallelogram are opposite. The weight of the parallelogram is

$$\quad = 2^{-1/4}[\sigma^x]_{a,b} = \begin{cases}0 & a = b\\ 2^{-1/4} & a \neq b.\end{cases} \tag{4.16}$$

With this definition, we can compute the effect of local manipulations and show that the spin defect can be moved around without changing the partition function i.e. it is a *topological defect*. In particular, for a defect to be topological, we must show the following defect commutation relations

$$\sum_{\text{internal spins}} \quad = \sum_{\text{internal spins}} \quad , \tag{4.17}$$

along with this diagram rotated by 90 degrees. We must also show

$$\sum_{\text{internal spins}}$$ 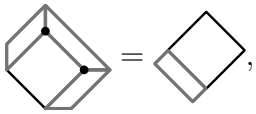 (4.18)

where the dots represent the weights d_v. These two relations for a general defect (represented by the gray parallelograms) show that you can move the defect line around the lattice without changing the partition function. It was shown by Aasen et al. [95] that with the definition of the spin defect in (4.16), these defect commutation relations are indeed satisfied.

Clearly stacking two spin-flip defects on top of each other is equivalent to having no defect at all. For this reason it will be convenient to introduce the identity defect which is constructed by inserting a string of parallelograms that simply identify the spins on each side

 $= 2^{-1/4}\delta_{ab}\,.$ (4.19)

4.4.3 The duality defect

The Ising model has one more non-trivial defect which implements the Kramers-Wannier duality of the Ising model [95]. The Kramers-Wannier duality replaces spins on the lattice with spins on the dual lattice. Hence, a duality defect must stitch together spins on G on one side with spins on G^* on the other – this is where the $\widetilde{G}$ picture comes into its own. We define the parallelogram for the duality defect as

 $= 2^{-1/2}(-1)^{ab}.$ (4.20)

It was shown in [95] that this too satisfies the defect commutation relations (4.17 - 4.18) proving that it is a topological defect. An important difference between the spin defect and the duality defect is the position of the spins. The spins are on diagonally opposite vertices of the parallelogram for the duality defect. This has the effect of changing the plaquettes from vertical to horizontal and vice versa i.e. $W^H(u_H) \to W^V(u_H)$ and $W^V(u_V) \to W^H(u_V)$.

As we already noted, the combination of two spin flip defects gives an identity defect. Further direct calculation [95] shows that any three defect lines, labelled α, β, γ, can interact at a triangle defect

(4.21)

which is non-zero only for certain allowed defect combinations. These are determined by the Ising *fusion category*, of which the identity, spin-flip and duality defects form a complete microscopic representation, and to which we now turn.

4.4.4 The Ising fusion category

The microscopic calculations shown in the previous sections and computed in detail in [95] allow us to forget about individual spins/plaquettes and instead deal directly with the extended defect lines. They form the structure of a *fusion category* that we will describe in this section. For completeness, we specify all the data of the Ising fusion category. We will not give a rigorous definition of fusion categories here but simply state the objects and the formal manipulations of them that are permitted. Any fusion category has a finite set of objects L, which in the case of the Ising category are the duality field σ, the spin field ψ and the identity $\mathbb{1}$. Each object is represented diagrammatically as a line in a graph. These objects satisfy an algebra, which in general, can be written as

$$a \times b = \sum_c N_{ab}^c \, c, \tag{4.22}$$

where $a, b, c \in \{\mathbb{1}, \psi, \sigma\}$ and $N_{ab}^c \in \mathbb{N}$. The Ising algebra is

$$\psi \times \psi = \mathbb{1}; \quad \psi \times \sigma = \sigma \times \psi = \sigma; \quad \sigma \times \sigma = \mathbb{1} + \psi. \tag{4.23}$$

The vertex factors d_a in (4.13) are called the *Frobenius-Perron dimensions* or *quantum dimensions* and are defined as the maximal eigenvalues of the algebra coefficient matrix $[N_a]_b^c$. Again, for the Ising category these are $d_\psi = d_\mathbb{1} = 1$ and $d_\sigma = \sqrt{2}$. The final piece of data in a fusion category is the set of *F-symbols*. These dictate the rules for

manipulations, called *F-moves*, of the diagrammatic representation of the combination properties of the objects in L. A general F-move takes the form

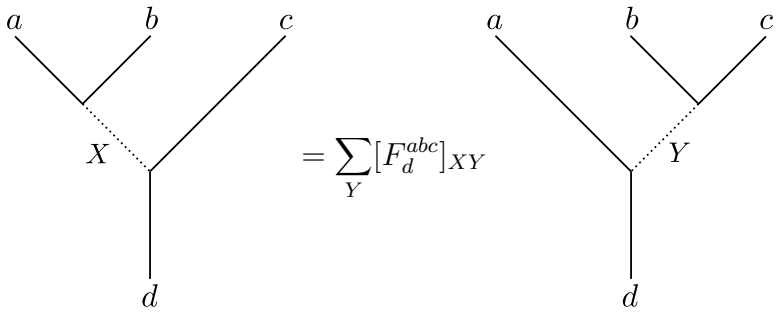

(4.24)

where the numbers $[F_d^{abc}]_{XY} \in \mathbb{R}$ are the F-symbols. These are not independent free parameters, they must satisfy a number of self-consistency conditions [102]. One such solution for the Ising category has the following non-trivial F-symbols:

$$\begin{aligned} &[F_\sigma^{\sigma\sigma\sigma}]_{\mathbb{1}\mathbb{1}} = [F_\sigma^{\sigma\sigma\sigma}]_{\mathbb{1}\psi} = [F_\sigma^{\sigma\sigma\sigma}]_{\psi\mathbb{1}} = \frac{1}{\sqrt{2}}, \\ &[F_\sigma^{\sigma\sigma\sigma}]_{\psi\psi} = -\frac{1}{\sqrt{2}}, \\ &[F_\psi^{\sigma\psi\sigma}]_{\sigma\sigma} = [F_\sigma^{\psi\sigma\psi}]_{\sigma\sigma} = -1. \end{aligned} \tag{4.25}$$

Any vertex that would imply the fusion of objects not allowed by the fusion algebra has a vanishing F-symbol. The remaining non-zero F-symbols in the Ising category are 1 if allowed by the fusion algebra. We can compute an arbitrary planar fusion diagram using (4.24–4.25) and the following rules:

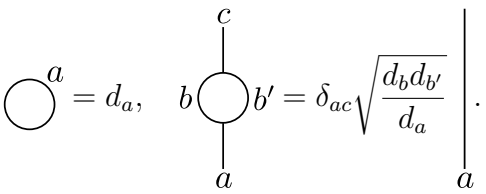

(4.26)

In Figure 4.4 we show some examples of the application of the F-moves to the manipulation of topological defects.

This association between topological defects in lattice models and fusion categories was fully established in [102] where it is shown that the construction extends to general height models.

4.4.5 Dehn twist operators on the lattice

A Dehn twist is an operation that cuts out a concentric circle at some finite distance from the origin, twists one half by a full revolution and glues the two halves back together at

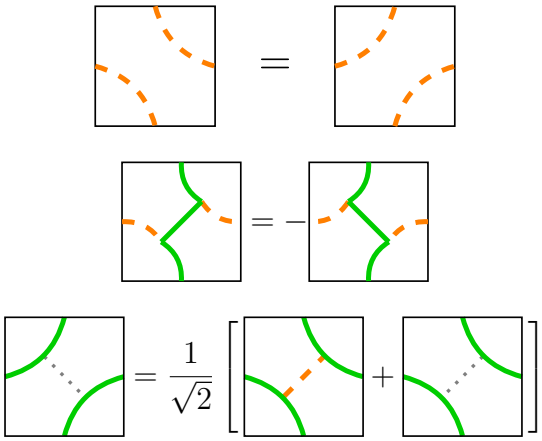

Figure 4.4: Non-trivial F-moves in the Ising fusion category. All of these moves are local and require no particular topology. The green solid line is the duality defect σ, the orange dashed line is the spin defect ψ and the thin dotted line is the identity $\mathbb{1}$ (which is often omitted in the diagrams).

the end. Here we show that operators that implement a Dehn twist can be constructed on a CT in a similar fashion to those constructed for a regular lattice in [95].

Consider the punctured plane $C \in \{\widetilde{C} \setminus D \mid \widetilde{C} \in \mathcal{C}_\infty\}$, where D is a topological disk. This is a natural space to consider for a CT because we often think of the graphs as starting from the inner boundary cycle $S_0(C)$ and evolving radially, equivalently in height. Let $C^h \subset C$ denote the subgraph of C consisting of all vertices and edges within a graph distance $h+1$ from $S_0(C)$ and including S_h as the outer boundary. Define $Z(C^h)$ to be the Ising partition function on C^h, with some boundary conditions described below, and represent it by the diagram

$$Z(C^h) = \quad , \tag{4.27}$$

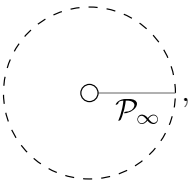

where $\mathcal{P}_\infty$ is a path from a marked point on the inner boundary to the outer boundary; it is convenient to choose $\mathcal{P}_\infty$ to be the relevant segment of the spine of $\beta^{-1}(\mathcal{C})$. Now insert an Ising topological defect that starts at a marked point on the inner boundary and extends to the outer boundary, crossing $\mathcal{P}_\infty$ n times; again it is convenient to choose the points where the defect intersects the boundaries to lie on the spine of $\beta^{-1}(\mathcal{C})$ as

these are always well defined. We denote the corresponding partition function $Z_n^\phi(C^h)$ where $\phi = \mathbb{1}, \psi, \sigma$ and represent it diagrammatically by

$$Z_n^\phi(C^h) =$$ 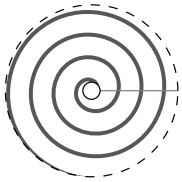 $$\mathcal{P}_\infty .$$ (4.28)

The boundary conditions are chosen so that the defects cannot be moved at the boundaries and hence unravelled. We show in Appendix A.1 that this can always be accomplished by an appropriate choice of spin values where the defect crosses the boundary.

This construction can also be viewed in a transfer matrix formalism [103]. For any height $0 \leq t \leq h$ we define the spin configuration $|\{h_i^t\}\rangle$ as a vector in a Hilbert space $\mathcal{H}_\phi$. The transfer matrix evolves a state $|\{h_i^t\}\rangle$ to a state $\left|\{h_i^{t+1}\}\right\rangle$. There is a subtle distinction here: unlike a regular square lattice, each height in a CT does not generally have the same number of spins. While this complicates writing a compact expression for the transfer matrix, this issue is purely aesthetic. Due to the topological nature of the defects, as guaranteed by (4.17) and (4.18), a defect whose plaquettes all sit at a height t can be moved to a height $t+1$ and hence commutes with the transfer matrix. As a result, we don't have to worry about at which height we define our defect operators in terms of plaquettes. We now show how to construct Dehn twists in the transfer matrix formalism.

Lemma 4.4.1 (Dehn twist operators)**.** *For all $C \in \{\widetilde{C} \setminus D \mid \widetilde{C} \in \mathcal{C}_\infty\}$, each defect $\phi = \psi, \sigma$ and every height t there is an operator $\mathbf{T}_\phi$ acting on the Hilbert space $\mathcal{H}_\phi$ at height t satisfying the relations*

1. $\mathbf{T}_\psi^2 - \mathbb{1}_\psi = 0$,

2. $\mathbf{T}_\sigma^4 - \sqrt{2}\mathbf{T}_\sigma^2 + \mathbb{1}_\sigma = 0$,

where the operators $\mathbb{1}_\phi$ act as the identity in the presence of a vertical defect ϕ, i.e. $\mathbb{1}_\phi |\{h_i\}\rangle = |\{h_i\}\rangle$.

Proof. Consider the first case, where we have a spin defect that runs from the inner boundary out to infinity without crossing $\mathcal{P}_\infty$ represented by the diagram

$$Z_0^{\psi}(C^h) = \quad . \tag{4.29}$$

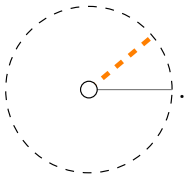

Choose $h > t' > t > 0$ and define the action of operators $\mathbb{1}_\psi$ and $\mathbf{T}_\psi$ at height t by cutting open the graph and inserting respectively a line of identity and spin-flip defect plaquettes as shown:

$\mathbb{1}_\psi =$ (4.30)

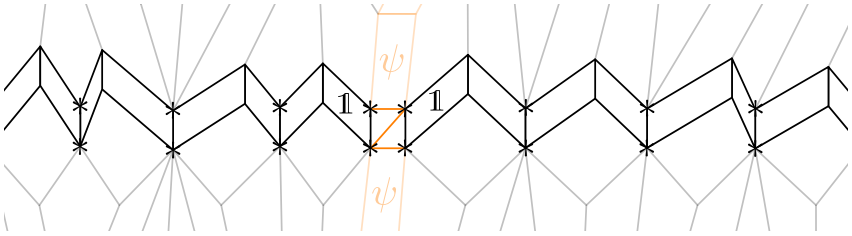

$\mathbf{T}_\psi =$ (4.31)

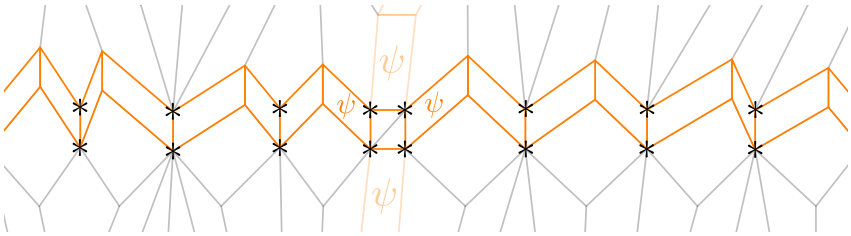

The square where the defects cross is simply two triangle defects (4.21) joined by an edge and summed over the defect label of that edge. Applying local moves in the partition function picture one can move the plaquettes to obtain:

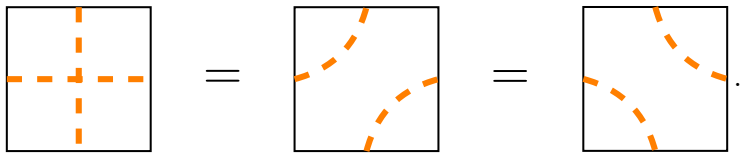

(4.32)

It follows that the partition function on C^h with a vertical spin-flip defect of twist number $n = 0$ and a horizontal spin-flip defect $\mathcal{D}_\psi$ inserted at height t satisfies

$$Z_0^{\psi\psi_t}(C^h) = Z_1^{\psi}(C^h). \tag{4.33}$$

That is to say the action of the operator $\mathbf{T}_\psi$ implements the Dehn twist. Now applying $\mathbf{T}_\psi^2$ at height t, we can use local moves to move one insertion of $\mathbf{T}_\psi$ to a height $t' > t$ and

apply F-moves to the defect lines to obtain

$$Z_0^{\psi\psi_t\psi_t}(C^h) = Z_2^{\psi}(C^h) =$$ 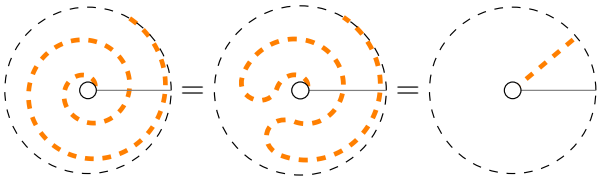 $$= Z_0^{\psi}(C^h)\,. \quad (4.34)$$

In the transfer matrix picture we therefore have $\mathbf{T}_\psi^2 \,|\{h_i\}\rangle = \mathbb{1}_\psi \,|\{h_i\}\rangle$. These manipulations apply for any $h > t+2$ so we can take h to infinity thus proving part 1 of the Lemma.

The calculation for the duality defect follows the same lines but with some added technical details. Consider a single duality defect that starts from the inner boundary and extends to infinity without wrapping around the centre shown diagrammatically by

$$Z_0^{\sigma}(C^h) =$$ 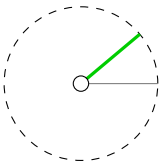 $$. \quad (4.35)$$

There is an additional subtlety in the duality case compared to the previous spin one. The duality defect interfaces between spins living on the vertices of C and spins living on the vertices of C^*. Due to the topology of the space we are considering, there must be another boundary where C and C^* meet again – this is the wall. We choose to place the wall along $\mathcal{P}_\infty$ for convenience. Crucially, we show in Appendix A.2 that the wall does not pose a problem in any manipulations that follow.

As before, we define an identity operator and an operator $\mathbf{T}_\sigma$ that act on the spins at height t in terms of the plaquettes

$\mathbb{1}_\sigma =$ 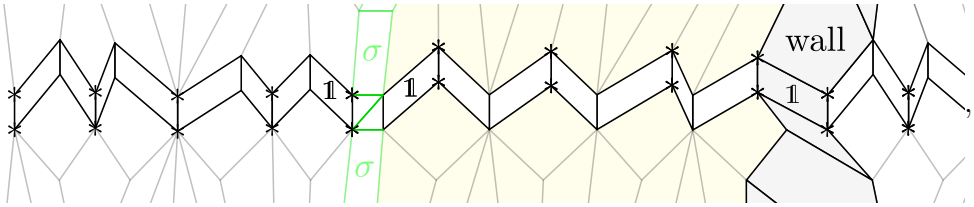

, (4.36)

$\mathbf{T}_\sigma =$ 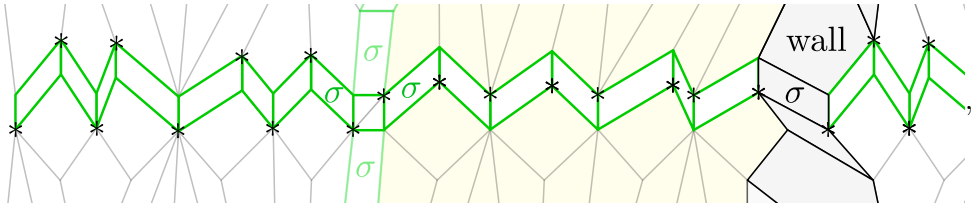

, (4.37)

where the appropriate wall plaquettes are included. The operators $\mathbb{1}_\sigma$ and $\mathbf{T}_\sigma$ can also be defined on the slice where the spins are on the other diagonals of the duality plaquettes. This gives us two isomorphic Hilbert spaces $\mathcal{H}_\sigma$ and $\hat{\mathcal{H}}_\sigma$. Currently, $\mathbf{T}_\sigma$ takes $\mathcal{H}_\sigma$ to $\hat{\mathcal{H}}_\sigma$ and vice-versa. Instead we can unify this into one operator that acts on $\mathcal{H}_\sigma \oplus \hat{\mathcal{H}}_\sigma$ [95].

Applying $\mathbf{T}_\sigma^2$ at height t and applying local topological moves, we can use the partition function picture and F-moves to compute the result:

$Z_2^\sigma(C^h) =$ 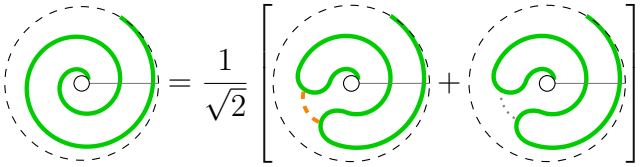 $= \frac{1}{\sqrt{2}}$,

$= \frac{1}{\sqrt{2}}$ 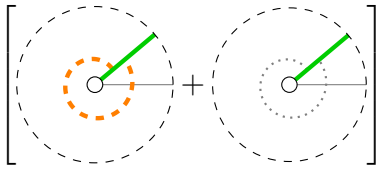 ,

where the details of how the defects pass through the wall can be found in Appendix A.2. In terms of the operators:

$$\mathbf{T}_\sigma^2 = \frac{1}{\sqrt{2}}\left(\psi_\sigma + \mathbb{1}_\sigma\right), \tag{4.38}$$

$$\mathbf{T}_\sigma^4 = \frac{1}{2}\left(\psi_\sigma + \mathbb{1}_\sigma\right)^2 = \frac{1}{2}\left(\mathbb{1}_\sigma + 2\psi_\sigma + \psi_\sigma^2\right), \tag{4.39}$$

where ψ_σ is an operator made of horizontal spin plaquettes in the presence of a vertical duality defect – we omit an explicit diagram for the sake of brevity. It remains to calculate ψ_σ^2, which is most easily done diagrammatically with the use of F-moves:

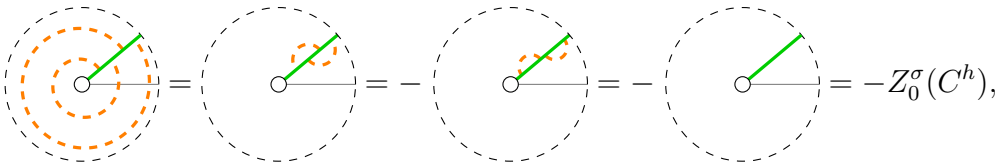

or in terms of operators $\psi_\sigma^2 = -\mathbb{1}_\sigma$, which gives us an algebraic equation for $\mathbf{T}_\sigma$:

$$\mathbf{T}_\sigma^4 = \sqrt{2}\mathbf{T}_\sigma^2 - \mathbb{1}_\sigma. \tag{4.40}$$

As before, this applies for any $h > t + 2$ so we can take h to infinity thus proving part 2 of the Lemma. □

Corollary 4.4.2 (Eigenvalues of Dehn twist operators)**.** *The eigenvalues of the operators* $\mathbf{T}_\psi$ *and* $\mathbf{T}_\sigma$ *are given by*

- $\mathbf{T}_\psi : \lambda = \pm 1$
- $\mathbf{T}_\sigma : \lambda = e^{2\pi i/16},\ e^{-2\pi i/16},\ e^{-2\pi i\cdot 7/16},\ e^{2\pi i\cdot 7/16}$

Proof. Both relations follow directly by turning the operator equations in Lemma 4.4.1 into eigenvalue equations. In the spin defect case, this becomes $\lambda^2 = 1$. In the duality defect case, we have $\lambda^4 - \sqrt{2}\lambda^2 + 1 = 0$. □

The Dehn twist operators described here are a topological construction on the graph C. Lemma 4.4.1 and Corollary 4.4.2 are exact statements of their properties which are independent of the values of the Ising weights and will persist in any continuum limit. Provided that the Dehn twist itself exists on continuum CTs, we can equate the eigenvalues of $\mathbf{T}_{\psi,\sigma}$ to those of $e^{2\pi i(L_0-\bar{L}_0)}$ which is the known form of the operator in the continuum. Before we can do this, we must first prove that it is possible to construct a Dehn twist on continuum CTs, which we do in the following section. Note that the above construction can be repeated for any height or Potts model whose fusion algebra has been worked out in [102] allowing us to extend the above arguments to those models.

4.5 Stochastic formulation of CDT

We derive a stochastic differential equation for the continuum length of the spatial slice $L(t)$ at time t starting from the discrete Galton-Watson process as an alternative to the results in [104, 105]. We then show how this generates a random measure on some base space in an exact analogy to the Liouville gravity picture.

4.5.1 The Lamperti-Ney Process

Theorem 4.5.1 (Lamperti-Ney Process)**.** *Let $L(t)$ be the length of the spatial slice at time t. Then $L(t)$ satisfies the Itô integral equation*

$$L(t) = L(0) + \int_0^t \sqrt{f''(1)L(s)}\, dW(s) + \int_0^t f''(1)\, ds, \tag{4.41}$$

or equivalently, the stochastic differential equation

$$dL(t) = \sqrt{f''(1)L(t)}dW(t) + f''(1)dt, \tag{4.42}$$

where $W(t)$ is a standard Wiener process and $f(s)$ is the generating function of the GW process. We call $L(t)$ a Lamperti-Ney Process (LNP) since it was first discovered by them [104].

Before we prove this we need to introduce some definitions and prove some lemmas. We mentioned that the ensemble of infinite CTs is in bijection to critical GW trees conditioned to survive forever. The number of points at height $k+1$, η_{k+1} is given by

$$\eta_{k+1} = \eta_k + \sum_{j=1}^{\eta_k - 1} Z_j + Z_0, \tag{4.43}$$

where $Z_j = Y_j - 1$ and $\{Y_j\}$ are i.i.d. random variables whose distribution is given by the generating function $f(s)$, i.e. they are the random variables whose value is the number of offspring of a point on the spatial slice. Similarly, $Z_0 = Y_0 - 1$ where Y_0 is the number of offspring of the special vertex on the infinite spine, which is distributed according to $sf'(s)$ [37]. We list the following results for future reference:

$$\begin{aligned} \mathbb{E}Z_k &= 0, \\ \mathbb{E}Z_0 &= f''(1), \\ \mathbb{E}[Z_k^2] &= f''(1). \end{aligned} \tag{4.44}$$

We define the re-scaled process $L_k^n := \eta_k/n$, where n is some integer which we will take to infinity at the end. Rewriting (4.43) in terms of L_k^n becomes

$$L_{k+1}^n = L_k^n + \frac{1}{n}\left(\sum_{j=1}^{nL_k^n - 1} Z_j + Z_0\right). \tag{4.45}$$

Lemma 4.5.2. *Define*

$$\xi_{k+1}^n = \frac{1}{\sqrt{nL_k^n}}\left[\sum_{j=1}^{nL_k^n - 1} Z_j + Z_0 - \mathbb{E}Z_0\right]. \tag{4.46}$$

Then $W_n(t) := \frac{1}{\sqrt{n}}\sum_{k=1}^{[nt]} \xi_k^n$ is a Martingale and $W_n(t) \Rightarrow W(f''(1)t) = \sqrt{f''(1)}W(t)$ where W is a standard Brownian motion. The convergence ($\Rightarrow$) is in distribution.

Proof. From Ethier & Kurtz [106] $W_n(t)$ is a Martingale if $\mathbb{E}[\xi_{k+1}^n | \mathcal{F}_k^n] = 0$, where $\mathcal{F}_k^n$ is the filtration at k. This is true since given L_k, ξ_{k+1}^n is a sum of random variables with mean 0. To show convergence in distribution as it is sufficient to show

$$\frac{1}{n}\sum_{k=1}^{[nt]} (\xi_k^n)^2 \to f''(1)t$$

in probability as $n \to \infty$.

$$\begin{aligned}\frac{1}{n}\sum_{k=1}^{[nt]}(\xi_k^n)^2 &= \frac{1}{n}\sum_{k=1}^{[nt]}\frac{1}{nL_k}\left(\sum_{i=1}^{nL_k-1} Z_i + Z_0 - \mathbb{E}[Z_0]\right)^2 \\ &= \frac{1}{n}\sum_{k=1}^{[nt]}\frac{1}{nL_k}\sum_{i=0}^{nL_k-1} Z_i^2 + \ldots \\ &\to f''(1)t\end{aligned} \tag{4.47}$$

where in the second to last line, we ignore cross terms (because the Z_i are independent) and the terms which will surely vanish as $n \to \infty$. In the final line, we used the law of large numbers and $\mathbb{E}[Z_i^2] = f''(1)$. □

Proof of Theorem 4.5.1. We can re-write equation 4.45 in terms of ξ_k as

$$L_{k+1}^n = L_k^n + \frac{\sqrt{L_k^n}}{\sqrt{n}}\xi_{k+1}^n + \frac{\mathbb{E}[Z_0]}{n}\,. \tag{4.48}$$

Following Kurtz and Protter [107] we define $L_n(t) := L_{[nt]}^n$, $W_n(t) := \frac{1}{\sqrt{n}}\sum_{k=1}^{[nt]}\xi_k^n$ and $V_n(t) := [nt]/n$ where $[nt]$ denotes the nearest integer to nt. It then follows that

$$L_n(t) = L_n(0) + \int_0^t \sqrt{L_n(s)}dW_n(s) + \int_0^t \mathbb{E}[Z_0]\; dV_n(s). \tag{4.49}$$

By Lemma 4.5.2 we know $W_n(t) \Rightarrow \sqrt{f''(1)}W(t)$ where W is a standard Wiener process and $V_n(t) \Rightarrow V(t) = t$. Kurtz and Protter [107] showed in general that for any process of this form, $L_n(t) \Rightarrow L(t)$ where $L(t)$ satisfies the integral stochastic equation

$$L(t) = L(0) + \int_0^t \sqrt{f''(1)L(s)}dW(s) + \int_0^t \mathbb{E}[Z_0]\; ds \tag{4.50}$$

or, in differential form,

$$dL(t) = \sqrt{f''(1)L(t)}dW(t) + f''(1)dt\,, \tag{4.51}$$

where we have used the fact that $\mathbb{E}[Z_0] = f''(1)$. □

Re-scaling $L(t) \to 2L(t)/f''(1)$ gives us exactly the result found in [105].

4.5.2 Scaling dimensions of Ising CFT fields

Equipped with the existence of the Lamperti-Ney Process, we can now explicitly construct a Dehn twist in a randomly sampled continuum CT as follows. Identify the ends of the spatial slices to obtain a space with the topology of a cylinder, where the circumference at height t is $L(t)$. Choose a curve c at height $t_0 + 1/2$ and let A be a neighbourhood of c which is homeomorphic to $S^1 \times [t_0, t_0 + 1]$. Noting that $L(t)$ is a continuous function, we define coordinates (s, t) on A where $s = e^{2\pi i x/L(t)}$, with $x \in [0, L(t)]$ and $t \in [t_0, t_0 + 1]$. Then the Dehn twist f is defined as

$$f : (e^{2\pi i x/L(t)}, t) \mapsto (e^{2\pi i (x+(t-t_0)L(t))/L(t)}, t)$$

or, in terms of the x coordinate, $x \mapsto x + (t - t_0)L(t)$. We observe that this construction does not exist for the Liouville case as the stochastic process described in Section 4.3 is not continuous.

Theorem 4.5.3 (Scaling dimensions of Ising CFT operators)**.** *Assume that a continuum limit of the Ising model on a CT exists and that the operators persist in the contiuum, then there exist fields in the CFT with spin $(L_0 - \bar{L}_0)$ given by*

- $h_\psi = 1/2 + n\,, n \in \mathbb{Z}$
- $h_\sigma = 1/16 + n\,, n \in \mathbb{Z}$

Proof. Firstly, the results of Corollary 4.4.2 are topological and so given the existence of a continuum limit, they persist at all scales. In the continuum, the known form of the Dehn twist operator is given by $e^{2\pi i(L_0 - \bar{L}_0)}$ and we have shown explicitly that it exists. Hence we can read off the spin of the field associated with ψ as $h_\psi = 1/2 + n,\ n \in \mathbb{Z}$, where we have chosen the $\lambda = -1$ sector. We are free to choose the sector because local manipulations of plaquettes prove that the Dehn twist operators $\mathbf{T}_\psi$ and $\mathbf{T}_\sigma$ always commute with the transfer matrix. Therefore, we can label a state by the eigenvalues λ_ψ, λ_σ and the spin configuration. Similarly for the duality defect, comparing the results of Corollary 4.4.2 to the continuum Dehn twist operator, we find that there is a sector where $h_\sigma = 1/16 + n,\ n \in \mathbb{Z}$. □

4.5.3 Properties of the Lamperti-Ney process

As we showed above, the LNP is defined by

$$dL(t) = \sqrt{f''(1)L(t)}\, dW(t) + f''(1)\, dt\,, \tag{4.52}$$

where $W(t)$ is a standard Wiener Process (WP) which has the property that

$$W_1(t) = x^{-\frac{1}{2}} W(xt) \tag{4.53}$$

$$W_2(t) = W(t+x) - W(x) \tag{4.54}$$

$$W_3(t) = tW(-t^{-1}) \tag{4.55}$$

are all WPs. In general if $g \in SL(2,\mathbb{R})/\{\pm\mathbb{1}\}$ (with the usual representation and $ad-bc=1$) then

$$W_g(t) = (ct+d)W\left(\frac{at+b}{ct+d}\right) - ct\, W\left(\frac{a}{c}\right) - d\, W\left(\frac{b}{d}\right) \tag{4.56}$$

is also a WP.

Lemma 4.5.4. *If $L(t)$ is an LNP, then so is $L_x(t) \equiv x^{-1}L(xt)$.*

Proof. From (4.52) we have

$$\begin{aligned} dL_x(t) = d(x^{-1}L(xt)) &= x^{-1}\, dL(xt) \\ &= \sqrt{f''(1)\, x^{-1}L(xt)}\, x^{-\frac{1}{2}} dW(xt) + f''(1)\, dt \\ &= \sqrt{f''(1)\, L_x(t)}\, dW_1(t) + f''(1)\, dt\,, \end{aligned} \tag{4.57}$$

where we have used (4.53). □

Now consider the 'square' segment of an LNP shown in Figure 4.5, then

Lemma 4.5.5. *The square area $S_x(L_0) \equiv x^{-2}S(xL_0)$, where $x > 0$, is equal in law to $S(L_0) = \int_{s=0,L(0)=L_0}^{L_0} L(s)\, ds$.*

Proof. Consider the scaled area process

$$S_x(L_0) = x^{-2}S(xL_0) = x^{-2}\int_{s=0,L(0)=xL_0}^{xL_0} L(s)\, ds. \tag{4.58}$$

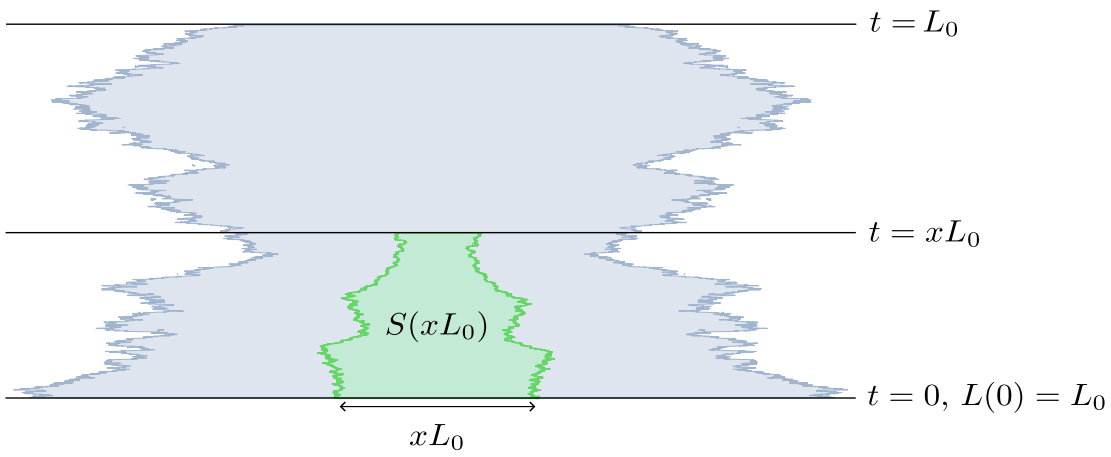

Figure 4.5: A segment of an LNP. The region shaded green is generated from a subset of the process at $t = 0$ and has area $S(xL_0)$.

Let $s = xt$, then

$$S_x(L_0) = \int_{s=0,\, x^{-1}L(0)=L_0}^{L_0} x^{-1} L(xt)\, dt. \tag{4.59}$$

Applying Lemma 4.5.4 to the r.h.s. then gives

$$S_x(L_0) = \int_{s=0, L_x(0)=L_0}^{L_0} L_x(t)\, dt, \tag{4.60}$$

which is equal in law to $S(L_0)$. □

In other words, $S(xL_0)$ is equal in law to $x^2 S(L_0)$ and so scales like a canonical 2D area.

Lemma 4.5.6. *The process $L(t), L(0) = L_0 > 0$ is strictly positive at all positive times.*

Proof. Let $L(t) = f''(1)L'(t)/4$, then

$$dL'(t) = 4dt + 2\sqrt{L'(t)}dW(t).$$

This is an $n = 4$ squared Bessel process which is strictly positive for all positive t [108].[1] □

As a consequence of being a scaled version of a squared Bessel process, (4.51) has a unique continuous solution provided $L_0 \geq 0$.

[1]The squared Bessel process governs the distance from the origin of a Brownian walk in $d = n + 1$ dimensions that starts at the origin. The process $L(t)$ thus describes the segment of such a walk from the time that it first reaches L_0. Brownian walks in $d > 2$ dimensions are non-recurrent so the walk never revisits the origin and $L(t)$ is strictly positive.

4.5.4 Classical and quantum scaling exponents in CDT

In this section we give another proof, in the spirit of the Duplantier-Sheffield construction, that scaling exponents on causal random geometry do not shift according to a KPZ-like relation. In the same way that DS used the volume term in the Liouville action to define a random measure $d\mu = e^{\gamma\phi}d^2z$ we can define a random measure for continuum CDTs as $d\mu = L(t)dtdx$, where $L(t)$ is a Lamperti-Ney Process (4.51). The spatial direction is uniform so we may write the two-dimensional measure as $d\mu = L(t)\,dt$, since the base space is $[0,1]\times[0,1]$. The solution $L(t)$ is a proper function of t so no regularisation of distributions is required in contrast to the case with the Liouville measure.

We are now in a position to show that the KPZ formula does not apply to CDTs in the continuum and in fact there is no shift in the scaling dimensions of fields on CDTs compared to a fixed lattice (up to logarithmic corrections). It will be convenient to rewrite the definitions of the scaling exponents (4.9–4.10) in a discrete form. First, consider dividing the base space $[0,1]\times[0,1]$ in two ways:

1. Into base cells $\mathcal{B} = \{B_\alpha,\, \alpha = 1, ..., 1/\varepsilon^2\}$ of classical area ε^2, $\varepsilon \ll 1$.

2. Into quantum cells $\{C_\alpha,\, \alpha = 1, ..., S(1)/\delta\}$ of quantum area δ, i.e. such that $\mu(C_\alpha) = \delta$. Let $\mathcal{B}_\alpha$ denote the set of base cells in C_α and $K_\alpha = |\mathcal{B}_\alpha|$.

Note that the decomposition according to the measure μ is much simpler than that of Liouville gravity. Due to the one–dimensional nature, the base space is divided into rows $i = 1, ..., n$, where each quantum cell in a row is the same size in the base space and has the same quantum area – see Figure 4.6. We use Greek subscripts when referring to an element of the complete set of cells and Latin subscripts to label the height of a cell. For example, C_i is a quantum cell at a height i in the base space – there is no need to distinguish the cell in the row, since they are all copies of each other.

Let X denote a random subset of $[0,1]\times[0,1]$ and $\mathcal{X} = \{b \in \mathcal{B} : b \cap X \neq \emptyset\}$ denote the set of base cells that intersect X.

Definition 4.5.1 (Discrete Euclidean and quantum scaling exponents)**.**

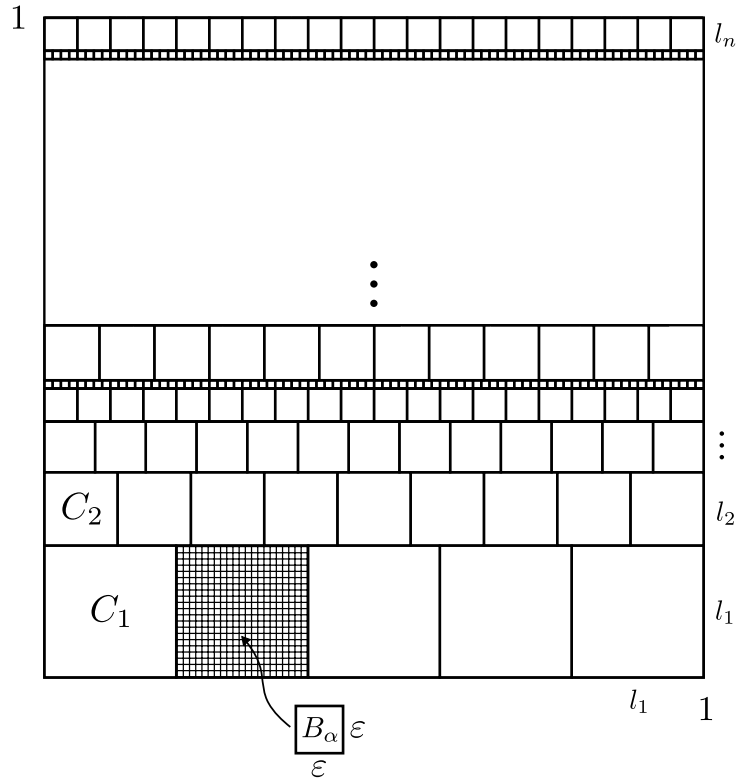

Figure 4.6: A decomposition of the base space $[0,1] \times [0,1]$ according to the measure μ.

- *The **Euclidean scaling exponent** $x = x(X)$ is defined as*

$$x(X) := \lim_{\varepsilon \to 0} \frac{\log \mathbb{E}_X[\varepsilon^2 N(\varepsilon, X)]}{\log \varepsilon^2}\,, \tag{4.61}$$

  where $N(\varepsilon, X)$ is the number of base cells that intersect X.

- *The **quantum scaling exponent** $\Delta = \Delta(X)$ is defined as*

$$\Delta(X) := \lim_{\delta \to 0} \frac{\log \mathbb{E}_X[\delta N_Q(\delta, X)]}{\log \delta}\,, \tag{4.62}$$

  where $N_Q(\delta, X)$ is the number of quantum cells that intersect X.

The expectation in both cases is over the ensemble of random subsets X.

Theorem 4.5.7. *The quantum scaling dimension $\Delta(X)$ and the classical scaling dimension $x(X)$ are equal for the measure $d\mu = L(t)dt$, where $L(t)$ is a LNP.*

Proof. By Lemma 4.5.5, a quantum cell C_i (see Figure 4.6) at height i and of quantum area δ covers a square in the base space of side length ℓ_i, where $\delta = \ell_i^2 S_i$ and S_i is sampled

from the law $S(1)$. Define the integer $n(\delta)$ by

$$n(\delta) = \max\{n : \sum_{i=1}^{n} l_i < 1\}\,. \tag{4.63}$$

As S_i is strictly positive and $\mathbb{E}[S_i^{-\frac{1}{2}}]$ is finite, this implies that, as $\delta \to 0$, we have $n(\delta)^2\delta = \mathcal{O}(1)$.

Let $p_X(\varepsilon) = \mathbb{P}[B_\alpha \cap X \neq \emptyset]$ be the *a priori* probability that X intersects a given base cell B_α. The probability $\mathbb{P}(C_i \cap X \neq \emptyset)$ that a given quantum cell C_i intersects the subset X is given by

$$\begin{aligned}\mathbb{P}[C_i \cap X \neq \emptyset] &= \mathbb{P}[\mathcal{B}_i \cap \mathcal{X} \neq \emptyset],\\ &= 1 - \mathbb{P}[\mathcal{B}_i \cap \mathcal{X} = \emptyset]\,.\end{aligned} \tag{4.64}$$

Letting

$$K_i^+ = \left\lceil \frac{l_i^2}{\varepsilon^2} \right\rceil \text{, and } K_i^- = \left\lfloor \frac{l_i^2}{\varepsilon^2} \right\rfloor, \tag{4.65}$$

we have

$$1 - (1 - p_X(\varepsilon))^{K_i^-} \leq \mathbb{P}(C_i \cap X \neq \emptyset) \leq 1 - (1 - p_X(\varepsilon))^{K_i^+}\,. \tag{4.66}$$

The quantity l_i^{-1} is not generally an integer, but we note that the quantum area, A_i, of the cells C_i satisfies

$$\delta \left\lfloor \frac{1}{l_i} \right\rfloor \leq A_i < \delta \left\lceil \frac{1}{l_i} \right\rceil\,. \tag{4.67}$$

Then, using (4.66) and (4.67), we find that the expectation of the area of quantum cells that intersect X is bounded above by

$$\mathbb{E}_X \delta N_Q(\delta, X) < \sum_{i=1}^{n(\delta)+1} \delta \left\lceil \frac{1}{l_i} \right\rceil (1 - (1 - p_X(\varepsilon))^{K_i^+}), \tag{4.68}$$

and below by

$$\sum_{i=1}^{n(\delta)} \delta \left\lfloor \frac{1}{l_i} \right\rfloor (1 - (1 - p_X(\varepsilon))^{K_i^-}) < \mathbb{E}_X \delta N_Q(\delta, X)\,. \tag{4.69}$$

Finally note that

$$p_X(\varepsilon) = \varepsilon^2 N(\varepsilon, X)\,, \tag{4.70}$$

and set $\delta = K\varepsilon^2$, where $K \gg 1$ is a fixed number. Then the quantum dimension converges to

$$\begin{aligned}\Delta(X) &= \lim_{\varepsilon\to 0} \frac{\log \mathbb{E}_X\left[\sum_{i=1}^{n(K\varepsilon^2)} \frac{K\varepsilon^2}{l_i}\left(\frac{l_i^2}{\varepsilon^2} + O\left(\frac{l_i}{\varepsilon}\right)\right)\varepsilon^2 N(\varepsilon, X)\right]}{\log K\varepsilon^2} \\ &= \lim_{\varepsilon\to 0} \frac{\log\left(K + O\sqrt{K}\right) + \log \mathbb{E}_X[\varepsilon^2 N(\varepsilon, X)]}{\log K\varepsilon^2} \\ &= x(X)\,, \end{aligned} \tag{4.71}$$

where we have used the fact that

$$\lim_{\varepsilon\to 0} \sum_{i}^{n(K\varepsilon^2)} l_i = 1. \tag{4.72}$$

□

We remark that this result is an inevitable outcome of the continuous, one dimensional nature of the measure.

4.6 Connection to Hořava–Lifshitz gravity

Before concluding this chapter, we comment on the connection to projectable Hořava–Lifshitz (HL) gravity that we first met in Chapter 2. Recall from Section 2.2, that the action for projectable HL gravity can be reduced to a one-dimensional action of the form [43]

$$S_E = \int dt \left(\frac{\dot{L}(t)^2}{4L(t)} + \Lambda L(t)\right). \tag{4.73}$$

We show that one can recover this action from the Lamperti-Ney Process. The Onsager-Machlup (OA) function allows us to write down a Lagrangian associated to any SDE [109–111]. In general, for an Itô process

$$dX_t = f(X_t)\,dt + \sigma(X_t)\,dW_t\,, \tag{4.74}$$

the OA function is given by

$$\mathcal{L}(\dot{x}, x) = \frac{(\dot{x} - f(x))^2}{2\sigma(x)^2}\,. \tag{4.75}$$

For the action (4.73), the OA function can be read off:

$$\mathcal{L}(\dot{L}, L) = \frac{\dot{L}^2}{4L}\,, \tag{4.76}$$

which is associated with the stochastic process satisfying the SDE

$$dL_t = \sqrt{2L_t}\, dW_t. \tag{4.77}$$

The associated formal path integral to the OA Lagrangian is

$$Z = \int \mathcal{D}L e^{-\int \mathcal{L}(\dot{L},L)dt}. \tag{4.78}$$

As is standard procedure in the probabilistic approach to quantum field theory (see [96]), we interpret the term

$$Z^{-1} e^{-\int \mathcal{L}(\dot{L},L)dt}\, \mathcal{D}L \tag{4.79}$$

as the measure which properly weights the paths given by the stochastic process.

The process in (4.77) is the Lamperti-Ney Process without the constant drift term. We now show that one can change measure to include the drift term and that the Radon-Nikodym derivative has a very simple and suggestive form.

Theorem 4.6.1. *Let $\mathbb{P}$ be the measure associated with the process defined by* (4.77) *and let $\widetilde{\mathbb{P}}$ be a new measure defined by the Radon-Nikodym derivative*

$$\frac{d\widetilde{\mathbb{P}}(t)}{d\mathbb{P}(t)} = \frac{L(t)}{L(0)}$$

then the process L_t satisfies

$$dL_t = 2dt + \sqrt{2L_t}\, d\widetilde{W}_t,$$

where

$$\widetilde{W}_t = W_t - \int_0^t \frac{2}{\sqrt{2L_t}} ds,$$

is standard Brownian motion under $\widetilde{\mathbb{P}}$.

Proof. The proof is a standard application of Girsanov's theorem. We first write the process (4.77) as

$$dL_t = 2dt + \sqrt{2L_t}\left(dW_t - \frac{2}{\sqrt{2L_t}} dt\right).$$

Girsanov's theorem states that the process

$$\widetilde{W}_t = W_t - \int_0^t \frac{2}{\sqrt{2L_t}} ds,$$

will be standard Brownian motion under the measure $\widetilde{\mathbb{P}}$ defined by the Radon-Nikodym derivative

$$\frac{d\widetilde{\mathbb{P}}(t)}{d\mathbb{P}(t)} = \exp\left\{\int_0^t \frac{2}{\sqrt{2L(s)}} dW(s) - \int_0^t \frac{1}{L(s)} ds\right\}.$$

A straightforward application of Itô's lemma shows that

$$d(\log L(t)) = \frac{2}{\sqrt{2L(s)}} dW(s) - \frac{1}{L(s)} ds,$$

hence

$$\log L(t) - \log L(0) = \int_0^t \frac{2}{\sqrt{2L(s)}} dW(s) - \int_0^t \frac{1}{L(s)} ds,$$

which proves the result. □

Under the change of measure defined in Theorem 4.6.1, expectations of random variables in the measure $\widetilde{\mathbb{P}}$ are given by $\widetilde{\mathbb{E}}[X] = \mathbb{E}[\frac{L(t)}{L(0)} X]$.

We are often interested in adding potential terms, such as a cosmological constant term, to the Lagrangian. These are then considered as observables whose expectation is being calculated with respect to the measure (4.79). For example, the partition function including a cosmological constant term is given by

$$\int \mathcal{D}L \, e^{-\int \mathcal{L}(\dot{L(t)}, L(t)) + \Lambda L(t)\, dt} = \mathbb{E}[e^{-\Lambda \int L(t)\, dt}], \tag{4.80}$$

where $\mathbb{E}$ is over paths sampled according to an SDE. For the LNP, this is indeed the correct cosmological constant term since $\int L(t)\, dt$ is the two dimensional volume. This particular observable also has the form of a killing term with rate function $r(l) = \Lambda\, l$. The expectation value of a general observable $F(L)$ is given by

$$\int \mathcal{D}L \, F(L(t)) e^{-\int \mathcal{L}(\dot{L}, L) dt} = \mathbb{E}[F(L(t))], \tag{4.81}$$

which may remind the reader of the expression that satisfies the Feynman-Kac formula. Indeed, if we specify an initial condition, say $L_0 = l$, then $\phi(l, \tau) = \widetilde{\mathbb{E}}[\, G(L(t)) e^{-\Lambda \int_0^\tau L(t)\, dt} \mid L_0 = l\,]$ satisfies the differential equation with a killing term

$$-\frac{\partial \phi}{\partial \tau} = -l \frac{\partial^2 \phi}{\partial l^2} - 2 \frac{\partial \phi}{\partial l} + \Lambda l \phi; \quad \phi(l, 0) = G(l), \tag{4.82}$$

where the expectation is taken with respect to the measure $\widetilde{\mathbb{P}}$. This is exactly the imaginary time Schrödinger equation with the CDT Hamiltonian [32, 105]. However, as discussed in [43], there is an ambiguity in the operator ordering of the Hamiltonian when it is quantised. The Hamiltonian is given by $H = L\Pi^2 + \Lambda L$, where $\Pi = -i\frac{\partial}{\partial L}$. The Hamiltonian in (4.82) corresponds to the ordering $H = -\frac{\partial^2}{\partial L^2}L + \Lambda L$, which is Hermitian on the space of square integrable functions with the measure $L\,dL$. This factor of L has its origin as the Radon-Nikodym derivative of changing from a process L_t without drift to one with a drift term $2\,dt$. It also corresponds to the discrete model where both entrance and exit loops are unmarked [43].

These results further corroborate the findings that 2D continuum CDT is 2D Projectable Hořava-Lifshitz gravity [43], this time showing the correspondence from the other direction.

4.7 Outlook and extension to the annealed case

In the quenched model, where a graph is first sampled from the UICT ensemble, and matter fields are subsequently placed on it, we have demonstrated that there is no change in the critical exponents compared to the flat lattice for any height model. In the particular case of the Ising model, Theorem 4.5.3 corroborates the numerical results in [40, 42, 112]. *If* a critical point exists, the topological defects and their associated fusion algebra persist in the continuum, being independent of any coupling constant. The continuity of the stochastic process $L(t)$, guarantees the existence of the Dehn twist in the continuum. Hence, the discrete arguments apply, showing that the conformal dimensions of the Ising operators are unchanged from their Onsager values.

This is in contrast to the KPZ relation in Liouville gravity, where even in the pure gravity case ($\gamma = \sqrt{8/3}$) we get a non-trivial relation between $x(X)$ and $\Delta(X)$. One way to explain this difference between causal and Euclidean random geometry is that there is no known way to define a Dehn twist in the Euclidean setting. In the discrete Euclidean picture, the set of vertices at a constant geodesic distance from a chosen origin is almost surely disconnected. The Dehn twist cannot be defined because there is no curve around which there exists a region homeomorphic to $S^1 \times [0, 1]$, due to the fractal nature of the

space. All that is to say, the unique properties of causal random geometry allow us to readily extend the arguments in [95, 102] to CTs but not to Euclidean triangulations.

In the *annealed model*, which amounts to sampling a graph $C \in \mathcal{C}_\infty$ according to the measure $\mu_J(C)$, we do not know the exact form of the process that describes the evolution of the random geometry. The immediate technical obstacle is the absence of a known tree bijection for the matter-coupled system, which is essential to construct the discrete difference equation (4.43) and hence the SDE in the continuum limit. One might bypass the explicit construction of a tree bijection by arguing that, due to the restriction to causal graphs with a global time foliation, a one-dimensional stochastic process $X(t)$ must still emerge and our results apply. This relies on the annealed model not undergoing a first-order phase transition that would destroy the extended structure of the graphs that is necessary for representing two-dimensional geometries. In any case, to fully extend our arguments to the annealed case, it is necessary and sufficient to prove the continuity of $X(t)$. If that can be done for any particular model that couples unitary matter to CDT, and there is a second order phase transition at which a continuum limit can be defined, then the corresponding conformal dimensions must be unchanged from the regular lattice case.

Another interesting observation comes from the functional renormalisation group equation (FRGE) analysis of the matrix model representation of CDT [49]. The authors find that the anomalous dimension vanishes due to the presence of the matrices C (not to be confused with the causal graph) that impose the causal structure in the ribbon graphs. Since it is exactly the anomalous dimension that shifts the scaling exponents, it follows that there should be no KPZ–like relation. The same analysis of the Ising–CDT matrix model defined in [51] comes to the same conclusion [113]. In fact, it is clear that any matrix model description of CDT coupled to matter that uses these C matrices to impose the causal constraint will contain vanishing anomalous dimensions. We elaborate on this further in the next chapter.

Finally, it is hard to say whether these results could be extended to higher dimensions. One would need to construct the equivalent topological defects, and the development of the constant time hypersurface would not be described by a simple one-dimensional stochastic process. This would be an interesting future direction.

5

A Renormalisation Group Analysis of the Ising Model Coupled to Causal Dynamical Triangulations

Contents

5.1 Introduction

Following on from Chapter 4, we continue to consider the interplay between matter and geometry in two-dimensional CDT coupled to the Ising model—our favourite toy model of matter. Specifically, we adopt a matrix model representation of this coupled Ising-CDT system, as introduced in [51], and investigate its fixed-point structure using Functional

Renormalisation Group (FRG) methods [52–55, 114]. Fixed points of the FRG represent potential double scaling limits of the matrix model, where $N \to \infty$ and couplings scale towards a critical value, the scaling being characterised by a critical exponent. Following the approach of [50], where FRG techniques were applied to tensor models, we extend the results of Castro and Koslowski [49], who first applied FRG methods to the pure CDT matrix model by Benedetti and Henson [48]. In particular, we demonstrate the existence of fixed points of RG flow in the Ising-CDT matrix model with precisely the right number of relevant directions to describe a continuum Ising CFT. More specifically, we show that the number of relevant directions matches the three primary fields of the Ising CFT [94]. Moreover, we find other types of fixed points with different numbers of relevant directions. These could, in principle, represent different continuum limits of the discrete theory. One of our main findings is that the parameter space has a rich structure, including segments such that all points on the segment are fixed points of the RG flow.

The chapter is organised as follows. In Section 5.2, we review the main features of the pure CDT and Ising-CDT matrix models. In Section 5.3, we set up the Functional Renormalisation Group Equation (FRGE) for the Ising-CDT matrix model. Section 5.4 presents the derivation of the general form of the beta-function equations. Finally, we analyse the fixed-point structure in Section 5.5.

5.2 A Matrix Model for Ising CDT

The matrix model for pure CDT was introduced by Benedetti and Henson (BH) [48] and is defined by the following partition function

$$Z = \int \mathcal{D}A\,\mathcal{D}B e^{-N\,\mathrm{Tr}\left[\frac{1}{2}A^2+\frac{1}{2}(C^{-1}B)^2-gA^2B\right]},$$

with Hermitian matrices A and B, along with the constant matrix C that satisfies (in the large N limit) the condition

$$\mathrm{Tr}[C^m] = N\delta_{m,2}\,, \quad m > 0\,. \tag{5.1}$$

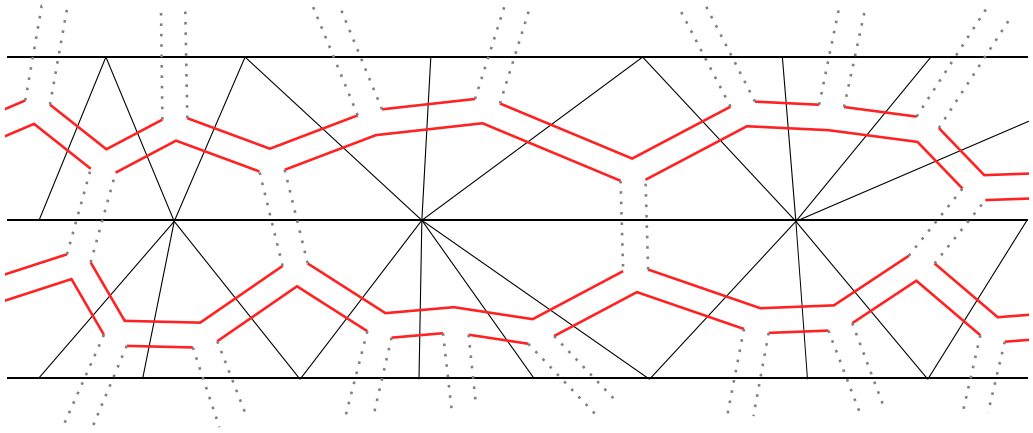

Figure 5.1: An example of a CDT strip and the dual ribbon graph. The red lines are the propagators for the A matrix and the gray dashed lines are the B propagators.

The propagators of the model are given by

$$\langle A_{ij}A_{kl}\rangle = \frac{1}{N}\delta_{il}\delta_{jk}, \quad \langle B_{ij}B_{kl}\rangle = \frac{1}{N}C_{il}C_{jk}, \quad \langle A_{ij}B_{kl}\rangle = 0\,.$$

In the perturbative expansion of the matrix integral, as we saw in Section 2.4.3, Wick contractions generate ribbon (fat) graphs. In the BH model, the generated graphs have two types of edges: A (space-like) and B (time-like). The generated graphs are *dual* to the standard construction of CDT graphs. That is to say, vertices of the triangulation are dual to faces of the fatgraph, and space-like edges in the triangulation are dual to time-like edges in the fatgraph and vice-versa (see Figure 5.1). CDT triangles have two time-like and one space-like edge, which in the dual graph become trivalent vertices of type AAB. The interaction $\mathrm{Tr}(A^2B)$ therefore produces precisely the allowed local vertex structure. The remaining CDT requirement, that is, the existence of a global foliation and absence of spatial topology change, can be enforced by a local "rigidity" condition: a connected fatgraph with only AAB vertices in which every face contains either exactly two or zero B-edges is equivalent to a 2D CDT configuration [48]. Each face with m internal B lines contributes a factor of $\mathrm{Tr}[C^m]$, hence the condition (5.1) ensures that, in the large N limit, each face has either two or zero B-lines (time-like edges). These local requirements are sufficient to generate valid CDT graphs with a global foliation [48].

The B field can be integrated out to obtain a simpler expression only in terms of the A matrix:

$$Z = \int \mathcal{D}A\, e^{-N \operatorname{Tr}\left[\frac{1}{2}A^2 - \frac{g^2}{2}(A^2C)^2\right]}. \tag{5.2}$$

The matrix model (5.2) was considered in [49] from the point of view of the Functional Renormalisation Group Equation (FRGE). In particular, it was shown that the theory admits different possible continuum limits, represented by the UV fixed points of the Renormalisation Group flow obtained by varying the matrix size N.

This work extends the analysis to CDT coupled to the Ising model. In order to do so, we need a matrix model which describes the coupling of the Ising model to CDT. In particular, the theory must account for the spin degree of freedom at each vertex of the dual fat graph, which takes values in $\{-1, +1\}$. Moreover, the edges connecting vertices with the same or different spins must be distinguished. It stands to reason therefore that we need to double the number of matrices. The matrix model that accounts for these requirements is the four-matrix model given by [51], which generalises the model by BH:

$$Z = \int \mathcal{D}A_+ \mathcal{D}A_- \mathcal{D}B_+ \mathcal{D}B_-\, e^{-NS},$$

where the action S is

$$S = \operatorname{Tr}\Big[\frac{1}{2}A_+^2 + \frac{1}{2}(C^{-1}B_+)^2 + \frac{1}{2}A_-^2 + \frac{1}{2}(C^{-1}B_-)^2 \\ - \gamma A_+A_- - \gamma(C^{-1}B_+)(C^{-1}B_-) - gA_+^2B_+ - gA_-^2B_-\Big].$$

The matrix C satisfies the property (5.1) and the propagators are given by

$$\begin{aligned}
\langle A_{+,ij}A_{+,kl}\rangle &= \langle A_{-,ij}A_{-,kl}\rangle = \frac{1}{N}\frac{1}{1-\gamma^2}\delta_{il}\delta_{jk},\\
\langle B_{+,ij}B_{+,kl}\rangle &= \langle B_{-,ij}B_{-,kl}\rangle = \frac{1}{N}\frac{1}{1-\gamma^2}C_{il}C_{jk},\\
\langle A_{+,ij}A_{-,kl}\rangle &= \frac{1}{N}\frac{\gamma}{1-\gamma^2}\delta_{il}\delta_{jk},\\
\langle B_{+,ij}B_{-,kl}\rangle &= \frac{1}{N}\frac{\gamma}{1-\gamma^2}C_{il}C_{jk}, \quad \langle A_{I,ij}B_{J,kl}\rangle = 0,
\end{aligned}$$

where $I, J = +, -$ in the last equation. The ribbon graphs generated by the perturbative expansion will have the same structure as the BH model since we still only have cubic

vertices and the same contraint on the matrix C. The matrices labelled A still represent space-like edges and B their time-like counterparts. Beyond the BH model, we now interpret the graphs to have spins on the vertices of the ribbon graph (faces of the triangulation) which is expressed in the matrix model by restricting the cubic interaction to only $A_+^2 B_+$ and $A_-^2 B_-$. Furthermore, we have propagators that allow for a different interaction between spins of the same parity and those with opposite parity—the interaction between opposite parity spins has an additional factor of γ. With these features, it is clear that this model generates graphs that both satisfy the CDT constraints and have interacting spins living on the vertices.

Once again, the matrices B_+ and B_- can be integrated out to obtain a simplified expression

$$Z = \int \mathcal{D}A_+ \mathcal{D}A_- \, e^{-N \operatorname{Tr}\left[\frac{1}{2}A_+^2 + \frac{1}{2}A_-^2 - \gamma A_+ A_- - \frac{1}{2}\frac{g^2}{1-\gamma}(A_+^2 C)^2 - \frac{1}{2}\frac{g^2}{1-\gamma}(A_-^2 C)^2 - \frac{1}{2}\frac{\gamma g^2}{1-\gamma^2}\left((A_+^2 + A_-^2)C\right)^2\right]}. \tag{5.3}$$

It is convenient to define $U = (A_+ + A_-)/\sqrt{2}$ and $V = (A_+ - A_-)/\sqrt{2}$ in order to diagonalise the kinetic part of the action.

$$Z = \int \mathcal{D}U \mathcal{D}V \, e^{-N \operatorname{Tr}\left[\frac{1}{2}(1-\gamma)U^2 + \frac{1}{2}(1+\gamma)V^2 - \frac{1}{4}\frac{g^2}{1-\gamma}((U^2+V^2)C)^2 - \frac{1}{4}\frac{g^2}{1+\gamma}((UV+VU)C)^2\right]}. \tag{5.4}$$

This transformation takes the Ising model with spins defined on the vertices of the ribbon graph to one where the spins live on the faces. Since the triangulation is the dual of the ribbon graph, the Ising spins now live on the vertices of the CDT. The matrices now have the interpretation that U defines an edge in the ribbon graph that separates faces of equal parity (i.e. both spin up or both spin down) and V separates faces of opposite parity. The action in (5.4) is symmetric under $U \to -U$ and $V \to -V$ and hence has a $\mathbb{Z}_2 \times \mathbb{Z}_2$ symmetry. This symmetry implements the logical consistency condition that the four spins that live on the faces around the 4-valent vertices cannot exist in any configuration where only one edge has opposite parity and the other three are all the same. The same is true if three of the edges have opposite parity; then this implies the fourth edge must have opposite parity. Hence, Us and Vs can only come in pairs. Furthermore, we follow [49] and write the action as

$$S = N \operatorname{Tr}\Big[\frac{1}{2}(1-\gamma)UU^T + \frac{1}{2}(1+\gamma)VV^T - \frac{1}{4}\frac{g^2}{1-\gamma}\Big((UU^T+VV^T)C\Big)^2 - \frac{1}{4}\frac{g^2}{1+\gamma}\Big((UV^T+VU^T)C\Big)^2\Big], \quad (5.5)$$

This creates a symmetry in the index structure of the action, which is convenient in our calculations. It does not change any of the above discussion and, from now on, we will deal exclusively with this action.

Analysing this matrix model from a Functional Renormalisation Group perspective will be the goal of the rest of the chapter. In particular, we will show that it admits a continuum limit at fixed points of the FRGE flow.

5.3 Functional Renormalisation Group Equation

In this section, we discuss the Functional Renormalisation Group Equation (FRGE) for the Ising-CDT matrix model given in (5.5), which will allow us to derive the β-function equations in the following section.

The following sections involve heavy use of index notation. To help with readability, we summarise our conventions in the following table.

Symbol	Meaning
a, b, c, d	Matrix indices in $\{1, \ldots, N\}$
$I, J, K \in \{1, 2\}$	"Parity" indices: $U_I \in \{U_1, U_2\}$ where $U_1 := U$, $U_2 := V$
i, j, k, l, h, m	Labels for couplings $g_4^{(i)}, g_6^{(h)}$ of distinct operators $O_4^{(i)}, O_6^{(h)}$

Table 5.1: Index and symbol conventions used in Sections 5.3 and 5.4.

The FRGE is a differential equation for a momentum-dependent effective average action $\Gamma_k[\phi]$, where ϕ is a general scalar field. See [114] for a general treatment and [50] for an application to matrix models. We provide a brief introduction as it applies to (5.3) here.

The idea is to construct an effective action where momentum modes above the scale k have been integrated out while maintaining those modes below k. The trick introduced in [114] is to give a momentum-dependent mass to modes below the scale k, which suppresses them in the functional integral and allows only the higher modes to be integrated. This

is achieved by adding a term $\Delta S_k = \frac{1}{2}\phi R_k \phi$ to the action. We can then define the effective generating functional $W_k[J]$ as

$$e^{-W_k[J]} = \int \mathcal{D}\phi e^{-S[\phi]+J\cdot\phi-\Delta S_k},$$

and the effective action as a modified Legendre transform

$$\Gamma_k[\phi] = \sup_J \{\int d^n x J(x)\phi(x) + W_k[J]\} - \Delta S_k. \tag{5.6}$$

Therefore, $\Gamma_k[\phi]$ interpolates between the quantum 1PI effective action and the bare action: $\lim_{k\to 0}\Gamma_k = \Gamma$ and $\lim_{k\to\Lambda}\Gamma_k = S$. The IR-suppression term R_k gives modes with $p^2 < k^2$ an effective mass of order k (heuristically, $R_k(p) \sim k^2\,\theta(k^2 - p^2)$), which suppresses their fluctuations in the path integral. In the matrix-model realisation used here, the role of k is played by the matrix size N and R_N acts as a mass term of order N for index modes with $(a+b)/2 < N$ [cf. eq. (5.16)].

The form of $R_k(p)$ in momentum space can be anything that satisfies the following conditions. It must give a mass to modes $p^2 < k^2$ and smoothly decrease to zero for $k^2 < p^2 < \Lambda^2$, where Λ is a UV cutoff. It must also satisfy,

$$\lim_{k\to 0} R_k(p) = 0$$

which ensures that

$$\lim_{k\to 0} \Gamma_k[\phi] = \Gamma[\phi],$$

the full effective action for the 1PI correlation functions. Finally, $R_k(p)$ must satisfy

$$\lim_{k\to\Lambda\to\infty} R_k(p) = \infty,$$

which ensures the saddle-point evaluation of the functional integral so that

$$\lim_{k\to\Lambda\to\infty} \Gamma_k[\phi] = S[\phi].$$

In the case of tensor (and matrix) models, $\phi_{a_1,\ldots,a_m}$ is a rank-m tensor and the scale k is given by the tensor (matrix) size N. The suppression term essentially gives a mass

to the matrix entries $a, b = 1, ..., N$. For the model in (5.3), we define the effective generating functional as

$$e^{-W_N[J]} = \frac{1}{\mathcal{N}_N} \int_\Lambda \mathcal{D}U\mathcal{D}V e^{-S[U,V]+J^U_{ab}U^{ab}+J^V_{ab}V^{ab}-\Delta S_N[U,V]} .$$

where $\mathcal{N}_N$ is an N-dependent normalisation factor, Λ is a UV cutoff on N and $\Delta S_N[U, V]$ is the IR suppression given by

$$\Delta S_N[U, V] = \sum_{I,J=1}^{2} \frac{1}{2} U^{ab}_I R^{IJ}_{N,abcd} U^{cd}_J ,$$

where we define $U_1 := U, U_2 := V$ for notational convenience. Then by analogy to (5.6), the effective action is given by

$$\Gamma_N[U, V] = \sup_J \{J^U_{ab}U^{ab} + J^V_{ab}V^{ab} + W_N[J]\} - \Delta S_N[U, V] . \tag{5.7}$$

In [114], Wetterich derived the following equation for Γ_N under a change of the IR scale N

$$\partial_t \Gamma_N = \frac{1}{2} \mathrm{Tr}\Big(\frac{\partial_t R_N}{R_N + \Gamma^{(2)}_N} \Big) , \tag{5.8}$$

where $t = \log N$ and $\Gamma^{(2)}_N$ is the second derivative with respect to the matrix components

$$\Gamma^{(2)}_{N,\,abcd}[U, V]_{IJ} = \frac{\delta}{\delta U^{ab}_I} \frac{\delta}{\delta U^{cd}_J} \Gamma_N[U, V] .$$

Equation (5.8) is the Functional Renormalisation Group Equation (FRGE).

The usual procedure to derive the effective action consists of writing down the most generic action compatible with symmetries. Then a suitable truncation is chosen to make explicit computations possible. Equation (5.8) translates into a beta-function equations for the coupling constants of operators in the effective action. As we explained in the previous section, we consider all operators with an even number of Us and Vs. Furthermore, we have an $O(N)$ symmetry acting on the right of the matrix fields

$$U \to UO, \quad V \to VO. \tag{5.9}$$

Therefore, we only consider the combinations UU^T, UV^T, VU^T and VV^T in the effective action.

Following [49], we choose a truncation of the effective action that only includes operators with two C matrices. We also restrict to the set of single trace operators, as this was shown to be a good approximation for matrix models [49, 50].

With this in mind, we can write the effective action as

$$\Gamma_N = \frac{Z_U}{2}\,\mathrm{Tr}\Big[UU^T\Big] + \frac{Z_V}{2}\,\mathrm{Tr}\Big[VV^T\Big] + \sum_{n=2}^{\infty}\sum_j \frac{\bar{g}_{2n}^{(j)}}{2n} O_{2n}^{(j)}\,, \tag{5.10}$$

where Z_U and Z_V are wavefunction renormalisation factors. The operators $O_{2n}^{(j)}$ are defined as

$$\begin{aligned} O_4^{(j)} &= \mathrm{Tr}\Big[U_{I_1}U_{I_2}^T C U_{I_3}U_{I_4}^T C\Big] \\ O_{2n}^{(j)} &= \mathrm{Tr}\Big[U_{I_1}U_{I_2}^T C U_{I_3}U_{I_4}^T C \underbrace{U_{I_5}U_{I_6}^T ... U_{I_{2n-1}}U_{I_{2n}}^T}_{n-2 \text{ terms}}\Big], \quad n>2, \end{aligned} \tag{5.11}$$

and $I_k \in \{1,2\}, \forall k$, $U_1 = U, U_2 = V$ as before and j labels the set of configurations permitted by the symmetries of the action discussed above. The ones that we will consider explicitly are $O_4^{(j)}$ and

$$O_6^{(j)} = \mathrm{Tr}\Big[U_{I_1}U_{I_2}^T C U_{I_3}U_{I_4}^T C U_{I_5}U_{I_6}^T\Big].$$

Following [49], we truncate the expansion in (5.10) at $n=3$, to account for the terms which contribute to the beta function of the bare action at one loop. There are 5 distinct O_4 operators allowed by the symmetries so $j = 1, ..., 5$. The symmetry allows any operator that has an even number of Us and Vs so we count them by simply summing the even binomial coefficients $\sum_{k=0}^{2}\binom{4}{2k} = 8$. However, this over-counts because

$$\mathrm{Tr}\Big[UU^T CVV^T C\Big] = \mathrm{Tr}\Big[VV^T CUU^T C\Big]$$

due to the cyclic property of the trace. The same is true for

$$\mathrm{Tr}\Big[UV^T CVU^T C\Big] = \mathrm{Tr}\Big[VU^T CUV^T C\Big]\,.$$

Moreover

$$UV^T CUV^T C = (VU^T CVU^T C)^T\,,$$

implying that their trace yields the same operator, namely

$$\mathrm{Tr}\Big[UV^T CUV^T C\Big] = \mathrm{Tr}\Big[VU^T CVU^T C\Big]\,.$$

Hence, we are left with 5 distinct operators at fourth-order. For O_6 operators, the over-counting is not due to the cyclicity of the trace because, in our basis, the two C matrices sit at fixed positions. Cyclic permutations of the index pattern generally move the C insertions and therefore produce distinct basis elements within our truncation. After modding out only by reversal (transpose) symmetry, the $2^5 = 32$ naive patterns reduce to 20 distinct O_6 operators.

We re-scale the kinetic term to its canonical coefficient and introduce the dimensionless couplings $g_{2n}^{(j)}$ for $n = 2, 3$, given by

$$\bar{g}_4^{(j)} = Z_U^{N_U^{(j)}/2} Z_V^{N_V^{(j)}/2} N^{\alpha_4} g_4^{(j)}, \quad \bar{g}_6^{(j)} = Z_U^{N_U^{(j)}/2} Z_V^{N_V^{(j)}/2} N^{\alpha_6} g_6^{(j)}, \tag{5.12}$$

where $N_U^{(j)}$ and $N_V^{(j)}$ are the numbers of U and V matrices respectively in the operator. For the O_4 operators, $N_U^{(j)} + N_V^{(j)} = 4$ and $N_U^{(j)} + N_V^{(j)} = 6$ for O_6 operators. The canonical scaling dimensions α_4 and α_6 are not determined by dimensional analysis because the RG flow scale is the dimensionless matrix size N. However, they can be fixed by requiring that the beta functions have no explicit dependence on N (they are "autonomous") in the large N limit. This sets an upper bound on the canonical scaling of the couplings [115]. Choosing the canonical dimensions below this bound only removes interactions from the beta functions, so the "most interacting" theory is one where the bound is saturated.

Having specified a consistent truncation of the effective action (5.10), we can now proceed to analyse the FRGE (5.8) in more detail. First, we define $G_N^{(2)}$ as the term in $\Gamma_N^{(2)}$ independent of any U, V field, which by looking at equation (5.10) is given by

$$G_N^{(2),abcd} = \begin{pmatrix} Z_U & 0 \\ 0 & Z_V \end{pmatrix} \delta^{ac}\delta^{bd}. \tag{5.13}$$

With this split, we can consider the expansion of the right-hand side of the FRGE (5.8)

$$\frac{1}{2}\,\mathrm{Tr}\Big(\frac{\partial_t R_N}{R_N + \Gamma_N^{(2)}}\Big) = \frac{1}{2}\,\mathrm{Tr}\Big(\dot{R}P\Big) - \frac{1}{2}\,\mathrm{Tr}\Big(\dot{R}PFP\Big) + \frac{1}{2}\,\mathrm{Tr}\Big(\dot{R}PFPFP\Big) + \ldots \tag{5.14}$$

where $\dot{R}$ indicates the derivative of R with respect to $t = \log N$,

$$P_N = (R_N + G_N^{(2)})^{-1}$$

is a field-independent term and F is the field-dependent term in $\Gamma_N^{(2)}$. Explicitly, for the truncation of (5.10) to $n = 3$,

$$F = \sum_{j=1}^{5} \bar{g}_4^{(j)} F_{N,(j)}^{(4)} + \sum_{j'=1}^{20} \bar{g}_6^{(j')} F_{N,(j')}^{(6)} \tag{5.15}$$

$F_{N,(j)}^{(4)}$ and $F_{N,(j)}^{(6)}$ are the terms obtained by taking the second derivative with respect to the matrix elements of operators containing four and six fields respectively, namely

$$F_{N,(j),IJ}^{(4),abcd} = \frac{\delta}{\delta U_I^{ab}} \frac{\delta}{\delta U_J^{cd}} O_4^{(j)}$$
$$F_{N,(j),IJ}^{(6),abcd} = \frac{\delta}{\delta U_I^{ab}} \frac{\delta}{\delta U_J^{cd}} O_6^{(j)}$$

Given the structure of the expansion (5.14) and the definition of the propagator P, we generalise the definition given in [49] of the IR-suppression term R_N to

$$R_{N,IJ}^{abcd} := \left(\frac{N}{a+b} - 1\right)\theta\left[1 - \frac{a+b}{N}\right] \begin{pmatrix} Z_U & 0 \\ 0 & Z_V \end{pmatrix}_{IJ} \delta^{ac}\delta^{bd}, \tag{5.16}$$

so that the sign indices factorise in $G_N^{(2)} + R_N$ and we can invert it separately. It follows that

$$P_{N,IJ}^{abcd} = P_N^{abcd} \otimes P_{IJ}^{\text{sign}}$$

where

$$P_{IJ}^{\text{sign}} = \begin{pmatrix} Z_U^{-1} & 0 \\ 0 & Z_V^{-1} \end{pmatrix}_{IJ}$$

is obtained by inverting the sign matrix in (5.13) and (5.16). Note that the propagators and the IR cutoff term in (5.14) are proportional to the identity in matrix space. Therefore, they will just contribute an overall N dependent factor, which we will keep track of in the final result. For the sake of notation, we will only keep track of the P^{sign} part of the propagator and suppress the dependence on $\dot{R}$ and P_N in the intermediate steps of the computation.

5.4 Beta Function Equations

Here we derive the beta functions within our single-trace, two-C truncation. We first extract the tensor structures that can appear on the right-hand side of the FRGE, then project them onto the operator basis $O_4^{(i)}$ and $O_6^{(j)}$, making the N-scaling explicit.

5.4.1 General form of the beta function equations

To find the structure of the beta functions, it is sufficient to only consider the terms F and P^{sign} in (5.14) – this is what we will do in this section. In the next subsection, we will be more careful in order to deduce the N dependence of the beta function equations. Let us first consider the left-hand side of the FRGE (5.8). The derivative acts on the couplings in (5.10), resulting in

$$\begin{aligned}\partial_t \Gamma_N &= \frac{Z_U}{2}\eta_U \,\mathrm{Tr}\left[UU^T\right] + \frac{Z_V}{2}\eta_V \,\mathrm{Tr}\left[VV^T\right] + \sum_{n=2}^{\infty}\sum_j \frac{\bar\beta_{2n}^{(j)}}{2n} O_{2n}^{(j)} \\ &= \frac{Z_U}{2}\eta_U \,\mathrm{Tr}\left[UU^T\right] + \frac{Z_V}{2}\eta_V \,\mathrm{Tr}\left[VV^T\right] \\ &+ \sum_{n=2}^{\infty}\sum_j \frac{Z_U^{N_U^{(j)}/2} Z_V^{N_V^{(j)}/2} N^{\alpha_{2n}} \left[\beta_{2n}^{(j)} + \left(\eta_U N_U^{(j)}/2 + \eta_V N_V^{(j)}/2 + \alpha_{2n}\right) g_{2n}^{(j)}\right]}{2n} O_{2n}^{(j)}\end{aligned} \tag{5.17}$$

where $\eta_{U/V} = \partial_t \log Z_{U/V}$ is the anomalous dimension of the operators $\mathrm{Tr}\left[UU^T\right]$ and $\mathrm{Tr}\left[VV^T\right]$ and

$$\bar\beta_4^{(j)} = \partial_t \bar g_4^{(j)}, \qquad \bar\beta_6^{(k)} = \partial_t \bar g_6^{(k)},$$

are the beta functions for $\bar g_4$ and $\bar g_6$ respectively. In the last line, we used the definitions of the dimensionless couplings in (5.12).

The next step is to compare this with the various terms on the right-hand side of the FRGE, namely the expansion (5.14), looking for operators which match those in our chosen truncation (5.17). This defines the projection rule onto a smaller set of operators, and by comparing the pre-factors, we can read off the beta functions.

Projection rule. After using (5.15) in the right-hand side of the FRGE expanded to the order of fields relevant for a given beta function, we apply the following projection rule onto a basis operator $O_{2n}^{(j)}$ by:

(a) discarding multi-trace terms (our truncation is single-trace);

(b) discarding monomials with C-power $\neq 2$ inside a single trace;

(c) matching the sequence of U, V and transposes to the canonical pattern of $O_{2n}^{(j)}$ (up to overall cyclic rotation and reversal, cf. the discussion above).

The coefficient left in front of $O_{2n}^{(j)}$ after these steps defines the projected contribution to $\beta_{2n}^{(j)}$.

Let us consider the $F_N^{(4)}$ contribution from (5.15) to first order in (5.14) given by:

$$\sum_j \bar{g}_4^{(j)} \sum_{\{I\}} \Big(c_{(j)}^{\{I\}} \operatorname{Tr}[C] \operatorname{Tr}\Big[U_{I_1}^T C U_{I_2}\Big] + (d_{(j)}^{\{I\}} + N f_{(j)}^{\{I\}}) \operatorname{Tr}\Big[C U_{I_1} U_{I_2}^T C\Big] \Big) = \operatorname{Tr}\Big[F_N^{(4)} P^{\text{sign}}\Big], \tag{5.18}$$

where we sum over all matrices and indices thereof in the trace. The constants $c_{(j)}^{\{I\}}$, $d_{(j)}^{\{I\}}$ and $f_{(j)}^{\{I\}}$ come from the combinatorics of the action of the derivatives and the label $\{I\} = \{I_1, I_2\}$. Within the single-trace, two-C truncation, the FRGE never generates $\operatorname{Tr}\Big[U_I U_J^T\Big]$ structures: all projected contributions carry two C insertions. Consequently, there is no running of Z_U or Z_V at this order, and the flow is entirely driven by the interaction couplings.

We now proceed to the computation of the beta functions $\beta_4^{(j)}$ and $\beta_6^{(j)}$, starting with the latter. In order to obtain contributions to $\beta_6^{(j)}$, we need to look for operators in the expansion of the right-hand side of the FRGE (5.14) which contain six U/V matrices. At the order of truncation we are considering for the effective action (equation (5.10) with $n = 3$), contributions can only arise from terms in the form of $F_N^{(4)} F_N^{(4)} F_N^{(4)}$ or $F_N^{(4)} F_N^{(6)}$. However, the first combination, once traced with respect to the matrix and sign indices, gives *single trace* terms with the following structure

$$\begin{aligned} \sum_{j,k,l} \bar{g}_4^{(j)} \bar{g}_4^{(k)} \bar{g}_4^{(l)} \Big(& \sum_{\{I\}} c_{(j,k,l)}^{\{I\}} \operatorname{Tr}\Big[C^3\Big] \operatorname{Tr}\Big[U_{I_1}^T C U_{I_2} U_{I_3}^T C U_{I_4} U_{I_5}^T C U_{I_6}\Big] \\ & + \sum_{\{J\}} d_{(j,k,l)}^{\{J\}} \operatorname{Tr}[\delta] \operatorname{Tr}\Big[C U_{J_1} U_{J_2}^T C C U_{J_2} U_{J_4}^T C C U_{J_5} U_{J_6}^T C\Big] \Big) \\ & = \operatorname{Tr}\Big[F_N^{(4)} P^{\text{sign}} F_N^{(4)} P^{\text{sign}} F_N^{(4)} P^{\text{sign}}\Big], \end{aligned} \tag{5.19}$$

where the constants $c_{(j,k,h)}^{\{I\}}$ and $d_{(j,k,h)}^{\{J\}}$ are combinatorial factors. In particular, we note that there are no terms proportional to the operator $O_6^{(j)}$ in (5.17) – the first term vanishes due to $\operatorname{Tr}(C^3) = 0$ and the second term has too many Cs and is therefore projected out.

The second possible contributing term to $\beta_6^{(j)}$ comes from $\operatorname{Tr}\Big[F_N^{(4)} P^{\text{sign}} F_N^{(6)} P^{\text{sign}}\Big]$ and takes the following form

$$\sum_{k,l} \bar{g}_4^{(k)} \bar{g}_6^{(l)} \Big(\sum_j E^{(j)}_{3,(k,l)} \operatorname{Tr}\Big[C^2\Big] O_6^{(j)} + \sum_{\{J\}} c^{\{J\}}_{(k,l)} \operatorname{Tr}[\delta] \operatorname{Tr}\Big[C U_{J_1} U^T_{J_2} C U_{J_3} U^T_{J_4} C U_{J_5} U^T_{J_6} C\Big] + \sum_{\{K\}} d^{\{K\}}_{(k,l)} \operatorname{Tr}[C] \operatorname{Tr}\Big[U^T_{K_1} C U_{K_2} U^T_{K_3} C U_{K_4} U^T_{K_5} C U_{K_6}\Big] \Big) = \operatorname{Tr}\Big[F_N^{(4)} P^{\text{sign}} F_N^{(6)} P^{\text{sign}}\Big], \quad (5.20)$$

where (j) labels the U, V configuration of the operator associated with each coupling constant $g_6^{(j)}$. Only the first term matches the structure of the operator $O_6^{(j)}$ in (5.17) and therefore, contributes to $\beta_6^{(j)}$. The factor $E^{(j)}_{3,(j,k)}$ is the combinatorial factor involved in making the operator $O_6^{(j)}$ in the expansion. From this expression and (5.17), we can read off the form of the beta function equations for $g_6^{(j)}$:

$$\beta_6^{(j)} = -\alpha_6 g_6^{(j)} + C_1(N) \sum_{k,l} E^{(j)}_{3,(k,l)} g_4^{(k)} g_6^{(l)} \,, \quad (5.21)$$

where we have set the anomalous dimensions to zero as discussed above. For the time being, we put all N-dependence in the factor $C_1(N)$ – we will elaborate on this in the next subsection.

Let us now compute the beta function for $g_4^{(j)}$. We need terms from the right-hand side of the FRGE that could generate the operators $O_4^{(j)}$ in equation (5.17). These operators require four U or V components, and they can originate from either $F_N^{(4)} F_N^{(4)}$ or $F_N^{(6)}$. Consider the former, which is a second-order contribution.

$$\sum_{k,l} \bar{g}_4^{(k)} \bar{g}_4^{(l)} \Big(\sum_j E^{(j)}_{2,(k,l)} \operatorname{Tr}\Big[C^2\Big] O_4^{(j)} + \sum_{\{I\}} f^{\{I\}}_{(k,l)} \operatorname{Tr}[\delta] \operatorname{Tr}\Big[C U_{I_1} U^T_{I_2} C C U_{I_3} U^T_{I_4} C\Big] \Big) = \operatorname{Tr}\Big[F_N^{(4)} P^{\text{sign}} F_N^{(4)} P^{\text{sign}}\Big]. \quad (5.22)$$

The first term reproduces the operator $O_4^{(j)}$ in (5.17), whereas the second term contains too many Cs and is projected out. The final contribution comes from the first-order term in the expansion and is given by

$$\sum_k \bar{g}_6^{(k)} \Big(\sum_j D^{(j)}_{2,(k)} \operatorname{Tr}[\delta] O_4^{(j)} + \sum_{\{I\}} r^{\{I\}}_{(k)} \operatorname{Tr}[C] \operatorname{Tr}\Big[U^T_{I_1} C U_{I_2} U^T_{I_3} U_{I_4}\Big] \Big) = \operatorname{Tr}\Big[F_N^{(6)} P^{\text{sign}}\Big] \,, \quad (5.23)$$

thus contributing to the beta function equations for $g_4^{(j)}$. Any other terms that match the structure of the operators will be subleading in N and are omitted. In all, the general form of $\beta_4^{(j)}$ is

$$\beta_4^{(j)} = -\alpha_4 g_4^{(j)} + C_2(N) \sum_{k,l} E^{(j)}_{2,(k,l)} g_4^{(k)} g_4^{(l)} + D(N) \sum_m D^{(j)}_{2,(m)} g_6^{(m)} \,, \tag{5.24}$$

where we have absorbed the N-dependence into $C_2(N)$ and $D(N)$.

5.4.2 N-dependence of the beta functions

In determining the general form of the beta function equations, we could ignore the factors from $\dot{R}$ and P in (5.14) but when it comes to doing calculations, we must treat this more carefully. Let us consider the term in (5.22) that we determined contributes to β_4. If we include all terms, this expression is given by

$$\begin{aligned} &Z_U^{N_U^{(j)}/2} Z_V^{N_V^{(j)}/2} N^{2\alpha_4} \sum_{k,l} E^{(j)}_{2,(k,l)} g_4^{(k)} g_4^{(l)} \\ &\qquad \times \sum_{a,b,c,d=1}^{N} \dot{R}(a,b) P(a,b)^2 P(c,d) C_{ac} C_{ca} (U_{J_1}^T C U_{J_2})_{bd} (U_{J_3}^T C U_{J_4})_{db} \,, \end{aligned} \tag{5.25}$$

where we have made use of (5.12). The terms $\dot{R}(a,b)$ and $P(a,b)$ are given by

$$\begin{aligned} \dot{R}(a,b) &= \frac{N}{a+b} \theta\Big[1 - \frac{a+b}{N}\Big], \\ P(a,b) &= \Big(\frac{a+b}{N} - 1\Big) \theta\Big[1 - \frac{a+b}{N}\Big] + 1, \end{aligned} \tag{5.26}$$

Note that the factors of Z_U and Z_V always match up with the appropriate scaling of the operator after using (5.12) and including the $1/Z_{U/V}$ terms in P^{sign}. Comparing (5.25) to (5.17) we have

$$\begin{aligned} \sum_{b,d=1}^{N} (U_{J_1}^T C U_{J_2})_{bd} (U_{J_3}^T C U_{J_4})_{db} \Big(&\beta_4^{(j)} + \alpha_4 g_4^{(j)} \\ &- N^{\alpha_4} \sum_{k,l} E^{(j)}_{2,(k,l)} g_4^{(k)} g_4^{(l)} \sum_{a,c=1}^{N} \dot{R}(a,b) P(a,b)^2 P(c,d) C_{ac} C_{ca} \Big) = 0. \end{aligned} \tag{5.27}$$

Since this is true for all U and V, then

$$\beta_4^{(j)} + \alpha_4 g_4^{(j)} - N^{\alpha_4} \sum_{k,l} E^{(j)}_{2,(k,l)} g_4^{(k)} g_4^{(l)} \sum_{a,c=1}^{N} \dot{R}(a,b) P(a,b)^2 P(c,d) C_{ac} C_{ca} = 0 \tag{5.28}$$

for all b, d. Reinstating the sum over b, d we get

$$\beta_4^{(j)} + \alpha_4 g_4^{(j)} - N^{\alpha_4 - 2} \sum_{k,l} E^{(j)}_{2,(k,l)} g_4^{(k)} g_4^{(l)} \sum_{a,b,c,d=1}^{N} \dot{R}(a,b) P(a,b)^2 P(c,d) C_{ac} C_{ca} = 0 \quad (5.29)$$

Finally, using the fact that the matrix C can be chosen to be diagonal in order to satisfy the constraint (5.1) in the large N limit [51], we can write the last term as

$$\sum_{a,b,c,d=1}^{N} \dot{R}(a,b) P(a,b)^2 P(c,d) C(a) C(d) \delta_{ac} \delta_{ca} = \sum_{a,b,d=1}^{N} \dot{R}(a,b) P(a,b)^2 P(a,d) C(a)^2, \quad (5.30)$$

where $C(a)$ are the diagonal terms of C. Since the diagonal terms in the large N limit are all bounded from above [51], (5.30) scales like N^3. Hence, we can write the beta function equation for $\beta_4^{(j)}$ as

$$\beta_4^{(j)} = -\alpha_4 g_4^{(j)} + N^{\alpha_4 + 1} C_2 \sum_{k,l} E^{(j)}_{2,(k,l)} g_4^{(k)} g_4^{(l)} + N^{\alpha_6 - \alpha_4 + 1} D \sum_m D^{(j)}_{2,(m)} g_6^{(m)}, \quad (5.31)$$

where C_2 depends on the exact calculation of (5.30) and D is found by an analogous calculation coming from the linear term in (5.14). Carrying out the same calculations for $\beta_6^{(j)}$ we get

$$\beta_6^{(j)} = -\alpha_6 g_6^{(j)} + N^{\alpha_4 + 1} C_2 \sum_{k,l} E^{(j)}_{3,(k,l)} g_4^{(k)} g_6^{(l)}. \quad (5.32)$$

It is now clear that the upper bounds on the canonical scaling of the couplings are $\alpha_4 = -1$ and $\alpha_6 = -2$. We could now choose to saturate these bounds in order to make the beta functions autonomous, but we allow for the freedom to choose values below these bounds. This freedom will be useful when analysing the fixed points in the next section. Note that the constant C_2 in (5.31) and (5.32) is the same. This will be crucial in the next section when we investigate the fixed points in the regime where $g_6 = 0$. The flow depends on three sets of numbers: $E^{(j)}_{2,(k,l)}$ from $F^{(4)}PF^{(4)}$, $E^{(j)}_{3,(k,l)}$ from $F^{(4)}PF^{(6)}$, and $D^{(j)}_{2,(m)}$ from $F^{(6)}P$.

5.5 Fixed Points Analysis

Having obtained the beta function equations for the couplings (5.21) and (5.24), we now analyse the fixed point structure, corresponding to a continuum, large N limit of the matrix

model (5.3). In particular, we focus on fixed points of the form $(g_4^{*(i)}, 0)$, namely $g_6^{(j)} = 0$. This is a necessary simplification in order to get analytic control of the equations that follow.

Before proceeding, it is useful to set up a convention for the fourth-order operators. This will be useful in the following discussion, where we will refer to couplings and their associated operators interchangeably. The operators corresponding to each $g_4^{(i)}$ coupling are listed in Table 5.2.

Coupling	Operator
$g_4^{(1)}$	$Tr[UU^TCUU^TC]$
$g_4^{(2)}$	$Tr[UU^TCVV^TC]$
$g_4^{(3)}$	$Tr[UV^TCUV^TC]$
$g_4^{(4)}$	$Tr[UV^TCVU^TC]$
$g_4^{(5)}$	$Tr[VV^TCVV^TC]$

Table 5.2: The fourth order operators and their associated couplings.

If we restrict ourselves to fixed points with $g_6^{*(i)} = 0$, $\beta_6^{(k)} = 0$ is automatically satisfied. The fixed point condition on $\beta_4^{(j)}$ implies

$$\beta_4^{(j)} = 0 \Rightarrow -\alpha_4 g_4^{*(j)} + N^{\alpha_4+1} C_2 \sum_{k,l} E_{2,(k,l)}^{(j)} g_4^{*(k)} g_4^{*(l)} = 0\,.$$

To be completely explicit, we list the non-zero contributions to the beta function equation for $\beta_4^{(j)}$ relevant to the $g_6^* = 0$ case in Table 5.3[1].

j	$(k,l) : E_{2,(k,l)}^{(j)}$
1	$(1,1):\ 16;\quad (4,4):\ 4$
2	$(2,2):\ 8;\quad (3,3):\ 8$
3	$(2,3):\ 16$
4	$(1,4):\ 16;\quad (4,5):\ 16$
5	$(4,4):\ 4;\quad (5,5):\ 16$

Table 5.3: Non-zero combinatorial factors $E_{2,(k,l)}^{(j)}$ entering β_4 via $F^{(4)}PF^{(4)}$ at $g_6^* = 0$.

[1]Details of the calculations leading to the results in Table 5.3 can be found in the accompanying Mathematica notebook on the JHEP website: https://link.springer.com/article/10.1007/JHEP10(2025)198. The notebook also computes the coefficients E_2 and D_2, which are not used in this chapter but are included for completeness and to facilitate future work.

Hence the beta function equations reduce to

$$\begin{aligned}
\beta_4^{(1)} &= -\alpha_4\, g_4^{(1)} + C_2(N)\left(16\,(g_4^{(1)})^2 + 4\,(g_4^{(4)})^2\right),\\
\beta_4^{(2)} &= -\alpha_4\, g_4^{(2)} + C_2(N)\left(8\,(g_4^{(2)})^2 + 8\,(g_4^{(3)})^2\right),\\
\beta_4^{(3)} &= -\alpha_4\, g_4^{(3)} + C_2(N)\left(16\, g_4^{(2)}\, g_4^{(3)}\right),\\
\beta_4^{(4)} &= -\alpha_4\, g_4^{(4)} + C_2(N)\left(16\, g_4^{(1)}\, g_4^{(4)} + 16\, g_4^{(4)}\, g_4^{(5)}\right),\\
\beta_4^{(5)} &= -\alpha_4\, g_4^{(5)} + C_2(N)\left(4\,(g_4^{(4)})^2 + 16\,(g_4^{(5)})^2\right).
\end{aligned}$$

It is worth noting that the solutions to the above beta-function equations, which we will list momentarily, can be divided into two classes of fixed points, according to their behaviour under the exchange $U \leftrightarrow V$:

- Fixed points which are symmetric under $U \leftrightarrow V$. This condition implies $g_4^{*(1)} = g_4^{*(5)}$;
- Fixed points which come in pairs, and are mapped into each other under $U \leftrightarrow V$.

Note that this is analogous to what happens in the $ABAB$ matrix model, as pointed out in [116]. It is also worth noting that, due to the specific form of the coefficients $E^{(j)}_{2,(k,l)}$, the equations for $g_4^{(1)}, g_4^{(4)}, g_4^{(5)}$ completely factorise from those for $g_4^{(2)}, g_4^{(3)}$. Hence, fixed points which live in the five-dimensional parameter space of $g_4^{(i)}$, can be factorised into the Cartesian product of solutions living in a two and a three-dimensional subspace respectively. There are four solutions in the $(g_4^{(2)}, g_4^{(3)})$ subspace, and we summarise them in Table 5.4.

Label	$g_4^{*(2)}$	$g_4^{*(3)}$
1	0	0
2	$\frac{\alpha_4}{16C_2(N)}$	$-\frac{\alpha_4}{16C_2(N)}$
3	$\frac{\alpha_4}{16C_2(N)}$	$\frac{\alpha_4}{16C_2(N)}$
4	$\frac{\alpha_4}{8C_2(N)}$	0

Table 5.4: Solutions to the beta-function equation in the $(g_4^{(2)}, g_4^{(3)})$ subspace.

Note that the corresponding operators are symmetric under $U \leftrightarrow V$, hence the symmetry is preserved at every point in this subspace.

By studying the solutions to the beta-function equation in the $(g_4^{(1)}, g_4^{(4)}, g_4^{(5)})$ subspace, we realise that there are two types of solutions. The first type consists of isolated fixed points and will be the object of the next subsection 5.5.1. The second type is represented by continuous line segments, where every point on the segment is a fixed point of the beta function equations. We will analyse these in subsection 5.5.2.

5.5.1 Isolated fixed points

The isolated fixed points solutions in the $(g_4^{(1)}, g_4^{(4)}, g_4^{(5)})$ subspace are presented in Table 5.5.

Label	$g_4^{*(1)}$	$g_4^{*(4)}$	$g_4^{*(5)}$
A	0	0	0
B	0	0	$\frac{\alpha_4}{16C_2(N)}$
C	$\frac{\alpha_4}{16C_2(N)}$	0	0
D	$\frac{\alpha_4}{16C_2(N)}$	0	$\frac{\alpha_4}{16C_2(N)}$

Table 5.5: Solutions to the beta-function equation in the $(g_4^{(1)}, g_4^{(4)}, g_4^{(5)})$ subspace.

Here, solutions A and D are symmetric under $U \leftrightarrow V$, whereas solutions B and C are mapped one into the other by the same transformation. Note that we have chosen a labelling that allows us to refer to the solution in the full space by combining solutions in the two subspaces. For example, solution 2B corresponds to

$$(g_4^{*(1)}, g_4^{*(2)}, g_4^{*(3)}, g_4^{*(4)}, g_4^{*(5)})_{2B} = \left(0, \frac{\alpha_4}{16C_2(N)}, -\frac{\alpha_4}{16C_2(N)}, 0, \frac{\alpha_4}{16C_2(N)}\right).$$

Therefore, there are 16 solutions in total, corresponding to all pairings across the two tables. Note that in all solutions, $g_4^{*(4)} = 0$. This is analogous to what happens in the $ABAB$ matrix model [116], where the coupling associated with the operator $Tr[ABBA]$ always vanishes at the fixed point.

Among these fixed points, there are some which lend themselves to a straightforward interpretation:

- Gaussian fixed point (solution 1A)

$$g_4^{*(i)} = (0, 0, 0, 0, 0)\,. \tag{5.33}$$

  On this fixed point, we have a free field theory;

- Pure CDT fixed points (solutions 1B and 1C)

$$g_4^{*(i)} = \left(\frac{\alpha_4}{16C_2(N)}, 0, 0, 0, 0\right) \tag{5.34}$$

$$g_4^{*(i)} = \left(0, 0, 0, 0, \frac{\alpha_4}{16C_2(N)}\right). \tag{5.35}$$

  On these fixed points, there is only one independent, non-vanishing coupling, representing the cosmological constant, which couples to the area operator. A fixed point of this kind also occurs in the analysis of the RG flow for the matrix model of pure CDT [49]. Therefore, we interpret this as a continuum limit in which the Ising model is switched off, and we are left with a theory of pure gravity.

Other solutions to the fixed-point equations represent non-trivial fixed points, which are specific to the matrix model we are considering.

The next step, in order to characterise these fixed points, is to compute the critical exponents, defined as the eigenvalues of the Hessian matrix $H_{ij} = -\frac{\partial \beta_i}{\partial g_j}$. They determine how couplings grow as we flow away from the critical point. In particular, a positive critical exponent corresponds to a relevant direction, a negative critical exponent characterises an irrelevant direction and a critical exponent of 0 is called marginal. Taking derivatives of (5.21) and (5.24), the Hessian matrix takes the block form

$$H = \left(\begin{array}{c|c} \alpha_4\delta^i_j - C_2(N)E^{(i)}_{2,(j,k)}g_4^{*(k)} & D(N)D^{(i)}_{2,(l)} \\ \hline C_2(N)E^{(h)}_{3,(j,k)}g_6^{*(k)} & \alpha_6\delta^h_l - C_2(N)E^{(h)}_{3,(l,k)}g_4^{*(k)} \end{array}\right),$$

with $i, j = 1, .., 5$ and $h, l = 1, ..., 20$. On the fixed points we are considering, this simplifies to

$$H = \left(\begin{array}{c|c} \alpha_4\delta^i_j - C_2(N)E^{(i)}_{2,(j,k)}g_4^{*(k)} & D(N)D^{(i)}_{2,(j)} \\ \hline 0 & \alpha_6\delta^h_l - C_2(N)E^{(h)}_{3,(l,k)}g_4^{*(k)} \end{array}\right),$$

so that the overall eigenvalues are given by the eigenvalues of the two blocks on the diagonal separately. Firstly, let us consider the critical exponents corresponding to the pure CDT solutions:

- Gaussian fixed point (solution 1A). The critical exponents corresponding to the upper-left block of the Hessian are

$$\lambda_4^{(i)} = \alpha_4, \quad \forall i = 1, ..., 5\,,$$

and the eigenvalues of the bottom-right block are given by

$$\lambda_6^{(h)} = \alpha_6, \quad \forall h = 1, ..., 20\,.$$

All directions of the RG flow from the Gaussian fixed point are irrelevant, and the theory is free, given $\alpha_4, \alpha_6 < 0$. The conditions on α_4 and α_6 are satisfied when the bounds are saturated. This continuum limit corresponds to topological gravity.

- Pure CDT fixed points. For both solutions 1B (5.34) and 1C (5.35), the critical exponents in the $g_4^{(i)}$ subspace are

$$\lambda_4^{(i)} = (\alpha_4, \alpha_4, 0, -\alpha_4, \alpha_4)\,,$$

therefore there are three irrelevant, one marginal and one relevant direction. On the bottom-right block, critical exponents associated with this solution are

$$\begin{aligned}
\lambda_6^{(h)} &= \alpha_6, \quad \text{for} \quad h = 1, ..., 12 \\
\lambda_6^{(h)} &= -\alpha_4 + \alpha_6, \quad \text{for} \quad h = 13, ..., 18 \\
\lambda_6^{(h)} &= -2\alpha_4 + \alpha_6, \quad \text{for} \quad h = 19, 20\,.
\end{aligned}$$

It follows that, for $\frac{\alpha_6}{\alpha_4} > 2$, all those directions are irrelevant. In particular, for the canonical values of α_4 and α_6, 18 directions are irrelevant and two are marginal. Hence, within this region of parameter space, there is only one relevant direction. This is consistent with the result of [49], for the continuum limit of the matrix model describing pure CDT, with the same value of the critical exponent for the relevant direction. Hence, this fixed point corresponds to gravity with a cosmological constant term and no matter. It was shown in [49] that, for the model of pure CDT, there is another fixed point which corresponds to the continuum limit of 2D gravity with a cosmological constant for complementary values of α_4 and α_6. We believe that such a fixed point should also be present in the Ising–CDT model. However, it will only exist in the $g_6^{(i)} \neq 0$ regime, where a full analytic or numerical study would be required to prove its existence.

Critical exponents corresponding to all solutions of the fixed-point equations are presented in Appendix B.1. One of the main features of solutions characterising non-trivial fixed points is that critical exponents in the bottom-right block only take three values, with different degeneracies depending on the solution. Those values are α_6, $\alpha_6 - \alpha_4$ and $\alpha_6 - 2\alpha_4$. This implies that those directions are all irrelevant or marginal for the canonical values of α_4, α_6, and they are all irrelevant in the region $\frac{\alpha_6}{\alpha_4} > 2$. This means that, as far as this region is concerned, there are no relevant directions coming from order six operators. Indeed, in different regions of parameter space, some of those directions will become relevant.

Let us now focus on the upper-left block. Different solutions are characterised by a different number of relevant, irrelevant and marginal directions. Note that critical exponents take three values α_4, 0 and $-\alpha_4$, corresponding to irrelevant, marginal and relevant directions respectively. In particular:

- Solution 1D has 2 irrelevant and 3 relevant directions;
- Solutions 2A and 3A have 4 irrelevant and 1 relevant directions;
- Solutions 2B, 3B, 2C and 3C have 2 irrelevant, 1 marginal and 2 relevant directions;
- Solutions 2D and 3D have 1 irrelevant and 4 relevant directions;
- Solution 4A has 3 irrelevant and 2 relevant directions;
- Solutions 4B and 4C have 1 irrelevant, 1 marginal and 3 relevant directions;
- Solution 4D has 5 relevant directions.

To summarise, besides recovering the fixed points corresponding to topological gravity and pure gravity with a cosmological constant, which can be obtained as the continuum limit of the pure CDT and no matter matrix model [49], we found new, non-trivial fixed points. In particular, within the region of the α_4, α_6 parameter space specified above, three of those fixed points, namely 1D, 4B and 4C, have three relevant directions. It follows that the corresponding CFT has the correct number of operators to represent the Ising CFT coupled to two-dimensional gravity. The operators in the Ising CFT are, namely, the cosmological constant term (identity), the energy operator ψ, and the duality operator σ.

5.5.2 Segments of fixed points

Alongside isolated fixed point solutions, beta-function equations in the $(g_4^{(1)}, g_4^{(4)}, g_4^{(5)})$ subspace admit lines of solutions such that each point on the line is a fixed point. We present them in Table 5.6.

Label	$g_4^{*(1)}$	$g_4^{*(4)}$	$g_4^{*(5)}$
R	$\frac{1}{32C_2(N)}\Big(\alpha_4 - s(g_4^{*(4)};\alpha_4)\Big)$	$\in \left(-\frac{\lvert\alpha_4\rvert}{16C_2(N)}, \frac{\lvert\alpha_4\rvert}{16C_2(N)}\right)$	$\frac{1}{32C_2(N)}\Big(\alpha_4 + s(g_4^{*(4)};\alpha_4)\Big)$
S	$\frac{1}{32C_2(N)}\Big(\alpha_4 + s(g_4^{*(4)};\alpha_4)\Big)$	$\in \left(-\frac{\lvert\alpha_4\rvert}{16C_2(N)}, \frac{\lvert\alpha_4\rvert}{16C_2(N)}\right)$	$\frac{1}{32C_2(N)}\Big(\alpha_4 - s(g_4^{*(4)};\alpha_4)\Big)$

Table 5.6: Lines of solutions to the beta-function equation in the $(g_4^{(1)}, g_4^{(4)}, g_4^{(5)})$ subspace. Here $s(g_4^{*(4)};\alpha_4) = \sqrt{\alpha_4^2 - 256 g_4^{*(4)\,2} C_2(N)^2}$.

The solutions in the extended parameter space are obtained by crossing entries of Table 5.6 with the ones in Table 5.4. It is worth noting that fixed points of type B and C from Table 5.5 can be obtained as particular points of the segments R and S respectively, with $g_4^{*(4)} = 0$. It follows that solutions of type B and C sit on the segments. These include the pure CDT solutions 1B (5.34) and 1C (5.35), which sit on segments 1R and 1S respectively. We show, in Figure 5.2, the projection of the phase space (restricted to the $(g_4^{*(i)}, 0)$ condition) to the $(g_4^{(1)}, g_4^{(4)}, g_4^{(5)})$ subspace, which includes critical points from Table 5.5 and critical segments from Table 5.6.

Along each segment one finds $g_4^{(1)} + g_4^{(5)} = \alpha_4/(16\,C_2)$ while $g_4^{(4)}$ varies within the interval in Table 5.6; we verified that (i) the spectrum of critical exponents and (ii) the autonomous beta polynomials are independent of $g_4^{(4)}$ along the segment. This indicates that the segment direction is generated by a redundant (reparameterisation) vector field in theory space: within the single-trace, two-C basis, a linear redefinition among $\{O_4^{(1)}, O_4^{(4)}, O_4^{(5)}\}$ leaves projected flows and spectra invariant, so points on the same segment are physically equivalent at the level of this truncation. A decisive test would require either (a) adding interactions outside this basis (e.g. multi-trace or three-C operators), or (b) computing an observable sensitive to $g_4^{(4)}$ (for instance a suitable four-point function from Γ_N) and checking its constancy along the segment. We leave this for future work. Consistent with this picture, Appendix B.1, Table B.2, shows that

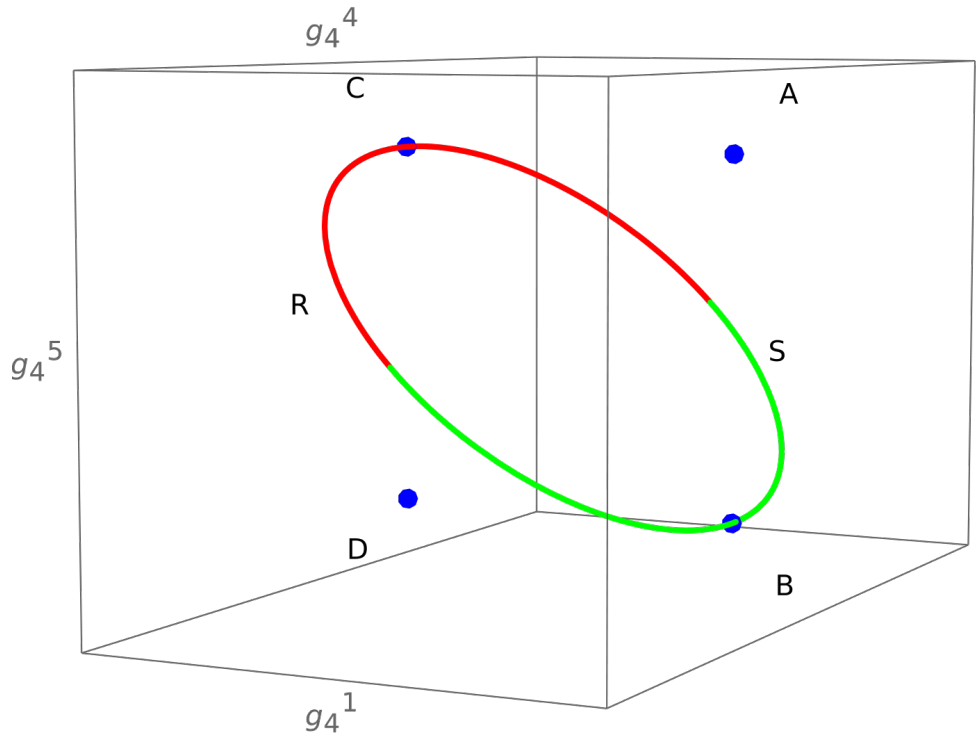

Figure 5.2: Projection of the phase space of the theory to the $(g_4^{(1)}, g_4^{(4)}, g_4^{(5)})$ subspace. This is composed by solutions A, B, C, D (blue), and critical segments R (red) and S (green).

every point on a given segment has identical critical exponents equal to those of the corresponding B or C fixed point with exactly one marginal direction in the quartic sector, interpreted as the RG flow along the segment. In particular, solutions 4R and 4S display three relevant directions and are therefore suitable to represent the Ising CFT.

5.6 Conclusion

In this work, we investigated the Ising model coupled to Causal Dynamical Triangulations (CDT) through the lens of the Functional Renormalisation Group Equation (FRGE). Using a matrix model representation, we analysed the fixed-point structure of the theory and demonstrated the existence of continuum limits. Our results confirm that the model not only reproduces known fixed points, such as those corresponding to topological gravity and pure CDT with a cosmological constant but also uncovers a new fixed point featuring three relevant directions, aligning with the number of primary operators of the Ising CFT.

The addition of Ising spin degrees of freedom significantly increased the complexity of the truncation, making the fixed-point analysis more challenging. However, by leveraging symmetry and simplifying assumptions, we successfully identified physically relevant fixed points, providing further evidence that the Ising CFT can emerge in this setting.

Future research could focus on extending this analysis to complementary regions of the parameter space (i.e. $g_6 \neq 0$) and exploring fixed points beyond the analytic reach of the current truncation. Numerical methods, in particular, could shed light on the existence of additional fixed points and their critical properties, providing a more comprehensive picture of the Ising-CDT model. The analysis could be further improved by adding higher order terms in the effective action, and by extending the truncation to also include multi-trace operators or operators with more than two C matrices. This would provide more quantitative results for the critical exponents.

6

Emergent Hyperbolic Space from CDT

Contents

6.1 Introduction

The final chapter of this thesis concerns the emergence of constant negative curvature spacetime from causal dynamical triangulations in the continuum. Recall the continuum limit of CDT from Section 2.3.3 with initial and final boundary cosmological constants X and Y respectively, separated by a continuum time T. It was shown in [1] that a hyperbolic spacetime emerges from this model by tuning the boundary cosmological constant $Y = -\sqrt{\Lambda}$ as $T \to \infty$. With this tuning, they achieve an average length process $\langle L(t) \rangle$, at $t \ll T$ with a sinh profile—hence the emergence of an AdS-like spacetime.

The problem with this calculation is the rather dubious limit $Y = -\sqrt{\Lambda}$. Recall that the continuum limit is taken by approaching the boundary of the region of convergence of the discrete generating function. This region for the boundary cosmological constant is $y < 1$ and so we must approach $y_c = 1$ (the boundary of this region) from below.

Recall from Section 2.3.3 that we achieve this by taking the continuum limit by setting $y = 1 - Y\theta\Lambda^{-1/2}$ and taking $\theta \to 0$. Hence, setting $Y = -\sqrt{\Lambda}$ abruptly jumps out of this region of convergence and it is unclear if this is a sensible operation.

As it turns out, all's well that ends well. We demonstrate another example of the power of the stochastic approach to analysing continuum CDT. We recover the sinh profile using only the machinery of stochastic calculus. Specifically, we find that the sinh profile emerges by conditioning the killed length process to survive up to time T. We go further by deriving another stochastic differential equation for the conditioned length process which encapsulates the full fluctuating geometry as well as the average sinh–profile.

Finally, we investigate a different source of emergent negative curvature space from CDT. This involves a stochastic time-change known as a Lamperti transformation [117] that turns the pure CDT process into an exponential Brownian process, whose exponential functionals are well studied [118, 119]. Therefore, the average length process also produces an AdS-like spacetime.

6.2 Conditioning the killed process

Firstly, recall the CDT Hamiltonian

$$\mathcal{L} = l\frac{\partial^2}{\partial l^2} + 2\frac{\partial}{\partial l} - \Lambda l,$$

which in keeping with the stochastic approach, we think of as the generator of a diffusion process with a killing term $-\Lambda l$ (explained in Section 3.7) [105]. We can read off the drift and diffusion terms for the SDE without the killing term, giving

$$dL_t = 2\,dt + \sqrt{2L_t}\,dW_t. \tag{6.1}$$

We claim that by conditioning on the killed process to survive up to some time T, we get a process whose average grows exponentially—giving a constant negative curvature space with fluctuations. We summarise the main result in the following theorem.

Theorem 6.2.1. *The generator of the process* (6.1) *with a killing term* $-\Lambda l$ *and conditioned to survive to time* T *is given by*

$$\mathcal{G} = l\frac{\partial^2}{\partial l^2} + \left(2 - 2\sqrt{\Lambda}l\coth\left(\sqrt{\Lambda}(T-t)\right)\right)\frac{\partial}{\partial l}. \tag{6.2}$$

The corresponding SDE is

$$dL_t = \left(2 - 2\sqrt{\Lambda} L_t \coth\left(\sqrt{\Lambda}(T-t)\right)\right) dt + \sqrt{2L_t}\, dW_t. \tag{6.3}$$

Proof. Consider the time-inhomogeneous equation

$$(\partial_t + \mathcal{L}) h(t,l) = 0, \tag{6.4}$$

whose solution is given by

$$h(t,l) = \frac{\Lambda}{\sinh^2 \sqrt{\Lambda}(T-t)} e^{-\sqrt{\Lambda} l \coth \sqrt{\Lambda}(T-t)}, \tag{6.5}$$

which can be checked by explicit substitution. This is the CDT two-loop propagator with one boundary shrunk to zero and $t \to T - t$, i.e. it is the kernel of the killed process (c.f. Example 3.8.5). Using the theory of h-transforms explained in Section 3.8 we know that if we have a space-time harmonic function $h(t,l)$ and a killed process, we can find the generator of the process conditioned to survive up to time T by calculating

$$\mathcal{G} = h^{-1}(\partial_t + \mathcal{L}) h.$$

Let $f(l)$ be a test function then

$$\begin{aligned} \partial_t(hf) + \mathcal{L}(hf) &= (\partial_t h) f + l(hf)'' + 2(hf)' - \Lambda l h f \\ &= \underbrace{\left(lh'' + 2h' - \Lambda l h + \partial_t h\right)}_{=0} f + 2hf' + 2lh'f' + lhf''. \end{aligned}$$

The term in brackets vanishes as h is a solution of (6.4), hence $\mathcal{G}$ reads

$$\mathcal{G} = l\frac{\partial^2}{\partial l^2} + \left(2 + 2l\frac{\partial}{\partial l}\log h\right)\frac{\partial}{\partial l},$$

and we get the desired result (6.2). The SDE follows directly by reading off the drift and diffusion coefficients from the generator. □

Note that this new process has no killing term, it is a pure diffusion process like (6.1) where the drift term enforces the 'no killing' condition. It is now straightforward to show how the sinh profile emerges from this process.

Proposition 6.2.1. *The average length* $\langle L_t \rangle := \mathbb{E}[L_t]$ *of the killed process conditioned to survive to time* T *is given by*

$$\langle L_t \rangle = \frac{1}{\sqrt{\Lambda}} \sinh\left(2\sqrt{\Lambda}(T-t)\right). \tag{6.6}$$

Proof. Taking the expectation of the SDE (6.3), we get the following ODE for the average process:

$$\frac{d\langle L_t \rangle}{dt} = 2 - 2\sqrt{\Lambda}\coth\left(\sqrt{\Lambda}(T-t)\right)\langle L_t \rangle .$$

It can be checked by direct substitution that (6.6) indeed satisfies this ODE which vanishes at $t = T$. □

This is exactly the result found in [1] if we let $t = 0$ and consider $\langle L_t \rangle$ as a function of the time T to the final boundary. Considering this profile to be the length of the classical surface at proper time T, we get the line element

$$ds^2 = dT^2 + \frac{C}{\Lambda}\sinh^2(2\sqrt{\Lambda}T)\, d\theta^2, \tag{6.7}$$

where $C > 0$ (to ensure a Euclidean signature) is fixed by comparing the line element to a continuum calculation as done in [1]. Regardless of the constant, this describes a spacetime of constant negative curvature with $R = -8\Lambda$.

It is also possible to consider the process conditioned to survive *forever* i.e. $T \to \infty$. In this case, we also find an emergent hyperbolic space but with an exponential profile. This is clearly consistent with the limit of (6.6) as $T \to \infty$. The following proposition summarises the result.

Proposition 6.2.2. *The generator of the process* (6.1) *with a killing term* $-\Lambda l$ *conditioned to survive forever is given by*

$$\mathcal{G} = l\frac{\partial^2}{\partial l^2} + 2\sqrt{\Lambda}\, l\frac{\partial}{\partial l}. \tag{6.8}$$

Equivalently, L_t *satisfies the stochastic differential equation*

$$dL_t = 2\sqrt{\Lambda}\, L_t\, dt + \sqrt{2L_t}\, dW_t. \tag{6.9}$$

Proof. As explained in Chapter 3, in order to condition on infinite survival, we must consider the process h that satisfies the time-homogeneous equation

$$\mathcal{L}\, h = 0.$$

A solution is given by the Wheeler-DeWitt wavefunction for CDT

$$h(l) = \frac{e^{\sqrt{\Lambda}\, l}}{l}.$$

The new generator is computed by conjugation

$$\mathcal{G} = h^{-1} \mathcal{L}\, h\,,$$

which applied to a test function f is given by

$$\begin{aligned} \mathcal{G} f &= l f'' + \left(2 + 2l \frac{h'}{h}\right) f' \\ &= l \frac{\partial^2}{\partial l^2} + 2\sqrt{\Lambda}\, l \frac{\partial}{\partial l}. \end{aligned} \tag{6.10}$$

Once again, the SDE is found by reading off the coefficients from the generator. □

Taking the expectation of (6.9) as before, we find the differential equation for the average length

$$\frac{d \langle L_t \rangle}{dt} = 2\sqrt{\Lambda}\, \langle L_t \rangle\,,$$

which has solution

$$\langle L_t \rangle = \frac{1}{\sqrt{\Lambda}}\, e^{2\sqrt{\Lambda}\, t}$$

and describes a universe of constant negative curvature with $R = -8\Lambda$. This is also the $T \to \infty$ limit of (6.6).

We have shown two ways where hyperbolic space emerges from CDT using the tools of the stochastic approach. These findings verify previous results and put them on a rigorous footing. Furthermore, we find explicit SDEs for the conditioned process which incorporate the average growth as well as the fluctuations. In the remainder of this chapter we will discuss another way that hyperbolic space emerges from CDT, this time from a random time-change of the canonical CDT time.

6.3 Time-changed CDT

The stochastic process (6.1) that describes the length is nothing more than a scaled squared Bessel process (BESQ$^{(\delta)}$) which obeys the SDE:

$$dL_t^{(\delta)} = \delta\, dt + 2\sqrt{L_t^{(\delta)}}\, dB_t, \quad L_0^{(\delta)} = l_1 > 0, \tag{6.11}$$

In fact, the process (6.1) is the process $L'_t = L_t^{(4)}/2$. For full generality, we keep the drift term as $\delta\, dt$. The following theorem due to Lamperti [117] transforms this process into an exponential Brownian motion from which we find another emergence of a constant negative curvature space.

Theorem 6.3.1 (Lamperti)**.** *Let $L_t^{(\delta)}$ satisfy the SDE in* (6.11) *and let $B_t^{(\mu)} := B_t + \mu\, t$, where $\mu := \frac{\delta-2}{2}$ and B_t is a standard Brownian motion starting at $x = \frac{1}{2}\log l_1$. Furthermore, define the process $A_t^{(\mu)} := \int_0^t e^{2B_s^{(\mu)}}\, ds$. Then*

$$L^{(\delta)}_{A_t^{(\mu)}} \overset{(law)}{=} e^{2B_t^{(\mu)}}, \tag{6.12}$$

where $\overset{(law)}{=}$ denotes equality in distribution (or equivalently, in law).

Proof. Lamperti first proved his result in [117]. Here we show the result for our setting. Let

$$Y_t := e^{B_t^{(\mu)}}, \qquad A_t := \int_0^t Y_s^2\, ds, \qquad \alpha_u := \inf\{t \geq 0 : A_t > u\}.$$

By Itô's formula,

$$dY_t = Y_t\, dB_t + \left(\mu + \tfrac{1}{2}\right) Y_t\, dt, \qquad Y_0 = \sqrt{l_1}.$$

Define $M_t := \int_0^t Y_s\, dB_s$, so that the quadratic variation is $\langle M\rangle_t = A_t$. By Lévy's characterization there is a Brownian motion $(\beta_u)_{u\geq 0}$ such that

$$M_t = \beta_{A_t} \quad \Rightarrow \quad Y_{\alpha_u}\, dB_{\alpha_u} = d\beta_u.$$

Let $Z_u := Y_{\alpha_u}$. Using $d\alpha_u = du/Z_u^2$,

$$dZ_u = dY_{\alpha_u} = Y_{\alpha_u}\, dB_{\alpha_u} + \left(\mu + \tfrac{1}{2}\right) Y_{\alpha_u}\, d\alpha_u = d\beta_u + \frac{\mu + \frac{1}{2}}{Z_u}\, du = d\beta_u + \frac{\delta - 1}{2Z_u}\, du,$$

which is the Bessel SDE. Squaring $X_u := Z_u^2$ and using Itô,

$$dX_u = 2Z_u\, dZ_u + d\langle Z\rangle_u = 2\sqrt{X_u}\, d\beta_u + \delta\, du, \qquad X_0 = Z_0^2 = Y_0^2 = l_1,$$

so $(X_u)_{u\geq 0}$ is a (weak) solution to the squared Bessel SDE (6.11). By uniqueness in law for (6.11),

$$(X_u)_{u\geq 0} \overset{(law)}{=} \left(L_u^{(\delta)}\right)_{u\geq 0}.$$

Finally, evaluating at the random time $u = A_t$,

$$L_{A_t}^{(\delta)} \overset{(law)}{=} X_{A_t} = Z_{A_t}^2 = Y_{\alpha_{A_t}}^2 = Y_t^2 = e^{2B_t^{(\mu)}}.$$

With the notational identification $A_t \equiv A_t^{(\mu)}$, this is $L_{A_t^{(\mu)}}^{(\delta)} \overset{(law)}{=} e^{2B_t^{(\mu)}}$. □

Remark 6.3.1 (Pathwise version)**.** *There is a coupling under which Lamperti's relation holds almost surely and not just in law. Let $B^{(\mu)}$ and $A^{(\mu)}$ be as in the theorem, set $Y_t := e^{B_t^{(\mu)}}$, $A_t := \int_0^t Y_s^2\, ds$, $\alpha_u := \inf\{t \geq 0 : A_t > u\}$, and define*

$$\beta_u := \int_0^{\alpha_u} Y_s\, dB_s.$$

One can verify that $(\beta_u)_{u\geq 0}$ is a Brownian motion by showing that $d\beta_u d\beta_u = du$ (Lévy's characterization). Using the fact that L is a squared bessel process, which has a unique strong solution, if we set

$$dL_u \;=\; 2\sqrt{L_u}\, d\beta_u + \delta\, du, \qquad L_0 = l_1$$

then

$$L_{A_t} \;=\; e^{2B_t^{(\mu)}} \qquad \textit{for all } t \geq 0 \quad \textit{a.s.}$$

A strong solution simply means that L is adapted to the filtration generated by β and not some other Brownian motion on some other probability space. However, if L and B are given a priori (e.g. with independent driving noises), one cannot expect a path-wise identity—only the stated identity in distribution.

Recall that pure CDT is a constant scaling of a BESQ$^{(4)}$ process. Hence, setting $\delta = 4$ ($\mu = 1$), under the time change, we get the following exponential Brownian motion

$$L_{A_t} = e^{2(B_t + t)}, \quad l_1 > 0.$$

Using this as the length of a slice of a continuum surface at time t, the average length is given by

$$\langle L_{A_t} \rangle := \mathbb{E}\left[L_{A_t}\right] = \mathbb{E}\left[e^{2(B_t+t)}\right] = e^{4t}.$$

Similarly to before, we define the line element to be

$$ds^2 = dt^2 + C\left\langle L_{A_t}\right\rangle^2 d\theta^2$$

from which we obtain an emergent hyperbolic space with $R = -2\frac{\langle L_{A_t}\rangle''}{\langle L_{A_t}\rangle} = -32$.

Despite the similarity of this result to that in [1], they come from different constructions: one from conditioning the killed process to survive forever and the other from taking the pure length process and performing a time-reparameterisation. It is interesting that both constructions yield a hyperbolic space and it would be a worthwhile endeavour to understand if there is a deeper connection between the two.

The machinery of stochastic calculus can be used to compute the two-loop propagator for pure CDT whose expression can be found in [32, 40]. In the following theorem and associated lemmas, we compute said propagator while implementing the time-change as an intermediate step. In doing so, we find a connection to Morse quantum mechanics which may hint towards the origin of the emergent hyperbolic space.

Theorem 6.3.2. *Consider the CDT Hamiltonian*

$$H_\Lambda(l, \frac{\partial}{\partial l}) = -2l\frac{\partial^2}{\partial l^2} - \delta\frac{\partial}{\partial l} + \Lambda\, l. \tag{6.13}$$

Then treating this as a generator for a diffusion process, we apply the Feynman-Kac formula. Hence the heat-kernel $G_\Lambda^{(\delta)}(l_1, l_2; T)$ of the semi-group e^{-TH_Λ} is given by

$$G_\Lambda^{(\delta)}(l_1, l_2; T) = \mathbb{E}_{L_0^{(\delta)}=l_1}[\delta(L_T^{(\delta)} - l_2)e^{-\Lambda\int_0^T L_s^{(\delta)}\,ds}]. \tag{6.14}$$

The closed-form expression for the heat kernel is

$$G_\Lambda^{(\delta)}(l_1, l_2; T) = \frac{1}{2}\left(\frac{l_2}{l_1}\right)^{\mu/2} \frac{\sqrt{2\Lambda}}{\sinh\left(\sqrt{2\Lambda}T\right)} e^{-\sqrt{\frac{\Lambda}{2}}(l_1+l_2)\coth\left(\sqrt{2\Lambda}T\right)} I_{|\mu|}\left(\frac{\sqrt{2\Lambda l_1 l_2}}{\sinh\left(\sqrt{2\Lambda}T\right)}\right) \tag{6.15}$$

where $\mu = (\delta - 2)/2$ and $I_{|\mu|}$ is the modified Bessel function of the first kind. This is the heat kernel for CDT with measure $m(dl) = \frac{1}{2}l^\mu\, dl$.

As promised, we will compute the propagator via the time-change. The following lemma rewrites the heat kernel in terms of the time-changed process.

Lemma 6.3.3. *Let* $\tilde{B}_t^{(\mu)} := B_t^{(\mu)} - \frac{1}{2}\log l_1$, $\tilde{C}_t^{(\mu)} := \int_0^t e^{4\tilde{B}_s^{(\mu)}}\,ds$, *and* $\tilde{A}_t^{(\mu)} := \int_0^t e^{2\tilde{B}_s^{(\mu)}}\,ds$ *then,*

$$G_\Lambda^{(\delta)}(l_1,l_2;T) = \frac{1}{2l_1}\int_0^\infty \mathbb{E}_{\tilde{B}_0^{(\mu)}=0}\Big[e^{-\Lambda\, l_1^2\,\tilde{C}_t^{(\mu)}}\;\Big|\;\tilde{A}_t^{(\mu)} = \tfrac{T}{l_1},\ \tilde{B}_t^{(\mu)} = \tfrac{1}{2}\log\tfrac{l_2}{l_1}\Big]\,\psi_t^{(\mu)}\left(\tfrac{T}{l_1}, \tfrac{1}{2}\log\tfrac{l_2}{l_1}\right)\,dt. \tag{6.16}$$

where $\psi_t^{(\mu)}$ *is the joint density of* $(\tilde{A}_t^{(\mu)}, \tilde{B}_t^{(\mu)})$.

Proof. We start by inserting the identity

$$1 = \int_0^\infty \delta(A_t^{(\mu)} - T)\,dA_t^{(\mu)},$$

into (6.14), where $A_t^{(\mu)} = \int_0^t e^{2B_s^{(\mu)}}\,ds$, $B_t^{(\mu)} = B_t + \mu\,t$ starting at $B_0^{(\mu)} = \frac{1}{2}\log l_1$. Then

$$\mathbb{E}_{L_0^{(\delta)}=l_1}\Big[\,\delta\Big(L_T^{(\delta)} - l_2\Big)\,e^{-\Lambda\int_0^T L_s^{(\delta)}\,ds}\Big] = \mathbb{E}\Big[\int_0^\infty \delta\Big(L^{(\delta)}_{A_t^{(\mu)}} - l_2\Big)\,e^{-\Lambda\int_0^{A_t^{(\mu)}} L_s^{(\delta)}\,ds}\,\delta\Big(A_t^{(\mu)} - T\Big)\,dA_t^{(\mu)}\Big].$$

Changing variables ($s = A_v^{(\mu)}$) in the integral and using $dA_t^{(\mu)} = e^{2B_t^{(\mu)}}dt$, $C_t^{(\mu)} := \int_0^t e^{4B_s^{(\mu)}}\,ds$, we arrive at

$$\begin{aligned} G_\Lambda^{(\delta)}(l_1,l_2;T) &= \mathbb{E}_{B_0^{(\mu)}=\frac{1}{2}\log l_1}\Big[\int_0^\infty \delta\Big(e^{2B_t^{(\mu)}} - l_2\Big)\,e^{-\Lambda\,C_t^{(\mu)}}\,\delta\Big(A_t^{(\mu)} - T\Big)\,e^{2B_t^{(\mu)}}\,dt\Big] \\ &= \frac{1}{2}\int_0^\infty \mathbb{E}_{B_0^{(\mu)}=\frac{1}{2}\log l_1}\Big[\delta\Big(B_t^{(\mu)} - \tfrac{1}{2}\log l_2\Big)\,\delta\Big(A_t^{(\mu)} - T\Big)\,e^{-\Lambda\,C_t^{(\mu)}}\Big]\,dt, \end{aligned} \tag{6.17}$$

where we have used the delta function identity

$$\delta\Big(e^{2x} - l_2\Big) = \frac{1}{2\,l_2}\,\delta\Big(x - \tfrac{1}{2}\log l_2\Big).$$

It will be useful to shift the Brownian motion to start at the origin. Clearly, the new Brownian motion $\tilde{B}_t^{(\mu)} = B_t^{(\mu)} - \frac{1}{2}\log l_1$ starts at 0. Furthermore,

$$A_t^{(\mu)} = \int_0^t e^{2B_s^{(\mu)}}\,ds = \int_0^t e^{2(\tilde{B}_s^{(\mu)} + \frac{1}{2}\log l_1)}\,ds = l_1\tilde{A}_t^{(\mu)},$$

$$C_t^{(\mu)} = \int_0^t e^{4B_s^{(\mu)}}\,ds = \int_0^t e^{4(\tilde{B}_s^{(\mu)} + \frac{1}{2}\log l_1)}\,ds = l_1^2\tilde{C}_t^{(\mu)},$$

$$\delta\Big(B_t^{(\mu)} - \tfrac{1}{2}\log l_2\Big) = \delta\Big(\tilde{B}_t^{(\mu)} - \tfrac{1}{2}\log\tfrac{l_2}{l_1}\Big),$$

$$\delta\Big(l_1 A_t^{(\mu)} - T\Big) = \frac{1}{l_1}\delta\Big(\tilde{A}_t^{(\mu)} - \tfrac{T}{l_1}\Big).$$

Hence we obtain

$$G_\Lambda^{(\delta)}(l_1, l_2; T) = \frac{1}{2l_1}\int_0^\infty \mathbb{E}_{\tilde{B}_0^{(\mu)}=0}\Big[\delta\Big(\tilde{B}_t^{(\mu)} - \tfrac{1}{2}\log\tfrac{l_2}{l_1}\Big)\,\delta\Big(\tilde{A}_t^{(\mu)} - \tfrac{T}{l_1}\Big)\,e^{-\Lambda\, l_1^2\,\tilde{C}_t^{(\mu)}}\Big]\,dt.$$

and the desired result (6.16). □

It remains to compute the expectation in (6.16) from which we can evaluate the heat kernel of CDT and make apparent the connection to Morse quantum mechanics.

Lemma 6.3.4.

$$\begin{aligned}&\mathbb{E}_{\tilde{B}_0^{(\mu)}=0}\Big[e^{-\Lambda\, l_1^2\,\tilde{C}_t^{(\mu)}}\;\Big|\;\tilde{A}_t^{(\mu)} = \tfrac{T}{l_1},\ \tilde{B}_t^{(\mu)} = \tfrac{1}{2}\log\tfrac{l_2}{l_1}\Big]\,\psi_t^{(\mu)}\left(\tfrac{T}{l_1}, \tfrac{1}{2}\log\tfrac{l_2}{l_1}\right)\\ &= \left(\frac{l_2}{l_1}\right)^{\mu/2} e^{-\mu^2 t/2}\frac{l_1\sqrt{2\Lambda}}{\sinh\Big(\sqrt{2\Lambda}T\Big)}e^{-\sqrt{\frac{\Lambda}{2}}(l_1+l_2)\coth\left(\sqrt{2\Lambda}T\right)}\theta\left(\frac{\sqrt{2\Lambda l_1 l_2}}{\sinh\Big(\sqrt{2\Lambda}T\Big)}, t\right)\end{aligned} \tag{6.18}$$

where

$$\theta(r,t) := \frac{r}{\sqrt{2\pi^3 t}}\,e^{\pi^2/2t}\int_0^\infty e^{-\frac{\xi^2}{2t} - r\cosh(\xi)}\sinh(\xi)\,\sin\left(\frac{\pi\,\xi}{t}\right)d\xi. \tag{6.19}$$

Proof. We give a proof for $\mu = 0$, the result for general μ can be recovered from the Cameron-Martin/Girsanov theorem. Since we are dealing with $\mu = 0$ we will drop the superscripts and consider the variables $\tilde{C}_t := \tilde{C}_t^{(0)}$, $\tilde{A}_t := \tilde{A}_t^{(0)}$, $\tilde{B}_t := \tilde{B}_t^{(0)}$. Consider the following Schrödinger operator with Morse potential,

$$\tilde{H}_{\Lambda,k} = -\frac{1}{2}\frac{d^2}{d\tilde{x}^2} + \Lambda e^{4\tilde{x}} - 2\sqrt{2\Lambda}ke^{2\tilde{x}}.$$

The heat kernel $\tilde{q}_{\Lambda,k}(t,\tilde{x},\tilde{y})$ of the semigroup generated by $\tilde{H}_{\Lambda,k}$ is, by the Feynman-Kac formula:

$$\tilde{q}_{\Lambda,k}(t,\tilde{x},\tilde{y}) = \mathbb{E}_{\tilde{B}_0=0}\Big[\exp\Big\{-\Lambda\, e^{4\tilde{x}}\,\tilde{C}_t + 2\sqrt{2\Lambda}ke^{2\tilde{x}}\tilde{A}_t\Big\}\;\Big|\;\tilde{B}_t = \tilde{y} - \tilde{x}\Big]\frac{1}{\sqrt{2\pi t}}e^{-|\tilde{y}-\tilde{x}|^2/2t}. \tag{6.20}$$

Using the scaling property of Brownian motion:

$$\tilde{B}_t \overset{\text{(law)}}{=} \frac{1}{2}B'_{4t},$$

where B'_t is another standard Brownian motion starting at 0, it follows that

$$\tilde{C}_t = \int_0^t e^{4\tilde{B}_s}ds \overset{\text{(law)}}{=} \int_0^t e^{2B'_{4s}}ds = \frac{1}{4}\int_0^{4t} e^{2B'_s}\,ds =: \frac{1}{4}A'_{4t}$$

and,

$$\tilde{A}_t = \frac{1}{4}\int_0^{4t} e^{B'_s}\, ds =: \frac{1}{4}a'_{4t}.$$

The Morse heat kernel becomes

$$\tilde{q}_{\Lambda,k}(t,\tilde{x},\tilde{y}) = \mathbb{E}_{B'_0=0}\Big[\exp\Big\{-\frac{\Lambda}{4}\,e^{2x}\,A'_{4t} + \sqrt{\frac{\Lambda}{2}}ke^{x}\tilde{a}'_{4t}\Big\}\,\Big|\,B'_{4t} = y-x\Big]\frac{1}{\sqrt{2\pi t}}e^{-|y-x|^2/8t},$$

where we have used the fact that $y = 2\tilde{y}$ and $x = 2\tilde{x}$. It was shown in [118], that this expectation is given by

$$\tilde{q}_{\Lambda,k}(t,\tilde{x},\tilde{y}) = \int_0^\infty \frac{e^{2ku}}{\sinh u}\, e^{-\sqrt{\frac{\Lambda}{2}}\,(e^x+e^y)\coth u}\,\theta\Big(\frac{\sqrt{2\Lambda}\,e^{(x+y)/2}}{\sinh u},\, t\Big)\,du$$

and after a change of integration variable can be written as

$$\tilde{q}_{\Lambda,k}(t,\tilde{x},\tilde{y}) = \int_0^\infty \frac{e^{2\sqrt{2\Lambda}kT}}{\sinh\big(\sqrt{2\Lambda}T\big)}\, e^{-\sqrt{\frac{\Lambda}{2}}\,(e^x+e^y)\coth\left(\sqrt{2\Lambda}T\right)}\,\theta\left(\frac{\sqrt{2\Lambda}\,e^{(x+y)/2}}{\sinh\big(\sqrt{2\Lambda}T\big)},\, t\right)\,\sqrt{2\Lambda}\,dT.$$

At the same time we can write the expectation in (6.20) as

$$\tilde{q}_{\Lambda,k}(t,\tilde{x},\tilde{y}) = \int_0^\infty \exp\Big\{2\sqrt{2\Lambda}ke^{2\tilde{x}}v\Big\}\,\mathbb{E}_{\tilde{B}_0=0}\Big[\exp\Big\{-\Lambda\,e^{4\tilde{x}}\,\tilde{C}_t\Big\}\,\Big|\,\tilde{A}_t = v,\,\tilde{B}_t = \tilde{y}-\tilde{x}\Big] \times \psi_t\,(v,\tilde{y}-\tilde{x})\,dv$$

after making the change of variables $v = e^{-2\tilde{x}}T$,

$$\tilde{q}_{\Lambda,k}(t,\tilde{x},\tilde{y}) = \int_0^\infty e^{2\sqrt{2\Lambda}kT}\,\mathbb{E}_{\tilde{B}_0=0}\Big[\exp\Big\{-\Lambda\,e^{4\tilde{x}}\,\tilde{C}_t\Big\}\,\Big|\,\tilde{A}_t = Te^{-2\tilde{x}},\,\tilde{B}_t = \tilde{y}-\tilde{x}\Big] \times \psi_t\left(Te^{-2\tilde{x}},\tilde{y}-\tilde{x}\right)e^{-2\tilde{x}}dT.$$

By the uniqueness of the Laplace transform and returning to the original variables $e^{2\tilde{x}} = l_1$, $e^{2\tilde{y}} = l_2$ we have the desired result for $\mu = 0$. Finally applying the Cameron-Martin theorem, we have the result for general drift. □

The proof of Theorem (6.3.2) follows almost immediately.

Proof of Theorem 6.3.2. Using the results of Lemmas 6.3.3 and 6.3.4 and the known relation [118]

$$\int_0^\infty e^{-\mu^2 t/2}\theta(r,t)\,dt = I_{|\mu|}(r),$$

the result follows immediately. □

When $\mu = 1$, (6.14) coincides with the known result for the continuum two-loop propagator of CDT as expected.

This long winded approach to computing the expectation in (6.14) via the time-change highlights an interesting connection between CDT and Morse quantum mechanics. It is known that Morse QM is unitarily equivalent to a particle in a magnetic field on the hyperbolic plane [118, 119] which hints at the origin of the emergent hyperbolic geometry latent in CDT. What's more, JT gravity also has a known description in terms of a particle in a magnetic field [120] on $\mathbf{H}^2$ which is famously a theory with constant negative curvature ($R = -2$).

6.4 Discussion and outlook

In this final chapter, we have demonstrated another use of the stochastic approach to investigating continuum CDT. We have made rigorous the findings in [1] and gone further to provide a full stochastic differential equation for the conditioned process. Furthermore, we implemented a stochastic time-change to the pure CDT process, transforming it into an exponential Brownian process.

The geometrical content of the time-change is transparent in expectation: Lamperti time makes the average spatial length grow exponentially, yielding an emergent constant negative curvature metric from CDT.

Using Doob h-transforms, we recovered the sinh profile of [1] by conditioning the killed CDT process and contrasted it with the Lamperti-induced hyperbolic geometry. Together, these results sharpen the sense in which hyperbolic space is latent in CDT and becomes manifest either by conditioning or by reparameterising time.

It would be interesting to explore further the connection between the time-changed model of CDT and Morse quantum mechanics. Not least because of the connection between the latter and the particle in a magnetic field description of JT gravity. This connection could provide a useful dictionary between the two theories of quantum gravity allowing for new computations in each direction.

Another direction for future work is whether we can incorporate generalised CDT with topology change into the stochastic framework. Would there be a sensible time-change and a deeper connection to JT gravity which includes geometries of all genus and boundaries?

Conceptually, it would be nice to find a microscopic, combinatorial origin of the Lamperti-type reparameterisation that can be engineered directly at the discretised level from which hyperbolic space would emerge dynamically.

7
Concluding Remarks

This thesis has explored causal random geometry in two dimensions from three complementary vantage points: discrete ensembles, stochastic analysis, and matrix models. Along the way, we established precise bridges between these descriptions and used them to address a long-standing question: how unitary matter couples to causal dynamical triangulations. The common thread is that causality enforces an essentially one-dimensional, continuous dynamical variable for the spatial length that shapes both critical behaviour and geometry and allows us to leverage the large technical machinery of stochastic calculus which has thus far been left untapped.

Matter coupling: why KPZ fails and conformal data remain classical. The first part of the thesis revisited two-dimensional quantum gravity in both its Euclidean (Liouville) and causal (CDT) incarnations. In the causal setting, the transfer-matrix/propagator analysis and the tree bijection lead to a continuum limit in which the length of a spatial slice, $L(t)$, evolves according to a diffusion with drift. We derived the associated Itô dynamics directly from the critical Galton–Watson process conditioned on infinite survival, recovering a Lamperti–Ney/Bessel-type stochastic differential equation with a strictly positive, continuous solution.

We then addressed the coupling of unitary matter to CDT, focusing on the Ising model as a canonical test case but with arguments that extend to RSOS/height models. Building

on the plaquette/defect formalism for lattice CFTs, we constructed topological defect lines (identity, spin-flip, and duality) on CDT graphs and established their fusion-category relations. We defined Dehn twist operators on CDT both microscopically and in the continuum, proving exact algebraic relations and extracting conformal dimensions. Because the continuum $L(t)$ is almost surely continuous and admits neighbourhoods homeomorphic to $S^1 \times [0,1]$, the Dehn twist exists in the continuum and commutes with the transfer matrix, letting us equate its eigenvalues with those of $e^{2\pi i(L_0-\bar{L}_0)}$. Consequently, the spins of the Ising primaries remain those of the flat lattice, $h_\psi = 1/2 + \mathbb{Z}$ and $h_\sigma = 1/16 + \mathbb{Z}$.

This analysis dovetails with an adapted Duplantier–Sheffield framework: defining the causal random measure by $d\mu = L(t)\,dt$, the one-dimensional and continuous nature of $L(t)$ implies that the "quantum" and Euclidean scaling exponents coincide (up to expected logarithmic corrections). There is, therefore, no KPZ dressing for unitary matter on CDT. The underlying mechanism is positivity and continuity: the CDT measure produces a genuine function $L(t)$ rather than a log-correlated distribution. This explains the robust numerical finding that unitary minimal models coupled to CDT retain their classical exponents, even beyond $c = 1$. It also clarifies the exception of non-unitary models (e.g. hard dimers), where complex weights destroy the probabilistic positivity underpinning the argument and KPZ-like shifts can reappear, albeit with possibly different values (see [36] for further discussion).

Matrix models and FRGE: causal constraints kill anomalous dimensions. A complementary perspective came from matrix models equipped with auxiliary matrices imposing causal ribbon-graph structure. Within a functional renormalisation group equation (FRGE) setup and a controlled truncation, we tracked the flow of single-trace interactions and identified fixed points relevant to pure CDT and to Ising–CDT. A central outcome is that the causal "C-matrix" structure enforces a vanishing anomalous dimension in the gravitational sector at the fixed points probed, making it impossible for there to be a KPZ-like relation that shifts the critical exponents and hence the conformal dimensions of any matter-coupled system. Moreover, we found non-trivial fixed points with three relevant directions, matching the number of Ising primaries. These FRGE

results corroborate the stochastic/defect-based picture and provide a renormalisation-group explanation for the absence of KPZ dressing in causal ensembles as well as providing evidence for the existence of an Ising–CDT continuum limit.

Emergent hyperbolic geometry. The stochastic formulation sheds light on the findings that there is an emergent hyperbolic space in CDT. It emerges by conditioning the killed process to survive and using the theory of Doob h-transforms. We find sinh/exponential profiles, thus exposing an intrinsic AdS_2-like character. Moreover, using Lamperti's time change links the squared-Bessel description to exponential Brownian motion—another emergence of hyperbolic geometry. We saw hints at the origin of this AdS-like spacetime by computing the two-loop propagator with the time-change as an intermediate step. This step reveals an underlying connection to Morse quantum mechanics and hints at a further connection to a particle in a magnetic field description of JT gravity that requires further investigation.

Summary and outlook

Taken together, the results are summarised as follows:

- Causality replaces the fractal, distributional Liouville geometry by a continuous, one-dimensional stochastic dynamics for the spatial length. This collapses the potential for KPZ dressing while preserving a rich continuum Hamiltonian structure.
- Topological defect lines and the fusion category survive the continuum limit on CDT. The existence of Dehn twists then fixes the spins of primary fields to their flat-lattice values for unitary matter, in agreement with numerics and in tension only with non-unitary cases where positivity fails.
- Within matrix-model FRGE, the causal constraint yields vanishing anomalous dimensions at the relevant fixed points, aligning renormalisation-group intuition with the stochastic/defect arguments and providing evidence for the existence of a continuum limit.

- Hyperbolic geometry emerges naturally by conditioning/time-changing the stochastic length process, revealing this latent feature in CDT and demonstrating the value of the stochastic picture.

Several directions require further work and appear promising:

1. Annealed CDT with unitary matter: the key technical step is to identify or derive the effective stochastic process $X(t)$ that governs the combined geometry–matter ensemble and to prove its almost-sure continuity in the scaling limit. If continuity holds and the limit is second order (no first-order transition), the defect/Dehn-twist argument should again freeze the conformal data to their flat-lattice values. Establishing the discrete–continuum bridge without an explicit tree bijection remains a central challenge.

2. Non-unitary matter (e.g. hard dimers) fall outside the positivity assumptions; quantifying the onset of KPZ-like dressing in such cases could clarify the boundary of the CDT universality class. In higher dimensions, the analogue of $L(t)$ will not be a single scalar, and constructing appropriate defect/twist operators and stochastic reductions is a major, but potentially tractable, problem.

3. Expanded FRGE truncations: include multi-trace couplings, couplings with more than two C matrices, and explore scheme dependencies to test the robustness of the fixed points.

4. Numerical methods could be used to further explore the parameter space of the Ising-CDT matrix model fixed points beyond the analytic reach of this thesis.

5. Finding a discrete origin of the Lamperti time-change. This would provide valuable insight into the physical meaning of what this new time represents and may shed further light on the connection to Morse quantum mechanics and possibly to JT gravity.

It is my hope that this thesis has demonstrated how causal constraints tame the two-dimensional gravitational path integral while still producing a rich model of quantum gravity. The technical machinery of stochastic calculus for causal random geometry has proven to be extremely powerful in analysing various aspects of this model. My hope and belief is that this new perspective will continue to be fruitful in tackling many remaining open problems in quantum gravity.

Appendices

A

Supplementary material for Chapter 4

A.1 Defects at the boundary

One is free to choose boundary conditions as part of the definition of the partition function. Two choices are *free* and *fixed*. In the free case, the boundary spins are summed over in the partition function just like any other bulk spin. In the fixed case, the boundary is defined by a state, $|B\rangle = |...0001101011...\rangle$ for example, which specifies the spin at every boundary vertex. We are interested in whether a defect is free to move at the boundary without altering the partition function. Figure A.1 shows the boundary spins a, b, c, d in the presence of a spin defect. Notice that the final plaquettes are horizontal to signify that an edge joins the boundary points.

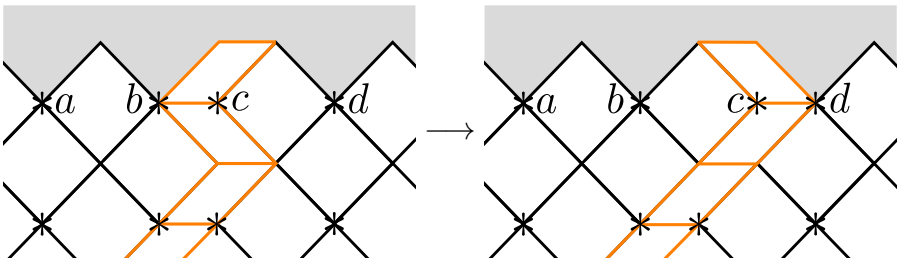

Figure A.1: Spin defect ending at the boundary (top) being moved one spin to the right. The boundary spins are those marked a, b, c, d.

If the boundary conditions are free, then by the same bulk moves in (4.17–4.18),

a spin defect move at the boundary is also topological. On the other hand, suppose we fix the boundary such that $a = 0, b = 0, c = 1, d = 1$, then before the move, the section of the boundary shown in Figure A.1 contributes a factor $W^H(u)_{00}W^H(u)_{11} \times 1$, where the factor of 1 comes from the spin defect. After the move the contribution is $W^H(u)_{00}W^H(u)_{10} \times 0$, where the factor of 0 also comes from the spin defect but with the same spin on each side of the plaquette. Hence this move does not preserve the partition function and is not topological. Moving the defect to the left is similarly not allowed. The defect can therefore be pinned by choosing a boundary condition in which all spins are 1, except for two adjacent spins that are 0.

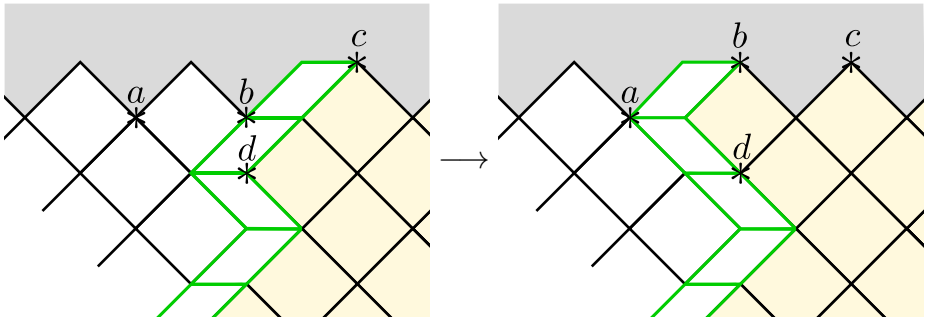

Figure A.2: Moving a duality defect at the boundary (top) one step to the left. The boundary spins are a, b, c. The yellow shading shows the difference between the dual and original plaquettes.

The case of the duality defect is slightly trickier – consider the diagram in Figure A.2. The left-hand side of the figure contributes a factor

$$W^H(u_H)_{ab}(-1)^{bd}(-1)^{bc}, \tag{A.1}$$

whereas the right-hand side is given by

$$W^V(u_H)_{bd}(-1)^{ad}(-1)^{ab}. \tag{A.2}$$

Now consider free boundary conditions. This amounts to summing over b since this is the only internal spin in the diagram. Evaluating $\sum_b$(A.1) and $\sum_b$(A.2), one finds that these can never be equal for all combinations of a, d, c. Thus the duality defect cannot be moved along the boundary without changing the partition function for all values of

u_H, u_V. A similar argument shows that for a magnetised boundary with $a = b = c = 0$ the duality defect cannot be moved freely.

We conclude that it is possible to pin any defect to the boundary by choosing suitable boundary conditions.

A.2 The domain wall

As we alluded to in Section 4.4, when considering a vertical duality defect in a space with periodic boundary conditions, we necessarily require a domain wall where the dual lattice meets the original again. In this appendix, we will elaborate on the details of the wall and show that defects can pass through the wall topologically.

One way to implement the wall is to introduce a new plaquette that identifies the spins at the wall. This plaquette is defined as

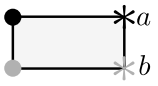

$= \delta_{ab},$ (A.3)

and Figure A.3 shows how it is implemented at the interface of the original and dual lattices.

Consider a horizontal sequence of duality defect plaquettes, such as those that constitute the Dehn twist in the presence of a vertical duality defect. At some point, there will be an intersection of the horizontal plaquettes with the wall, as shown in Figure A.4. Notice that at the intersection of the wall and the horizontal defect, there is a new type of object

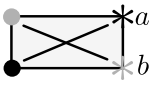

$= \delta_{ab}$ (A.4)

which is almost identical to (A.3) but differs with the relative positions of the original and dual empty sites.

The question is whether the horizontal defect can be moved along the wall and what happens when two horizontal defects meet at the wall. To answer the first question,

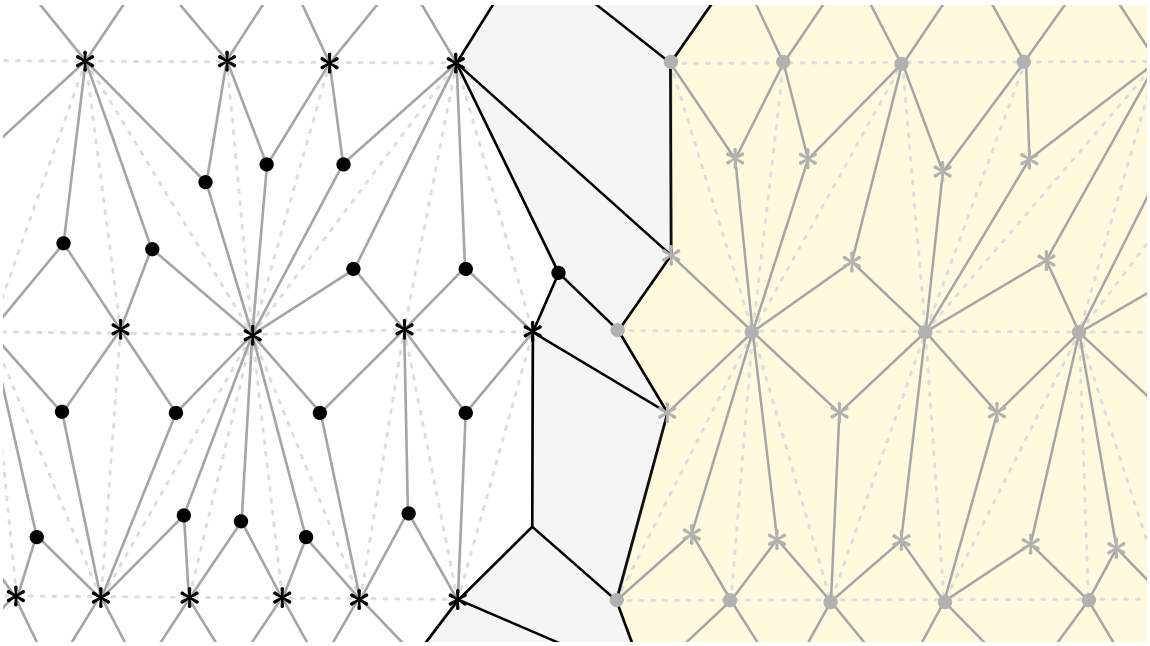

Figure A.3: The domain wall where the original and dual lattice meet again in the presence of a vertical duality defect. Black asterisks indicate the positions of the spins on G, while gray asterisks mark the positions of the spins on G^*. Black dots denote empty positions in G, and gray dots denote empty positions in G^*. The dotted lines depict the underlying triangulation.

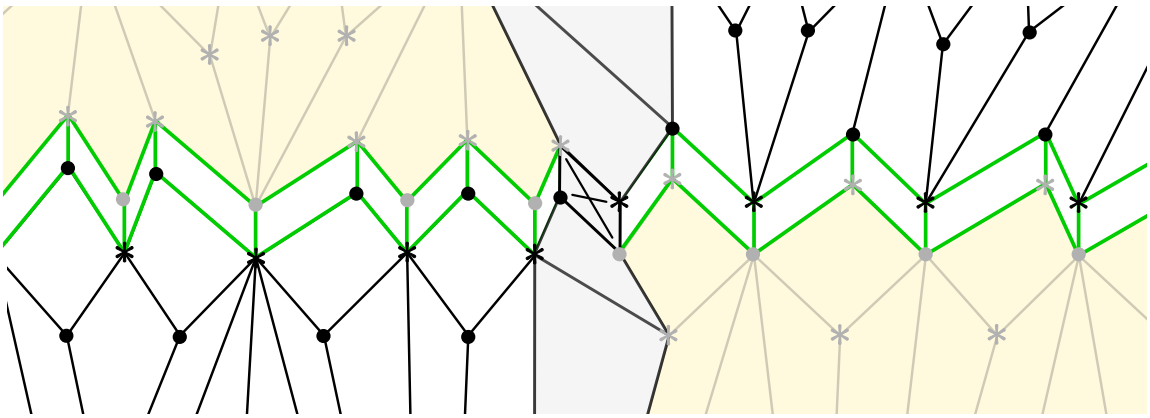

Figure A.4: The intersection of a horizontal duality defect and the domain wall.

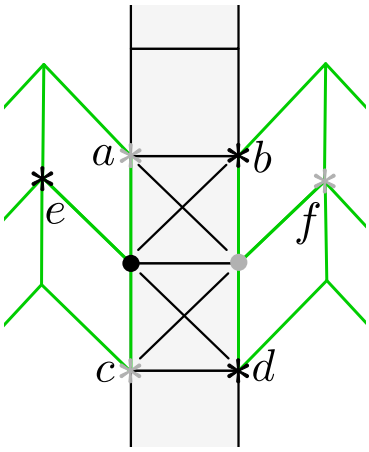

Figure A.5: Two horizontal duality defects meeting at the wall.

consider the following diagram

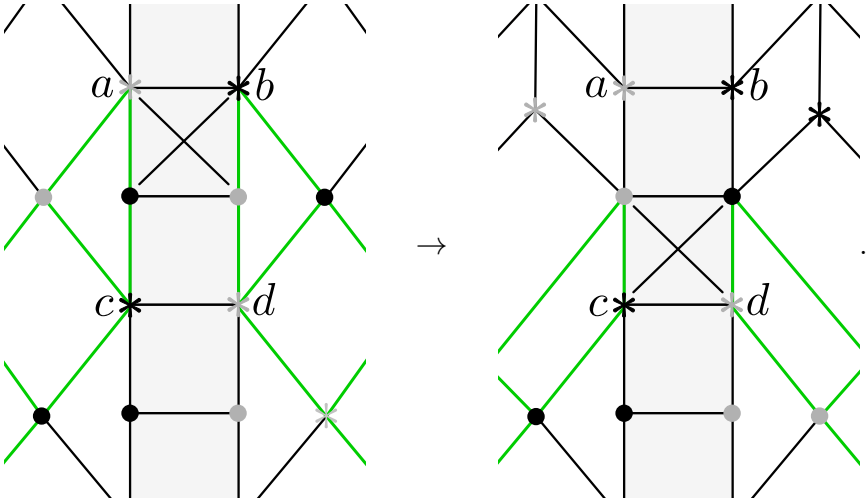

(A.5)

Evaluating the left-hand side,

$$\begin{aligned} &= 2^{-1/2}(-1)^{ac} \times 2^{-1/2}(-1)^{bd} \times \delta_{ab}\delta_{cd} \times 2^{1/2} \times 2^{1/2} \\ &= (-1)^{ac}(-1)^{bd}\delta_{ab}\delta_{cd} = \delta_{ab}\delta_{cd} \end{aligned} \tag{A.6}$$

where the final factors of $\sqrt{2}$ come from the additional blank vertices on the left-hand side compared to the right-hand side. The right-hand side of (A.5) gives the same result. Therefore, we have shown that the duality defect can be moved along the wall without obstruction. Finally, we must show what happens when two horizontal duality defects meet at the wall. Consider the diagram in Figure A.5, as was shown in [95] when two duality defects meet, it is equivalent to the sum of an identity and a spin defect.

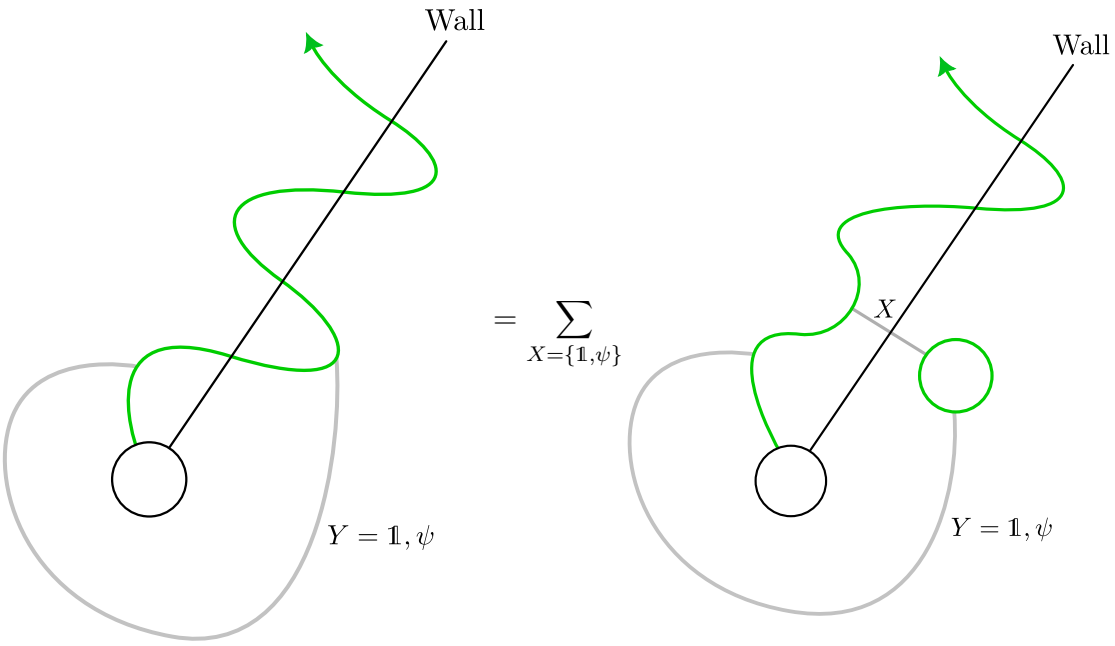

Figure A.6: Macroscopic view of applying (A.7) to the set up in Section 4.4.5. If $Y = \mathbb{1}$, the non-zero contribution is the identity defect passing through the wall. Otherwise, if $Y = \psi$, then the spin defect passes through the wall.

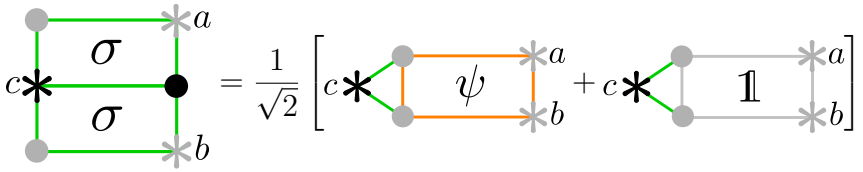

$$= \frac{1}{\sqrt{2}} \left[\delta_{ab} + \sigma^x_{ab}\right] \tag{A.7}$$

Since the spins across the wall are identified, the only non-zero contributions are those in which there is either an identity or a spin defect on both sides of Figure A.5. Contributions where there is an identity on one side but a spin on the other vanish.

We are interested in whether we can perform the topological moves needed at the end of Section 4.4 in the presence of a wall. In this setup, a single duality defect crosses the wall multiple times, as shown in Figure A.6. As we concluded above, merging two duality lines at the wall produces a sum over an identity defect and a spin defect that passes through the wall. Depending on the type of defect that wraps around the centre of the space, either the identity or the spin defect will pass through the wall as shown in

Figure A.6. In each case, the remaining duality bubble shrinks to zero, contributing a factor of $\sqrt{2}$ which cancels the factor in the sum in (A.7). Hence, we have shown that the duality defect can be moved through the wall, allowing us to perform the necessary moves in calculating the conformal dimensions in Section 4.4.5.

B

Supplementary material for Chapter 5

B.1 Critical exponents for the RG fixed points

In this section, we present the values of the critical exponents, obtained by diagonalising the Hessian matrix $H_{ij} = -\frac{\partial \beta_i}{\partial g_j}$. As explained in the main text, eigenvalues in the upper-left block take three different values, corresponding to irrelevant, marginal and relevant directions. We specify the degeneracy of these eigenvalues for each solution of the beta-function equations in the left half of Table B.1. We have also seen that in the bottom-right block of the Hessian, the eigenvalues take three possible values. We specify the degeneracies of these eigenvalues for each solution on the right half of the same table.

Solution	α_4	0	-α_4	α_6	$\alpha_6 - \alpha_4$	$\alpha_6 - 2\alpha_4$
1A	5	0	0	20	0	0
1B	3	1	1	12	6	2
1C	3	1	1	12	6	2
1D	2	0	3	6	8	6
2A	4	0	1	12	6	2
2B	2	1	2	6	8	6
2C	2	1	2	6	8	6
2D	1	0	4	2	6	12
3A	4	0	1	12	6	2
3B	2	1	2	6	8	6
3C	2	1	2	6	8	6
3D	1	0	4	2	6	12
4A	3	0	2	6	8	6
4B	1	1	3	2	6	12
4C	1	1	3	2	6	12
4D	0	0	5	0	0	20

Table B.1: Degeneracy of the eigenvalues in both the upper-left and the bottom-right blocks of the Hessian for each fixed point.

Note that the order six operators are all irrelevant for $\frac{\alpha_6}{\alpha_4} > 2$ and all irrelevant or marginal for the canonical values $\alpha_4 = -1$ and $\alpha_6 = -2$.

We list the degeneracies of the critical exponents on the fixed line segments (section 5.5.2) in Table B.2.

Solution	α_4	0	-α_4	α_6	$\alpha_6 - \alpha_4$	$\alpha_6 - 2\alpha_4$
1R	3	1	1	12	6	2
1S	3	1	1	12	6	2
2R	2	1	2	6	8	6
2S	2	1	2	6	8	6
3R	2	1	2	6	8	6
3S	2	1	2	6	8	6
4R	1	1	3	2	6	12
4S	1	1	3	2	6	12

Table B.2: Degeneracy of the eigenvalues in both the upper-left and the bottom-right blocks of the Hessian for fixed line segments.

Segments of fixed points have the same critical exponents as the corresponding B and C type solutions. They feature exactly one marginal direction in the order four parameter space, corresponding to the direction along the segment.

To steal ideas from one person is plagiarism; to steal from many is research.

— Wilson Mizner

References

[1] J. Ambjørn et al. "The emergence of background geometry from quantum fluctuations". In: *Physics Letters B* 641.1 (Sept. 2006), pp. 94–98. DOI: 10.1016/j.physletb.2006.08.021. arXiv: gr-qc/0607013 [gr-qc].

[2] Gerard 't Hooft and M. J. G. Veltman. "One-loop divergencies in the theory of gravitation". In: *Ann. Inst. H. Poincare Phys. Theor. A* 20.1 (1974), pp. 69–94. DOI: 10.1142/9789814539395_0001.

[3] Marc H. Goroff and Augusto Sagnotti. "Quantum gravity at two loops". In: *Phys. Lett. B* 160 (1985), pp. 81–86. DOI: 10.1016/0370-2693(85)91470-4.

[4] Marc H. Goroff and Augusto Sagnotti. "The Ultraviolet Behavior of Einstein Gravity". In: *Nucl. Phys. B* 266 (1986), pp. 709–736. DOI: 10.1016/0550-3213(86)90193-8.

[5] Carlo Rovelli. "What Is Observable in Classical and Quantum Gravity?" In: *Class. Quant. Grav.* 8 (1991), pp. 297–316. DOI: 10.1088/0264-9381/8/2/011.

[6] A.M. Polyakov. "Quantum geometry of bosonic strings". In: *Physics Letters B* 103.3 (1981), pp. 207–210. DOI: https://doi.org/10.1016/0370-2693(81)90743-7.

[7] Nathan Seiberg. "Notes on quantum Liouville theory and quantum gravity". In: *Prog. Theor. Phys. Suppl.* 102 (1990), pp. 319–349. DOI: 10.1143/PTPS.102.319.

[8] J Teschner. "Liouville theory revisited". In: *Classical and Quantum Gravity* 18.23 (Nov. 2001), R153–R222. DOI: 10.1088/0264-9381/18/23/201. arXiv: hep-th/0104158 [hep-th].

[9] Yu Nakayama. "Liouville field theory: A Decade after the revolution". In: *Int. J. Mod. Phys. A* 19 (2004), pp. 2771–2930. DOI: 10.1142/S0217751X04019500. arXiv: hep-th/0402009.

[10] A. Zamolodchikov and Al. Zamolodchikov. "Conformal bootstrap in Liouville field theory". In: *Nuclear Physics B* 477.2 (Oct. 1996), pp. 577–605. DOI: 10.1016/0550-3213(96)00351-3. arXiv: hep-th/9506136 [hep-th].

[11] A. A. Belavin, Alexander M. Polyakov, and A. B. Zamolodchikov. "Infinite Conformal Symmetry in Two-Dimensional Quantum Field Theory". In: *Nucl. Phys. B* 241 (1984). Ed. by I. M. Khalatnikov and V. P. Mineev, pp. 333–380. DOI: 10.1016/0550-3213(84)90052-X. arXiv: hep-th/0601056 [hep-th].

[12] P. Ginsparg and Gregory Moore. "Lectures on 2D gravity and 2D string theory (TASI 1992)". In: 1993. arXiv: hep-th/9304011 [hep-th].

[13] Philippe Di Francesco, Pierre Mathieu, and David Sénéchal. *Conformal Field Theory*. New York: Springer, 1997. DOI: 10.1007/978-1-4612-2256-9.

[14] Tullio Eugenio Regge. "General relativity without coordinates". In: *Il Nuovo Cimento (1955-1965)* 19 (1961), pp. 558–571.

[15] Jan Ambjørn, Bergfinnur Durhuus, and Thordur Jonsson. *Quantum Geometry: A Statistical Field Theory Approach*. Cambridge Monographs on Mathematical Physics. Cambridge, UK: Cambridge Univ. Press, Dec. 2005. DOI: 10.1017/CBO9780511524417.

[16] V.A. Kazakov, I.K. Kostov, and A.A. Migdal. "Critical properties of randomly triangulated planar random surfaces". In: *Physics Letters B* 157.4 (1985), pp. 295–300. DOI: https://doi.org/10.1016/0370-2693(85)90669-0.

[17] F. David. "A model of random surfaces with non-trivial critical behaviour". In: *Nuclear Physics B* 257 (1985), pp. 543–576. DOI: https://doi.org/10.1016/0550-3213(85)90363-3.

[18] E. Brezin and V. A. Kazakov. "Exactly Solvable Field Theories of Closed Strings". In: *Phys. Lett. B* 236 (1990), pp. 144–150. DOI: 10.1016/0370-2693(90)90818-Q.

[19] Michael R. Douglas and Stephen H. Shenker. "Strings in Less Than One-Dimension". In: *Nucl. Phys. B* 335 (1990). Ed. by E. Brezin and S. R. Wadia, p. 635. DOI: 10.1016/0550-3213(90)90522-F.

[20] David J. Gross and Alexander A. Migdal. "Nonperturbative Two-Dimensional Quantum Gravity". In: *Phys. Rev. Lett.* 64 (1990). Ed. by E. Brezin and S. R. Wadia, p. 127. DOI: 10.1103/PhysRevLett.64.127.

[21] Dionysios Anninos and Beatrix Mühlmann. "Notes on matrix models (matrix musings)". In: *J. Stat. Mech.* 2008 (2020), p. 083109. DOI: 10.1088/1742-5468/aba499. arXiv: 2004.01171 [hep-th].

[22] B. Eynard. *Counting Surfaces*. Vol. 70. Progress in Mathematical Physics. Springer, 2016. DOI: 10.1007/978-3-7643-8797-6. arXiv: 2208.09474 [math.AG].

[23] Jean-François Le Gall. "The topological structure of scaling limits of large planar maps". In: *Inventiones mathematicae* 169.3 (Sept. 2007), pp. 621–670. DOI: 10.1007/s00222-007-0059-9. arXiv: math/0607567 [math.PR].

[24] Jean-François Le Gall. "Uniqueness and universality of the Brownian map". In: *The Annals of Probability* 41.4 (July 2013), pp. 2880–2960. DOI: 10.1214/12-AOP792. arXiv: 1105.4842 [math.PR].

[25] Grégory Miermont. "The Brownian map is the scaling limit of uniform random plane quadrangulations". In: (2011). arXiv: 1104.1606 [math.PR].

[26] Bertrand Duplantier and Scott Sheffield. "Liouville quantum gravity and KPZ". In: *Inventiones mathematicae* 185.2 (2011), pp. 333–393. DOI: 10.1007/s00222-010-0308-1. arXiv: 0808.1560 [math.PR].

[27] Rémi Rhodes and Vincent Vargas. "Gaussian multiplicative chaos and applications: a review". In: *Probab. Surv.* 11 (2014), pp. 315–392. DOI: 10.1214/13-PS218. arXiv: 1305.6221 [math.PR].

[28] Ewain Gwynne and Jason Miller. "Existence and uniqueness of the Liouville quantum gravity metric for $\gamma \in (0, 2)$". In: (2020). arXiv: 1905.00383 [math.PR].

[29] Omer Angel and Oded Schramm. "Uniform Infinite Planar Triangulations". In: *Communications in Mathematical Physics* 241.2–3 (Sept. 2003), pp. 191–213. DOI: 10.1007/s00220-003-0932-3. arXiv: math/0207153 [math.PR].

[30] Gregory F. Lawler, Oded Schramm, and Wendelin Werner. "Values of Brownian intersection exponents, I: Half-plane exponents". In: *Acta Mathematica* 187.2 (2001), pp. 237–273. DOI: 10.1007/BF02392618. arXiv: math/9911084 [math.PR].

[31] Bertrand Duplantier. "Random Walks and Quantum Gravity in Two Dimensions". In: *Phys. Rev. Lett.* 81 (25 Dec. 1998), pp. 5489–5492. DOI: 10.1103/PhysRevLett.81.5489.

[32] Jan Ambjorn and R. Loll. "Nonperturbative Lorentzian quantum gravity, causality and topology change". In: *Nucl. Phys. B* 536 (1998), pp. 407–434. DOI: 10.1016/S0550-3213(98)00692-0. arXiv: hep-th/9805108.

[33] J. Ambjørn, J. Jurkiewicz, and R. Loll. "Dynamically triangulating Lorentzian quantum gravity". In: *Nuclear Physics B* 610.1–2 (Sept. 2001), pp. 347–382. DOI: 10.1016/s0550-3213(01)00297-8. arXiv: hep-th/0105267 [hep-th].

[34] J. Ambjørn, J. Jurkiewicz, and R. Loll. "The universe from scratch". In: *Contemporary Physics* 47.2 (Mar. 2006), pp. 103–117. DOI: 10.1080/00107510600603344. arXiv: hep-th/0509010 [hep-th].

[35] J. Ambjørn et al. "A $c = 1$ phase transition in two-dimensional CDT/Horava– Lifshitz gravity?" In: *Physics Letters B* 743 (Apr. 2015), pp. 435–439. DOI: 10.1016/j.physletb.2015.03.008. arXiv: 1412.3873 [gr-qc].

[36] John F Wheater and P D Xavier. "The cylinder amplitude in the hard dimer model on 2D causal dynamical triangulations". In: *Classical and Quantum Gravity* 39.7 (Mar. 2022), p. 075004. DOI: 10.1088/1361-6382/ac50ec. arXiv: 2109.04414 [hep-th].

[37] Bergfinnur Durhuus, Thordur Jonsson, and John Wheater. "From Trees to Gravity". In: *Handbook of Quantum Gravity*. Ed. by Cosimo Bambi, Leonardo Modesto, and Ilya Shapiro. Singapore: Springer Nature Singapore, 2024, pp. 3385–3435. DOI: 10.1007/978-981-99-7681-2_86. arXiv: 2211.15247 [hep-th].

[38] R Loll. "Quantum gravity from causal dynamical triangulations: a review". In: *Classical and Quantum Gravity* 37.1 (Dec. 2019), p. 013002. DOI: 10.1088/1361-6382/ab57c7. arXiv: 1905.08669 [hep-th].

[39] Bergfinnur Durhuus, Thordur Jonsson, and John F. Wheater. "On the spectral dimension of causal triangulations". In: *J. Statist. Phys.* 139 (2010), p. 859. DOI: 10.1007/s10955-010-9968-x. arXiv: 0908.3643 [math-ph].

[40] J. Ambjørn, K. N. Anagnostopoulos, and R. Loll. "New perspective on matter coupling in 2D quantum gravity". In: *Physical Review D* 60.10 (Oct. 1999). DOI: 10.1103/physrevd.60.104035. arXiv: hep-th/9904012 [hep-th].

[41] J. Ambjorn, J. Jurkiewicz, and R. Loll. "Lorentzian and Euclidean Quantum Gravity - Analytical and Numerical Results". In: (2000). arXiv: hep-th/0001124 [hep-th].

[42] J.A. Ambjørn et al. "Shaken, but not stirred—Potts model coupled to quantum gravity". In: *Nuclear Physics B* 807.1-2 (Jan. 2009), pp. 251–264. DOI: 10.1016/j.nuclphysb.2008.08.030. arXiv: 0806.3506 [hep-lat].

[43] Jan Ambjørn et al. "2d CDT is 2d Hořava–Lifshitz quantum gravity". In: *Physics Letters B* 722.1 (2013), pp. 172–175. DOI: https://doi.org/10.1016/j.physletb.2013.04.006. arXiv: 1302.6359 [hep-th].

[44] Ryan Barouki, Henry Stubbs, and John Wheater. "Conformal Dimensions On Causal Random Geometry". In: (2025). arXiv: 2501.17930 [hep-th].

[45] J. Ambjorn, J. Jurkiewicz, and R. Loll. "Reconstructing the universe". In: *Phys. Rev. D* 72 (2005), p. 064014. DOI: 10.1103/PhysRevD.72.064014. arXiv: hep-th/0505154.

[46] J. Ambjorn, J. Jurkiewicz, and R. Loll. "Spectral dimension of the universe". In: *Phys. Rev. Lett.* 95 (2005), p. 171301. DOI: 10.1103/PhysRevLett.95.171301. arXiv: hep-th/0505113.

[47] J. Ambjørn et al. "Planckian Birth of the Quantum de Sitter Universe". In: *Phys. Rev. Lett.* 100 (2008), p. 091304. DOI: 10.1103/PhysRevLett.100.091304. arXiv: 0712.2485 [hep-th].

[48] Dario Benedetti and Joe Henson. "Imposing causality on a matrix model". In: *Phys. Lett. B* 678 (2009), pp. 222–226. DOI: 10.1016/j.physletb.2009.06.027. arXiv: 0812.4261 [hep-th].

[49] Alicia Castro and Tim Koslowski. "Renormalization Group Approach to the Continuum Limit of Matrix Models of Quantum Gravity with Preferred Foliation". In: *Frontiers in Physics* 9 (2021). DOI: 10.3389/fphy.2021.531766. arXiv: 2008.10090 [gr-qc].

[50] Astrid Eichhorn and Tim Koslowski. "Continuum limit in matrix models for quantum gravity from the Functional Renormalization Group". In: *Phys. Rev. D* 88 (2013), p. 084016. DOI: 10.1103/PhysRevD.88.084016. arXiv: 1309.1690 [gr-qc].

[51] Juan L. A. Abranches, Antonio D. Pereira, and Reiko Toriumi. "Dually Weighted Multi-matrix Models as a Path to Causal Gravity-Matter Systems". In: *Annales Henri Poincaré* 26.3 (Mar. 2025), pp. 947–1008. DOI: 10.1007/s00023-024-01442-1. arXiv: 2310.13503 [math-ph].

[52] Jürgen Berges, Nikolaos Tetradis, and Christof Wetterich. "Non-perturbative renormalization flow in quantum field theory and statistical physics". In: *Physics Reports* 363.4–6 (June 2002), pp. 223–386. DOI: 10.1016/s0370-1573(01)00098-9. arXiv: hep-ph/0005122 [hep-ph].

[53] N. Dupuis et al. "The nonperturbative functional renormalization group and its applications". In: *Physics Reports* 910 (May 2021), pp. 1–114. DOI: 10.1016/j.physrep.2021.01.001. arXiv: 2006.04853 [cond-mat.stat-mech].

[54] Joseph Polchinski. "Renormalization and Effective Lagrangians". In: *Nucl. Phys. B* 231 (1984), pp. 269–295. DOI: 10.1016/0550-3213(84)90287-6.

[55] Tim R. Morris. "The Exact Renormalization Group And Approximate Solutions". In: *International Journal of Modern Physics A* 09.14 (June 1994), pp. 2411–2449. DOI: 10.1142/s0217751x94000972. arXiv: hep-ph/9308265 [hep-ph].

[56] Matt Visser. "How to Wick rotate generic curved spacetime". In: (2017). arXiv: 1702.05572 [gr-qc].

[57] G. W. Gibbons and S. W. Hawking. "Action Integrals and Partition Functions in Quantum Gravity". In: *Phys. Rev. D* 15 (1977), pp. 2752–2756. DOI: 10.1103/PhysRevD.15.2752.

[58] G. W. Gibbons, S. W. Hawking, and M. J. Perry. "Path Integrals and the Indefiniteness of the Gravitational Action". In: *Nucl. Phys. B* 138 (1978), pp. 141–150. DOI: 10.1016/0550-3213(78)90161-X.

[59] Robert M. Wald. *Quantum Field Theory in Curved Space-Time and Black Hole Thermodynamics*. Chicago Lectures in Physics. Chicago, IL: University of Chicago Press, 1995.

[60] Petr Hořava. "Quantum gravity at a Lifshitz point". In: *Physical Review D* 79.8 (Apr. 2009). DOI: 10.1103/physrevd.79.084008. arXiv: 0901.3775 [hep-th].

[61] Petr Hořava. "Spectral Dimension of the Universe in Quantum Gravity at a Lifshitz Point". In: *Physical Review Letters* 102.16 (Apr. 2009). DOI: 10.1103/physrevlett.102.161301. arXiv: 0902.3657 [hep-th].

[62] Christian Anderson et al. "Quantizing Hořava-Lifshitz gravity via causal dynamical triangulations". In: *Physical Review D* 85.4 (Feb. 2012). DOI: 10.1103/physrevd.85.044027. arXiv: 1111.6634 [hep-th].

[63] Jan Ambjørn et al. "Second-Order Phase Transition in Causal Dynamical Triangulations". In: *Physical Review Letters* 107.21 (Nov. 2011). DOI: 10.1103/physrevlett.107.211303. arXiv: 1108.3932 [hep-th].

[64] J. Ambjørn et al. "CDT meets Hořava–Lifshitz gravity". In: *Physics Letters B* 690.4 (June 2010), pp. 413–419. DOI: 10.1016/j.physletb.2010.05.054. arXiv: 1002.3298 [hep-th].

[65] William T. Tutte. "A Census of Hamiltonian Polygons". In: *Canadian Journal of Mathematics* 14 (1962), pp. 402–417.

[66] William T. Tutte. "A Census of Planar Triangulations". In: *Canadian Journal of Mathematics* 14 (1962), pp. 21–38.

[67] William T. Tutte. "A Census of Slicings". In: *Canadian Journal of Mathematics* 14 (1962), pp. 708–722.

[68] William T. Tutte. "A Census of Planar Maps". In: *Canadian Journal of Mathematics* 15 (1963), pp. 249–271.

[69] E. Brezin et al. "Planar Diagrams". In: *Commun. Math. Phys.* 59 (1978), p. 35. DOI: 10.1007/BF01614153. arXiv: 1701.01171 [hep-th].

[70] Alexander A. Migdal. "Loop Equations and 1/N Expansion". In: *Phys. Rept.* 102 (1983), pp. 199–290. DOI: 10.1016/0370-1573(83)90076-5.

[71] Yu.M. Makeenko and A.A. Migdal. "Exact equation for the loop average in multicolor QCD". In: *Physics Letters B* 88.1 (1979), pp. 135–137. DOI: https://doi.org/10.1016/0370-2693(79)90131-X.

[72] Igor R. Klebanov. "String theory in two-dimensions". In: *Spring School on String Theory and Quantum Gravity (to be followed by Workshop)*. July 1991. arXiv: hep-th/9108019.

[73] Jérémie Bettinelli. *Planar map with 30,000 vertices*. URL: http://www.normalesup.org/~bettinel/maps/maps.html.

[74] J. Ambjørn, J. Jurkiewicz, and R. Loll. "Nonperturbative Lorentzian Path Integral for Gravity". In: *Physical Review Letters* 85.5 (July 2000), pp. 924–927. DOI: 10.1103/physrevlett.85.924. arXiv: hep-th/0002050 [hep-th].

[75] Rafael Sorkin. "Time-evolution problem in Regge calculus". In: *Phys. Rev. D* 12 (2 July 1975), pp. 385–396. DOI: 10.1103/PhysRevD.12.385.

[76] Maxim Krikun and Anatoly Yambartsev. "Phase transition for the Ising model on the Critical Lorentzian triangulation". In: *J Stat Phys* 148 (2008), pp. 422–439. DOI: https://doi.org/10.1007/s10955-012-0548-0. arXiv: 0810.2182 [math.PR].

[77] K.B. Athreya, P.E. Ney, and P.E. Ney. *Branching Processes*. Dover Books on Mathematics. Dover Publications, 2004.

[78] Russell Lyons and Yuval Peres. *Probability on Trees and Networks*. Vol. 42. Cambridge Series in Statistical and Probabilistic Mathematics. Available at https://rdlyons.pages.iu.edu/. Cambridge University Press, New York, 2016, pp. xv+699. DOI: 10.1017/9781316672815.

[79] Bergfinnur Durhuus. "Probabilistic Aspects of Infinite Trees and Surfaces". In: *Acta Physica Polonica B* 34.10 (Oct. 2003), p. 4795.

[80] P. Di Francesco, E. Guitter, and C. Kristjansen. "Integrable 2D Lorentzian gravity and random walks". In: *Nuclear Physics B* 567.3 (Feb. 2000), pp. 515–553. DOI: 10.1016/s0550-3213(99)00661-6. arXiv: hep-th/9907084 [hep-th].

[81] G.'t Hooft. "A planar diagram theory for strong interactions". In: *Nuclear Physics B* 72.3 (1974), pp. 461–473. DOI: https://doi.org/10.1016/0550-3213(74)90154-0.

[82] Phil Saad, Stephen H. Shenker, and Douglas Stanford. "JT gravity as a matrix integral". In: (Mar. 2019). arXiv: 1903.11115 [hep-th].

[83] Scott Collier et al. "The Virasoro minimal string". In: *SciPost Phys.* 16.2 (2024), p. 057. DOI: 10.21468/SciPostPhys.16.2.057. arXiv: 2309.10846 [hep-th].

[84] Scott Collier et al. "The complex Liouville string: the matrix integral". In: (Oct. 2024). arXiv: 2410.07345 [hep-th].

[85] P. Di Francesco, Paul H. Ginsparg, and Jean Zinn-Justin. "2-D Gravity and random matrices". In: *Phys. Rept.* 254 (1995), pp. 1–133. DOI: 10.1016/0370-1573(94)00084-G. arXiv: hep-th/9306153.

[86] Paul H. Ginsparg. "Matrix models of 2-d gravity". In: Dec. 1991. arXiv: hep-th/9112013.

[87] Ioannis Karatzas and Steven E. Shreve. *Brownian Motion and Stochastic Calculus*. 2nd. Vol. 113. Graduate Texts in Mathematics. New York: Springer-Verlag, 1991. DOI: 10.1007/978-1-4612-0949-2.

[88] Bernt Øksendal. *Stochastic Differential Equations: An Introduction with Applications*. 6th. Universitext. Berlin, Heidelberg: Springer-Verlag, 2003. DOI: 10.1007/978-3-642-14394-6.

[89] Steven E. Shreve. *Stochastic Calculus for Finance II: Continuous-Time Models*. Springer Finance. New York: Springer-Verlag, 2004. DOI: 10.1007/978-1-4757-4296-1.

[90] V. G. Knizhnik, Alexander M. Polyakov, and A. B. Zamolodchikov. "Fractal Structure of 2D Quantum Gravity". In: *Mod. Phys. Lett. A* 3 (1988). Ed. by I. M. Khalatnikov and V. P. Mineev, p. 819. DOI: 10.1142/S0217732388000982. arXiv: hep-th/9312157 [hep-th].

[91] F. David. "Conformal Field Theories Coupled to 2D Gravity in the Conformal Gauge". In: *Mod. Phys. Lett. A* 3 (1988), p. 1651. DOI: 10.1142/S0217732388001975.

[92] Jacques Distler and Hikaru Kawai. "Conformal field theory and 2D quantum gravity". In: *Nuclear Physics B* 321.2 (1989), pp. 509–527. DOI: https://doi.org/10.1016/0550-3213(89)90354-4.

[93] V.A. Kazakov. "Ising model on a dynamical planar random lattice: Exact solution". en. In: *Physics Letters A* 119.3 (Dec. 1986), pp. 140–144. DOI: 10.1016/0375-9601(86)90433-0.

[94] D. V. Boulatov and V. A. Kazakov. "The Ising Model on Random Planar Lattice: The Structure of Phase Transition and the Exact Critical Exponents". In: *Phys. Lett. B* 186 (1987), p. 379. DOI: 10.1016/0370-2693(87)90312-1.

[95] David Aasen, Roger S K Mong, and Paul Fendley. "Topological defects on the lattice: I. The Ising model". In: *Journal of Physics A: Mathematical and Theoretical* 49.35 (Aug. 2016), p. 354001. DOI: 10.1088/1751-8113/49/35/354001. arXiv: 1601.07185 [cond-mat.stat-mech].

[96] F. Guerra, L. Rosen, and B. Simon. "The $P(\phi)_2$ Euclidean Quantum Field Theory as Classical Statistical Mechanics". In: *Annals of Mathematics* 101.1 (1975), pp. 111–189. DOI: https://doi.org/10.2307/1970988.

[97] Rémi Rhodes and Vincent Vargas. *Two Decades of Probabilistic Approach to Liouville Conformal Field Theory*. 2025. arXiv: 2509.21053 [math-ph].

[98] François David et al. *Liouville Quantum Gravity on the Riemann sphere*. 2015. arXiv: 1410.7318 [math.PR].

[99] Bertrand Duplantier et al. "Critical Gaussian multiplicative chaos: Convergence of the derivative martingale". In: *The Annals of Probability* 42.5 (Sept. 2014). DOI: 10.1214/13-aop890.

[100] Bertrand Duplantier et al. "Renormalization of Critical Gaussian Multiplicative Chaos and KPZ Relation". In: *Communications in Mathematical Physics* 330.1 (2014), pp. 283–330. DOI: 10.1007/s00220-014-2000-6.

[101] Scott Sheffield. "Gaussian free fields for mathematicians". In: *Probability Theory and Related Fields* 139.3 (2007), pp. 521–541. DOI: 10.1007/s00440-006-0050-1. arXiv: math/0312099 [math.PR].

[102] David Aasen, Paul Fendley, and Roger S. K. Mong. "Topological Defects on the Lattice: Dualities and Degeneracies". In: (2020). arXiv: 2008.08598 [cond-mat.stat-mech].

[103] J. C. Hernandez et al. "Bounds on the critical line via transfer matrix methods for an Ising model coupled to causal dynamical triangulations". In: *Journal of Mathematical Physics* 54.6 (June 2013), p. 063301. DOI: 10.1063/1.4808101. arXiv: 1301.1483 [math-ph].

[104] John Lamperti and Peter Ney. "Conditioned Branching Processes and Their Limiting Diffusions". In: *Theory of Probability & Its Applications* 13.1 (1968), pp. 128–139. DOI: 10.1137/1113009. eprint: https://doi.org/10.1137/1113009.

[105] Valentin Sisko, Anatoly Yambartsev, and Stefan Zohren. "A note on weak convergence results for infinite causal triangulations". In: *Brazilian Journal of Probability and Statistics* 32.3 (2018), pp. 597–615. DOI: 10.1214/17-BJPS356. arXiv: 1201.0264 [math-ph].

[106] Stewart N. Ethier and Thomas G. Kurtz. *Markov processes – characterization and convergence*. Wiley Series in Probability and Mathematical Statistics: Probability and Mathematical Statistics. New York: John Wiley & Sons Inc., 1986, pp. x+534.

[107] Thomas G. Kurtz and Philip Protter. "Weak Limit Theorems for Stochastic Integrals and Stochastic Differential Equations". In: *The Annals of Probability* 19.3 (1991), pp. 1035–1070. DOI: 10.1214/aop/1176990334.

[108] Daniel. Revuz and Marc. Yor. *Continuous Martingales and Brownian Motion*. eng. 3rd ed. 1999. Grundlehren der mathematischen Wissenschaften, A Series of Comprehensive Studies in Mathematics, 293. Berlin, Heidelberg: Springer Berlin Heidelberg, 1999.

[109] L. Onsager and S. Machlup. "Fluctuations and Irreversible Processes". In: *Phys. Rev.* 91 (6 Sept. 1953), pp. 1505–1512. DOI: 10.1103/PhysRev.91.1505.

[110] W. Horsthemke and A. Bach. "Onsager-Machlup Function for one dimensional nonlinear diffusion processes". In: *Zeitschrift fur Physik B Condensed Matter* 22.2 (June 1975), pp. 189–192. DOI: 10.1007/BF01322364.

[111] Markus F Weber and Erwin Frey. "Master equations and the theory of stochastic path integrals". In: *Reports on Progress in Physics* 80.4 (Mar. 2017), p. 046601. DOI: 10.1088/1361-6633/aa5ae2. arXiv: 1609.02849 [cond-mat.stat-mech].

[112] D. Benedetti and R. Loll. "Unexpected spin-off from quantum gravity". In: *Physica A: Statistical Mechanics and its Applications* 377.2 (Apr. 2007), pp. 373–380. DOI: 10.1016/j.physa.2006.11.032. arXiv: hep-lat/0603013 [hep-lat].

[113] Ryan Barouki and Davide Laurenzano. "A Renormalization Group Analysis of the Ising Model Coupled to Causal Dynamical Triangulations". In: (Apr. 2025). arXiv: 2504.01134 [hep-th].

[114] Christof Wetterich. "Exact evolution equation for the effective potential". In: *Physics Letters B* 301.1 (Feb. 1993), pp. 90–94. DOI: 10.1016/0370-2693(93)90726-x. arXiv: 1710.05815 [hep-th].

[115] Astrid Eichhorn, Tim Koslowski, and Antonio D. Pereira. "Status of background-independent coarse-graining in tensor models for quantum gravity". In: (2018). arXiv: 1811.12909 [gr-qc].

[116] Astrid Eichhorn, Antonio D. Pereira, and Andreas G. A. Pithis. "The phase diagram of the multi-matrix model with ABAB-interaction from functional renormalization". In: *JHEP* 12 (2020), p. 131. DOI: 10.1007/JHEP12(2020)131. arXiv: 2009.05111 [gr-qc].

[117] John Lamperti. "Semi-stable Markov processes. I". In: *Zeitschrift für Wahrscheinlichkeitstheorie und Verwandte Gebiete* 22.3 (Sept. 1972), pp. 205–225. DOI: 10.1007/BF00536091.

[118] Hiroyuki Matsumoto and Marc Yor. "Exponential functionals of Brownian motion, I: Probability laws at fixed time". In: *Probability Surveys* 2.none (Jan. 2005). DOI: 10.1214/154957805100000159. arXiv: math/0511517 [math.PR].

[119] Hiroyuki Matsumoto and Marc Yor. "Exponential functionals of Brownian motion, II: Some related diffusion processes". In: *Probability Surveys* 2.none (Jan. 2005). DOI: 10.1214/154957805100000168. arXiv: math/0511519 [math.PR].

[120] Zhenbin Yang. "The Quantum Gravity Dynamics of Near Extremal Black Holes". en. In: *Journal of High Energy Physics* 2019.5 (May 2019), p. 205. DOI: 10.1007/JHEP05(2019)205. arXiv: 1809.08647 [hep-th].